# FINAL REPORT

## FEBRUARY 1963 TO JULY 1964

Contract No. NAS7-107

19 JULY 1964

# VOLUME II
## NEW CONCEPTS

Prepared for

CHIEF, LIQUID-PROPULSION SYSTEMS, CODE RPL

NATIONAL AERONAUTICS AND SPACE ADMINISTRATION

Washington, D.C.

# TRW SPACE TECHNOLOGY LABORATORIES
THOMPSON RAMO WOOLDRIDGE INC.
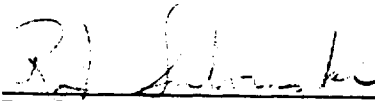
FINAL REPORT

FEBRUARY 1963 TO JULY 1964

ADVANCED VALVE TECHNOLOGY FOR SPACECRAFT ENGINES (U)

VOLUME II -- NEW CONCEPTS
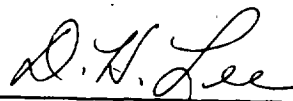
O. O. Fiet                R. J. Salvinski
D. I. Friedlander         L. D. Young

PREPARED FOR

CHIEF, LIQUID-PROPULSION SYSTEMS, CODE RPL
NATIONAL AERONAUTICS AND SPACE ADMINISTRATION
WASHINGTON, D.C.

CONTRACT NAS7-107

19 JULY 1964

R. J. Salvinski, Program Manager

Approved

D. H. Lee
Propulsion Development Department

TRW SPACE TECHNOLOGY LABORATORIES
REDONDO BEACH, CALIFORNIA

# FOREWORD

This is Volume II of two volumes constituting the final report and
including the work accomplished between 26 February 1963 and 17 July
1964, representing an extension of NASA Contract NAS7-107 entitled
"Advanced Valve Technology for Spacecraft Engines." This volume,
which has been made an independent portion of the report because of
the Confidential nature of its contents, presents the results of an
electromagnetic actuator study and the new design concepts initiated
under this study. The program was originated under Dr. Henry Burlage,
Chief, Liquid Propulsion Systems, Headquarters, Washington, D.C., in
February 1962 and Final Report No. 8651-6016-RU000 was issued in March
1963. The Headquarters Project Manager is Mr. Frank E. Compitello.
The program is under the technical direction of Mr. Louis R. Toth of
Jet Propulsion Laboratory, Pasadena, California.

The Propulsion Laboratory of TRW-STL Mechanics Division was responsible
for the work performed on this program. Acknowledgment is made of the
technical assistance provided on this volume by the following personnel
at STL:

| | |
|---|---|
| Mr. R. J. Berg | Propulsion Development Department |
| Dr. C. L. Dailey | Solid State Physics Department |
| Mr. R. L. Hammel | "       "       "       " |
| Dr. J. S. Martinez | Propulsion Research Department |
| Mr. J. R. McDougall | "       "       " |
| Mr. C. Salts, Jr. | Solid State Physics Department |

Further acknowledgment is made to Mrs. Bess Smith, whose assistance has
been invaluable in the preparation of this report.

ABSTRACT

This final report describes the work undertaken to advance the state-of-the-art of valves used on spacecraft propulsion systems. The work is a continuation of a NASA program initiated in February 1962 for which a final report entitled "Advanced Valve Technology for Spacecraft Engines" was submitted March 1963.

Interviews were held with personnel of major prime manufacturers and NASA agencies to determine current problems and future requirements of valves operating in the space environments. A literature search was maintained throughout the program to obtain required information.

Studies were conducted on valve and valve elements, including zero-g venting, electromagnetic and pyrotechnic actuators, and permeation of Teflon composite seal materials. Other studies undertaken include liquid propellant material compatibility, space maintenance, meteoroidal impact, and requirements for valve qualification testing in the space environments.

SUMMARY

Volume II presents the results of an investigation of four new concepts developed under the Advanced Valve Technology Program. Also included in this volume is an electromagnetic actuator study which led to the evolution of a lightweight high-temperature solenoid coil.

## WET SEAL CONCEPT

This concept involves the use of liquids for application as a seal between valve seats and fitting joints. Liquid metals have been coated on simulated closures and tested for helium leakage. Helium pressures to 2200 psi have been successfully held between two flat surfaces, while no leakage was detected using a mass spectrometer having a sensitivity of $10^{-9}$ scc/sec helium.

Preliminary tests were performed on a dynamic seal utilizing rotary motion between two flat surfaces wetted with liquid gallium eutectic. A helium probe was used to provide a leak medium. No leakage was detected using a helium mass spectrometer. After several turning motions, sticking was noticed. Examination of the surfaces showed that sticking was due to poor compatibility and lubricity of the liquid metal with the substrate material.

## ELECTROMAGNETIC ACTUATOR STUDY

This study investigates the state-of-the-art capability of high temperature solenoids and includes material limitations, coil resistivity, magnetic saturation, effects of solenoid transient forces on spacecraft, the effects of space environments and design configuration data for optimum performance.

A lightweight high temperature electromagnetic solenoid utilizing beryllium wire was developed. The solenoid coil was designed to operate at $1800^{\circ}F$, the temperature limit of available magnetic core materials. The coil is believed to represent a weight saving of 50 percent over presently designed solenoids.

ZERO-G VENT VALVE

A new technique for venting excessive propellant tank pressures has been originated.  In this process the principles of refrigeration are applied in a novel and efficient manner in order to remove the energy additions responsible for the overpressure condition.  This concept has been treated in a patent disclosure.  A system analysis and model test have been performed.

RADIOACTIVE PROXIMETER

The use of radioisotopes for the purpose of monitoring valve position was investigated.  It is felt that this concept can, with proper development, provide a high reliable, no-load, temperature and pressure insensitive method of valve position detection.  An analysis has been performed which considers the relationship of some alpha, beta, and gamma source levels with respect to representative valve requirements, e.g. stroke, response, resolution, etc.  In addition, in order to present a realistic set of design requirements against which to evaluate this concept, a special case was chosen:  the propellant valve actuator for the STL version of the Lunar Excursion Module descent engine was felt to represent a practical approach to current spacecraft requirements.

VALVE ANALYSIS CHART

A valve analysis chart was used throughout the program to aid in defining valve problem areas.  This was accomplished by assigning a reliability rating to each valve and valve elements in relation to their functional parameters and their performance with propellants and space environments.  The ratings indicated on the chart were based on several interviews with prime manufacturers and NASA agencies, a propellant study and a literature search.  A review of the analysis chart is presented; several problem areas are defined and discussed.  Valve serviceability data obtained through personal interviews are also included.

## ADVANCED VALVE STUDIES

Several new valve concepts were reviewed: A contamination insensitive metal valve closure; zero-g-vent valves; a pneumatic regulator; a diffusion valve and a freeze valve. The valves selected for review contained concepts which represent solutions or potential solutions to outstanding valve problem areas.

A series of tests was performed to establish probable problem areas which reflect on the state-of-the-art of electropyrotechnic cartridges. The tests involved exposure to sterilization thermal cycles and ethylene oxide, radiation, vacuum, and helium leakage.

Teflon composite materials were fabricated and tested to investigate permeability characteristics of polymeric composites which might be used as seal materials.

## LIQUID PROPELLANT STUDY

Sixteen propellants were investigated pertaining to materials compatibility, shock sensitivity, lubricity, viscosity, radiation tolerances, and effects of leakage. A propellant rating chart is included which enables one to assess quickly the more serious problem areas. The information contained in this section has been extracted from the best technical sources available.

## SPACE MAINTENANCE

A preliminary evaluation has been made of the several forms that maintenance of the control valving function can take. This evaluation is summarized in a set of tables which attempt to define the preferential form of maintenance (i.e., in-flight servicing, redundant circuits, and/ or override systems) for each valve type being considered and for representative space missions. In a second phase of this study, a series of high vacuum tests--in the $10^{-9}$ torr region--was performed to investigate the tendency toward inadvertent adhesion, sometimes referred to as cold welding. Line fittings and representative valve elements were subjected

to repeated torquing cycles in this environment to determine whether the cold welding phenomenon would affect in-flight servicing of space valves.

## METEOROIDAL IMPACT STUDY

Discussions have been held with several authorities in the field of meteoroidal impact who are currently conducting studies at NASA's Lewis Research Laboratories, General Motors Defense Research Laboratory, and the Aerojet General Corporation Terminal Ballistics Department. These discussions have provided appreciable insight into the phenomena involved and into the potential hazards for spacecraft valving. A series of tests was performed to determine the practical effects of simulated meteoroidal bombardment on representative valve elements. Cast valve housings of corrosion resistant steel and aluminum alloys were bombarded, through a skin-like aluminum shield, by projectiles traveling at the low end of the micrometeorite velocity spectrum. Projectile properties and valve damage have been recorded.

## VALVE QUALIFICATION TESTING

Valve qualification testing for the space environments is discussed including vacuum simulation testing, radiation exposure, and meteoroidal bombardment. Two new testing concepts are discussed for possible further development and include a dynamic electropyrotechnic cartridge tester and a leak detector.

CONTENTS

TABLES

FIGURES

FIGURES (Cont'd)

FIGURES (Cont'd)

INTRODUCTION

This report represents a continuation of the work accomplished under the
Advanced Valve Technology Program initiated February 1962.  An interim
report, No. 8651-6016-RU000, was issued in March 1963.  Volume II includes
the new concepts originated during the period February 1963 to July 1964.

In the course of conducting work on the program, new concepts were evolved
in many instances resulting from systematic valve studies.  Ideally, new
concepts would be evolved after defining the problem to which a solution
is required.  Generating new concepts requires freedom of thought, or
brainstorming.  Sometimes a systematic procedure such as the morphological
approach can be used to evolve new ideas, but this is limited to those
techniques already evolved, and further advancements in the state-of-the-
art cannot be efficiently made.  The program plan was conducted in a man-
ner in which the methodic or systematic approach was taken to define the
problem areas and accomplish the various valve studies.  Directing the
effort of the valve studies toward investigation of the defined problem
areas, with emphasis on generating new ideas, stimulated the brainstorming
technique among the technical personnel working on the program, resulting
in several new concepts.

PROGRAM OBJECTIVES

The objectives of the Advanced Valve Technology Program are to advance the
state-of-the-art of valves used on spacecraft liquid propulsion engines,
evaluate valve problem areas, and evolve new concepts.

PROGRAM PLAN

An outline of the program plan including specific tasks is presented in
the Summary Chart on the following pages.  Tasks I through VI depicted on
the program plan are presented in Volume I.  Task VII, New Concepts, is
presented in Volume II.

## NAS 7-107 ADVANCED VALVE TECHNOLOGY FOR SPACECRAFT ENGINES
### PROGRAM PLAN — Period February 1963 to July 1964

Objective: To advance the state of the art of valves used in liquid propulsion spacecraft engines.

**I. VALVE ANALYSIS CHART**

Program management aid in defining and evaluating problems related to propulsion valves operating in the space environment. Includes functional parameters and valve performance with propellants.

**II. ADVANCED VALVE STUDY**

Evaluate problem areas, review new concepts for propulsion valves.

- A. VALVES - Review New Concepts
  1. Cone Labyrinth Valve
  2. Zero-g Vent Valves
  3. Cold Gas Regulator
  4. Diffusion Valve
  5. Freeze Valve

- B. RELATED SUBCOMPONENTS (Also see New Concepts, VII)
  1. Electropyrotechnic Cartridge Test

| | |
|---|---|
| Leak Test | Helium mass spectrometer test to 2000 psi helium |
| Radiation Exposure | $10^6$ r gamma radiation |
| Sterilization | Ambient to 300°F cycle; ethylene oxide exposure |
| Vacuum Exposure | $10^{-9}$ mm Hg exposure includes −150°F to 300°F cycle, fire in vacuum |

  2. Teflon Composite Permeability Test

Gold-Teflon
Silver-Teflon
Iron-Teflon

**III. LIQUID PROPELLANT STUDY**

Effect of propellants and parameters on valve

| Liquid Propellants Studied | | | Parameters |
|---|---|---|---|
| Fuels | Oxidizers | Cryogenics | |
| Aerozine-50 | Chlorine Trifluoride | Liquid Fluorine | Compatibility |
| Hybaline $A_5$ | Nitrogen Tetroxide | Liquid Hydrogen | Control of Flow |
| Hybaline B | Oxygen Difluoride | Liquid Oxygen | Leakage |
| Hydrazine | Perchloryl Fluoride | | Lubricity |
| Monomethylhydrazine | | **Gels** | Radiation Tolerance |
| Pentaborane | | | Shock Sensitivity |
| U-Dimethylhydrazine | | Metalized | Viscosity |
| | | Nonmetalized | |

**IV. SPACE MAINTENANCE STUDY**

- A. Evaluation of the most appropriate of three methods of valve maintenance—redundancy, override, and in-flight service or replacement—for typical vehicle missions and component functions.

- B. Investigation into one of the problems associated with the servicing of valves during extended space missions; e.g., cold welding of fluid fittings.

**V. METEOROIDAL IMPACT**

Evaluation of the damaging effects of micrometeoroid bombardment on valve elements. Includes a bibliography of significant papers, a brief review of industry opinion, and a report of the simulated meteoroidal impact tests performed on typical cast valve housings.

**VI. VALVE QUALIFICATION TESTING**

- A. Investigate and evaluate testing techniques necessary for qualifying spacecraft engine valves.

- B. Evolve new testing techniques
  1. Electropyrotechnic cartridge dynamic tester
  2. Leak measurements utilizing volumetric buoyancy techniques

**VII. NEW CONCEPTS**

- A. WET SEAL — Test liquid metal coatings (gallium and mercury) between valve seats and joints for sealing capability.
  Phase I: Static Seal Test. Phase II: Dynamic Seal Test.

| | Test Parameters | | |
|---|---|---|---|
| Media | Helium | Bearing Load | Ambient to 80 percent yield |
| Maximum Leak | $10^{-8}$ scc/sec helium | Pressure | Ambient to 2000 psi |

- B. ELECTROMAGNETIC ACTUATOR
  1. STUDY:

| Parameters | Environments |
|---|---|
| Coil Resistivity | High Temperatures |
| Magnetic Permeability | Planetary Magnetic Fields |
| Magnetic Saturation | Radiation |
| Transient Forces | Space Vacuum |
| Weight | |

  2. LIGHTWEIGHT ACTUATOR — manufacture, test lightweight solenoid actuator coil.

- C. ZERO-G VENT VALVE — Concept using heat exchange techniques — perform analysis and preliminary design.

- D. RADIOACTIVE PROXIMETER — Analytical evaluation of the merits of an environment-insensitive proximity measuring device, based on detection of isotope-generated radiation, for use in feedback control and simple position detection of flow control valves.

R. J. Salvinski
Program Manager
Propulsion Development Department

NAS 7-107 ADVANCED VALVE TECHNOLOGY FOR SPACECRAFT ENGINES

PROGRAM PLAN — Period February 1963 to July 1964

Objective: To advance the state of the art of valves used in liquid propulsion spacecraft engines.

I. **VALVE ANALYSIS CHART**

Program management aid in defining and evaluating problems related to propulsion valves operating in the space environment. Includes functional parameters and valve performance with propellants.

II. **ADVANCED VALVE STUDY**

Evaluate problem areas, review new concepts for propulsion valves.

A. VALVES - Review New Concepts
1. Cone Labyrinth Valve
2. Zero-g Vent Valves
3. Cold Gas Regulator
4. Diffusion Valve
5. Freeze Valve

B. RELATED SUBCOMPONENTS (Also see New Concepts, VII)
1. Electropyrotechnic Cartridge Test

| | |
|---|---|
| Leak Test | Helium mass spectrometer test to 2000 psi helium |
| Radiation Exposure | $10^6$ r gamma radiation |
| Sterilization | Ambient to 300°F cycle; ethylene oxide exposure |
| Vacuum Exposure | $10^{-9}$ mm Hg exposure includes –150°F to 300°F cycle, fire in vacuum |

2. Teflon Composite Permeability Test

Gold-Teflon
Silver-Teflon
Iron-Teflon

III. **LIQUID PROPELLANT STUDY**

Effect of propellants and parameters on valve

| Liquid Propellants Studied | | | Parameters |
|---|---|---|---|
| **Fuels** | **Oxidizers** | **Cryogenics** | Compatibility |
| Aerozine-50 | Chlorine Trifluoride | Liquid Fluorine | Control of Flow |
| Hybaline $A_5$ | Nitrogen Tetroxide | Liquid Hydrogen | Leakage |
| Hybaline B | Oxygen Difluoride | Liquid Oxygen | Lubricity |
| Hydrazine | Perchloryl Fluoride | | Radiation Tolerance |
| Monomethylhydrazine | | **Gels** | Shock Sensitivity |
| Pentaborane | | Metalized | Viscosity |
| U-Dimethylhydrazine | | Nonmetalized | |

IV. **SPACE MAINTENANCE STUDY**

A. Evaluation of the most appropriate of three methods of valve maintenance—redundancy, override, and in-flight service or replacement—for typical vehicle missions and component functions.

B. Investigation into one of the problems associated with the servicing of valves during extended space missions; e.g., cold welding of fluid fittings.

V. **METEOROIDAL IMPACT**

Evaluation of the damaging effects of micrometeoroid bombardment on valve elements. Includes a bibliography of significant papers, a brief review of industry opinion, and a report of the simulated meteoroidal impact tests performed on typical cast valve housings.

VI. **VALVE QUALIFICATION TESTING**

A. Investigate and evaluate testing techniques necessary for qualifying spacecraft engine valves.

B. Evolve new testing techniques
1. Electropyrotechnic cartridge dynamic tester
2. Leak measurements utilizing volumetric buoyancy techniques

VII. **NEW CONCEPTS**

A. WET SEAL — Test liquid metal coatings (gallium and mercury) between valve seats and joints for sealing capability.
Phase I: Static Seal Test. Phase II: Dynamic Seal Test.

| Test Parameters | | | |
|---|---|---|---|
| Media | Helium | Bearing Load | Ambient to 80 percent yield |
| Maximum Leak | $10^{-8}$ scc/sec helium | Pressure | Ambient to 2000 psi |

B. ELECTROMAGNETIC ACTUATOR
1. STUDY:

| Parameters | Environments |
|---|---|
| Coil Resistivity | High Temperatures |
| Magnetic Permeability | Planetary Magnetic Fields |
| Magnetic Saturation | Radiation |
| Transient Forces | Space Vacuum |
| Weight | |

2. LIGHTWEIGHT ACTUATOR — manufacture, test lightweight solenoid actuator coil.

C. ZERO-G VENT VALVE — Concept using heat exchange techniques — perform analysis and preliminary design.

D. RADIOACTIVE PROXIMETER — Analytical evaluation of the merits of an environment-insensitive proximity measuring device, based on detection of isotope-generated radiation, for use in feedback control and simple position detection of flow control valves.

R. J. Salvinski
Program Manager
Propulsion Development Department

I.  WET SEAL STUDY

## INTRODUCTION

The purpose of this study was to develop a zero leak seal for static and dynamic applications by using liquid metal coatings between metal sealing surfaces.  Zero leakage has been defined to be a leakage of less than $10^{-8}$ std cc/sec helium (Ref. 1).  Metal-to-metal seals maintaining zero leakage are possible by plastically deforming soft metals.  Static seals such as those used in flare tube fittings and flange gaskets utilize plastically deformed materials.  Such seals are not recommended, however, for re-use after the joint is broken.  When a large number of valve poppet cycles are required, soft metal sealing materials which are plastically deformed are unacceptable due to their low cycle life.  The result is the common use of metal-to-metal seats which involve no plastic deformation and require hard seat materials with extremely fine surface finishes.  A major problem with such a seat is the inherently high leakage rate and extreme sensitivity to contamination.

## THEORY

When two highly polished surfaces are placed in contact, a small volume of porous structure can be visualized as existing between the two contacting surfaces.  Numerous leakage paths result from the microscopic nonuniformity between the two surfaces.

Utilizing this concept, sealing by a liquid metal can then be visualized as the closing of the capillary leakage paths by the liquid metal.  The force necessary to overcome the retention of the liquid or break down the seal is directly related to the capillary forces.

The capillary force between a liquid-solid interface depends upon the manner in which they meet.  Between a liquid and a solid the contact angle is the angle between the solid and the tangent to the liquid at the point of contact.  The surface tension of the solid and liquid phases and interfacial tension between these phases determines the

magnitude of the contact angle and thus the capillary force. In a
confined volume the contact angle results in the formation of a
meniscus. The contact angle (Ref. 2) is directly related to
wettability of the liquid which is described at equilibrium and
neglecting gravitational effects as:

$$\lambda_{SV} = \lambda_{LS} + \lambda_{LV} \cos \theta \tag{1}$$

where

$$\lambda_{SV} = \text{surface tension solid: vapor}$$

$$\lambda_{LS} = \text{interfacial tension liquid: solid}$$

$$\lambda_{LV} = \text{surface tension liquid: vapor}$$

For complete wettability $\theta = 0^{\circ}$ so that:

$$\lambda_{SV} = \lambda_{LS} + \lambda_{LV} \tag{2}$$

The general equation relating the pressure difference across a curved
liquid surface is:

$$\Delta P = -\lambda \left( \frac{1}{R_1} + \frac{1}{R_2} \right) \tag{3}$$

where $\lambda$ is the interfacial tension of the liquid surface film and $R_1$
and $R_2$ are the radius of curvature of a curved liquid surface.

For closely spaced parallel plates

$$R_2 = \infty \text{ and } R_1 = D/2 \text{ the above equation reduces to:}$$

$$\Delta P = -\lambda 2/D \tag{4}$$

where perfect wetting is assumed ($\cos \theta = 1$).

This equation is plotted in Figure 1-1.

Figure 1-1 illustrates the significance of surface finishes for wet seals.
Surface finish is important in reducing the spacing between parallel

plates. For both mercury and gallium alloy liquid metal systems at room temperature, the surface tension is greater than 500+ dynes/cm$^2$. Any contaminants present in the liquid phase or on the surface of the solid will, in general, tend to degrade wettability by lowering the surface tension.

While more rigorous mathematical solutions are available (Ref. 3) for treatment of idealized geometries, their contribution does not provide more direction to the engineering problem than this simple model.

## LIQUID METALS AND LITERATURE REVIEW

A partial review of the literature was made concerning applications of liquid metals to surfaces. Particular attention was given to physical properties of liquid metal systems, wettability characteristics and wetting techniques, corrosiveness, and known compatibilities, and related usage (Ref. 4). As a result of the initial review, two liquid metal systems were selected for use in the experimental phase. These are mercury-indium-thallium and gallium-indium-tin. The primary considerations in selecting these two systems were their generally noted wettability for a wide range of materials and their liquid state at room temperature.

The Mercury-Indium-Thallium system was purchased from the Victor King Materials Laboratory as Viking LS232 and the Gallium-Indium-Tin from United Mineral and Chemical Corporation as UG-1 Alloy.

## Compatibilities

As the surface finish is important to the sealing effectiveness of liquid metals, reactions between the liquid metal and the wetted surface which would produce roughening are of concern. Roughening could occur in the form of etching, pitting, or material buildup through amalgamation and alloying. The Aluminum Company of America (Ref. 5) summarizes the compatibilities of gallium as readily alloying with all metals at elevated temperatures and forming alloys with tin, zinc, cadmium, aluminum, silver, magnesium, copper, and others at room temperature. Tantalum resists attack up to 842°F and tungsten to 1472°F. Graphite is not attacked by gallium at any temperature and silicon base refractories are satisfactory

to 1832°F. Gallium reacts with sulphuric, nitric, perchloric, and hydro-
chloric acids and sodium hydroxide. Aqua regia and concentrated caustics
attack pure gallium very rapidly. Alcoa (Ref. 6) also indicates gallium
is being used as a sealant for glass joints in laboratory vacuum equipment,
in particular with mass spectrometers. The Metals Department of United
Mineral and Chemical Corporation (Ref. 7) likewise indicates the applica-
tion of gallium for vacuum seals. United Mineral indicates mild steel,
stainless steels, such as the 14 percent chrome and 18/8 nickel/chrome
types, Monel, nickel, copper, and brass have been wetted and left for six
weeks at room temperature and 212°F. All metals were found intact with
the exception of copper and brass, which showed slight corrosion at 212°F.
At temperatures over 572°F these metals are attacked by gallium and its
eutectics. Columbium resists corrosion up to 842°F, beryllium up to 932°F.
Tungsten, rhenium, and zirconium are not attacked at temperatures up to
1472°F. Beryllia, alumina, and silica resist attack at temperatures of
1832° and higher. United Mineral also reports the ability of the liquid
metal to withstand atmospheric pressure across a $10^{-3}$ cm gap provided the
liquid metal wets and bridges the sides continuously. They report the
application of such a seal at $10^{-7}$ torr vacuum retained a 3 psi helium
pressure which corresponds well with the curve of Figure 1-1.

The mercury-thallium alloy is highly reactive with oxygen and will rapidly
degrade to form thallium oxides or hydroxides. Boag (Reference 8) has
found treatment with purified hydrogen can reduce the absorbed oxygen and
prevent or retard additional reaction. It is the formation of the thal-
lium oxide which probably produces the widespread wettability of this
liquid metal system for most materials. For sealing purposes the presence
of oxides is not clearly detrimental. The mercury-thallium system does
not require special care (Reference 9) and handling, although precautions
are not prohibitively complex. The alloy system is reported to have in-
curred no apparent degradation after nuclear exposure to $1.35 \times 10^{16}$ $n/cm^2$
greater than 1 Mev, $4.75 \times 10^{15}$ $n/cm^2$ breater than 2.9 Mev, and $2.5 \times 10^{8}$R
gamma.

Table 1-1 (Taken from Ref. 10) compares the indicated corrosion resist-
ance of gallium and mercury for a number of metals. References (11),

(12), and (13) provide additional detailed solubility data on both liquid metals. While summarization of the gross compatibilities between liquid metals and substrate materials and solubilities are available in the literature, it was concluded no definitive information regarding minor surface attack or reaction kinetics appropriate to highly finished sealing surfaces was available. The known effects of liquid metals on mechanical properties have been well summarized by Rostoker, et al. (Ref. 14). In addition to the alteration of mechanical properties, the possibility of liquid metals in contact between two substrate materials resulting in welding or bond formation between the solid components has been reported.

Beneficial results in applying liquid metals have been noted by using chemical attack to remove surface contaminants from metallic substrates. Lowering the sample to be coated through the cleaning agent which is floating above the liquid metal is one such technique. Likewise, the use of sonic and ultrasonic mechanical breakdown of surface oxides while the material to be wetted is immersed in the liquid metal has been used to improve wettabilities. With the materials tested, such techniques were not found to be necessary. The results of the screening tests and wetting techniques are summarized as follows:

1. The qualitatively observed wettability for both liquid metal systems appeared very satisfactory. Tests performed prior to the wetting of seal surfaces indicated reasonable adherence to tungsten, nickel, iron, copper, tantalum, molybdenum, niobium, coil silver, sintered $Al_2O_3$, and glass.

2. The liquid metal was applied with a cotton bud to the surface to be wetted, and the liquid was swabbed over the desired area. Subsequent light mechanical burnishing with a disposable paper wiper insured complete coverage while striking the excess liquid metal from the wetted surface. This procedure was used on all subsequent seal surfaces.

Table 1-2 compares some of the physical properties of the liquid metals of interest.

SUMMARY

On the basis of general wettability characteristics, both the mercury and the gallium alloys appear comparable. Likewise, the surface tension of both alloys appears adequate for seal applications. However, one distinction between the two systems can be made on the basis of their solidification points: The mercury alloy may permit operation at significantly lower temperatures than the gallium system. The most attractive property of the gallium system is its relatively low vapor pressure, permitting applications as high as $800^{\circ}F$ without significant evaporative loss. The mercury system, on the other hand, has an exceedingly high vapor pressure for elevated temperature usage and thus must be confined to ambient and below ambient applications. Because of gallium's superior vapor pressure, the primary effort in the investigation was based on the gallium.

The indicated tendency of both liquid metals to attack base metals, especially at elevated temperatures, would appear to be a significantly detrimental factor for applying them to many common valve materials. In seal applications where the surface finish is extremely critical, this becomes a dominant point.

STATIC SEAL TESTS

Preliminary Leakage Tests

A preliminary feasibility test was performed using a simple test setup and three common engineering materials. The test samples consisted of 1/2 by 2 inch long rods of ordinary drill rod stock and 304 stainless steel and a 3/8 inch diameter high-speed tool steel. The ends of these rods were surface ground to a number 16 rms finish and one of each subsequently hand polished to a burnished finish. These finishes were obtained using normal metallographic polishing practices; however, they were not checked for flatness or measured surface finish. The polished surfaces were scrubbed with MEK (methyl ethyl ketone) and the gallium liquid metal alloy applied, using the technique previously described. For all three materials the apparent wettability was excellent. In order to measure the sealing ability quantitatively, a 1/4 inch diameter hole was drilled through the 304

stainless steel rod along its longitudinal axis. One end of the rod was attached to the vacuum line of a helium mass spectrometer leak detector. The other end was coated with the liquid metal. The wetted end of the two solid sample materials was alternately tested by placing them on top of the drilled rod. Figure 1-2 schematically shows the specimen arrangement. With this test it was not possible to provide continuous application of helium, and leakage was determined by intermittently spraying helium from a pressurized cylinder over the joint area. The effective pressure differential across the seal consisted only of the approximately 15 psi pressure produced by the application of vacuum to the inner side of the seal. All tests were conducted at ambient temperatures. The leak detector was calibrated to have a sensitivity of $5 \times 10^{-10}$ cc/sec/division or a minimum detectable leak of $1 \times 10^{-9}$ std cc/sec (helium). Numerous short-term and long-term exposures of the seal were made under vacuum. Using helium probe techniques, the observed leak rate with all single contact static seals was less than $1 \times 10^{-8}$ std cc/sec helium. The background sometimes exceeded a $1 \times 10^{-9}$ std cc/sec leak; therefore, while no deflection was noted, a conservative figure is used for reporting the general results. On two occasions 72-hour continuous exposures were performed between the drill rod and the 304 stainless steel. From these tests no deterioration of the seal properties was observed due to the 15 psi pressure differential. However, it was determined that the seal configuration could only be separated a few times before complete loss of the seal occurred. Consequently, the surfaces were rescrubbed with MEK and rewet with gallium alloy following a few separations of the joint. Similar results were obtained with the 3/8 inch diameter high-speed tool steel sample against 304 stainless steel; that is, any leak was less than $1 \times 10^{-8}$ std cc/sec helium. After 14 days of continuous wetting by the liquid metal, it was found the surfaces would no longer seal. It was noted the mirror-like polished surfaces showed some indication of attack as evidenced by a loss of luster. A light repolishing immediately restored the original surface finish and the effectiveness of the seal. From these tests it was concluded the gallium liquid metal served as a very adequate seal for a 15 psi pressure differential in the liquid state on metallic surfaces. It was likewise concluded the effectiveness of the seal degraded rapidly with the number of seal separations and, while the degree of liquid

metal attack with the substrate material was minimal, the destruction of the surface finish would be intolerable for sealing applications.

High Pressure Tests

In order to perform static high-pressure tests, a special test cell was designed and fabricated. The purpose of this cell was to permit:

1.  A quantitative measurement of leakage using helium mass spectrometer leak detector methods;

2.  The application of various controlled bearing loads to the seal surfaces;

3.  The application of controlled high-pressure helium gas to the seal.

Figure 1-3 shows the test cell assembly as designed and initially utilized in the investigation. The fixture was designed to allow testing of various seat materials by permitting interchange of the samples. While this latter flexibility was a desirable feature, it was found that the seals necessary to permit such flexibility compromised interpretation of the results. The initial problem resulted from permeation leakage of helium through the elastomeric seal between the test cell body and the lower surface of the lip seat sample. As designed, the fixture employed this seal in normal elastic compression. The inconsistency as well as the magnitude of permeation leakage compromised conclusions of the liquid metal seal at leak rates $1 \times 10^{-8}$ std cc/sec. This resulted in modification of the fixture in order to overcome these difficulties. The initial attempt to remedy this situation consisted of placing the O-ring seal into "fluid" compression by eliminating the normal expansion volume of the O-ring groove with a filler ring. While this resulted in a marked improvement of the permeation characteristics, it did not eliminate the problem. The second solution, shown in Figure 1-4, required modification of the sample support area. The elastomeric O-ring seal was removed and replaced with a cylindrical copper shear gasket. With this seal the lipped test specimen was pressed into the test fixture housing, compressing the cylindrical copper

ring gasket at the same time. While satisfactorily sealing some of the samples, it was found a fixed dimension of the gasket and housing were incompatible with variations in the sample material diameters and hardness. Therefore, this solution was abandoned as not being reproducibly leaktight to high helium pressures. The final solution eliminated the problem but no longer permitted testing of similar materials for both seal surfaces. This solution consisted of making the upper end of the test support fixture the lower sealing surface upon which the flat specimen was placed. Thus, the only possible leak to the leak detector was that of the liquid metal coated surface. To accomplish this, the upper end of the support was ground flat and subsequently polished using metallographic techniques. All results reported with 4340 steel are with the test fixture in this configuration.

The test materials used in this phase of the investigation consisted of common valve seat materials. While it was recognized that compatibility between the liquid metals and these materials might present a problem, it was decided evaluation of the severity could only be made by experiment. Table 1-3 summarizes the materials tested. Surface finishes on these samples were initially ground and lapped flat to within a few microinches over 90 percent of their surface area. Subsequent repolishing tended to increase curvature at the outer edges, although measurement with optical flats after each repolish indicated flatness was retained for a majority of the samples to less than one fringe.

Results

A number of the specimens were checked with helium probe techniques under no mechanical load. These tests were comparable to those performed in the "preliminary leakage tests." Table 1-4 gives the material couples which were wetted with the gallium alloy and helium leak checked.

As there were several samples of each material, multiple tests in each category were actually performed. With almost all the tests, the seals showed no indicated leakage when probed with helium. The leak detector background was in all cases between $1 \times 10^{-9}$ and $1 \times 10^{-8}$ std cc/sec

(helium). A few samples would not seal under the no-load condition and were eliminated from further use.

Typical results obtained with the O-ring beneath a lipped specimen are given in tabulated form, Tables 1-5 and 1-6. The test results of Tables 1-5 and 1-6 were obtained with gallium-indium-tin wetted 440C versus 440C samples under 55-psig helium pressure. Table 1-7 shows the results of a similar test of only the O ring using a solid flat specimen to seal the fixture.

High-pressure helium tests were performed both with copper gasketed lipped specimens and the 4340 support fixture surface. The maximum pressure used in any of these tests was 2250 psig (the limit of the bottle gas pressure). Figure 1-8 summarizes the results of the high pressure tests. It was observed the seals gave no indication of leakage higher than the background of the leak detector, until either a reduction of the applied load or an increase in the helium pressure resulted in a sudden catastrophic breakdown of the seal. Examination of the seals following such breakdown showed the liquid metal to have been forced off the sealing surfaces into the center section of the solid specimen. Figure 1-5 plots the applied maximum pressure without breakdown versus a normalization factor. All tests, except as noted, were performed with the liquid gallium alloy as the sealant. The seal area for the lipped specimens was $0.0192$ in.$^2$ and for the 4340 test fixture surface was $0.185$ in.$^2$.

The bearing load was applied in an Instron load frame where mechanical loading was measured with a load cell. With no internal pressure the indicated load was a direct measure of the total bearing load. Minor error due to outer O-ring friction was introduced. At higher pressures the indicated load was the sum of the initial mechanical load plus the forces of the internal gas pressure. The internal cross sectional area of the pressure cell was about $0.4$ in$^2$. With increased internal pressure the frictional losses due to the O-ring as well as hysteresis were nonlinear so as to make the observed load only approximate. Since the mechanical load applied on the wetted surfaces was transmitted

through the pressure cell to the specimen support, the result of
applying internal pressure was, in effect, to reduce the applied mechan-
ical load. Figure 1-5 is based only on the initial applied mechanical
load (P) where A is the bearing area and L is the radius of the seal.
Tables 1-8 and 1-9 tabulate two tests which withstood 2250 psig with
no indicated leak. It should be noted the test of 4340 versus HSS of
Table 1-9 was kept under 500 psi helium pressure overnight without loss
of the seal.

## SPECIAL PROBLEMS DISCUSSION

While a large number of high-pressure seals were observed, several
important aspects relating to the use of liquid metals for both dynamic
and static seals were noted and will be discussed.

Compatibility Problems - Microscopic examination of sample surfaces which
had been cleaned after being wetted and contacted showed evidence of a
solid or semi-solid material buildup. This observation was noted with
high-speed steel, 440C, tungsten carbide, and beryllium copper. The
buildup was not uniform and appeared greatest on the bearing areas. The
buildup could be easily discerned by visual observation of the lip
impression on the flat specimen samples. For this reason, between each
re-use of a given sample, repolishing of the surface was necessary.
Initially, it was thought buildup might be associated with oxide
formation and subsequently a series of weight measurements of wetted
samples was performed. In addition to the weight measurements, photo-
micrographs of specimen surfaces before and following several days wetting
by the gallium alloy were made. Also, a small portion of the solid
material was taken from the surface of a high-speed steel sample and an
X-ray diffraction pattern obtained. The results of all three observations
confirm that the buildup of a solid or semi-solid film on the surface is
the result of interaction between the liquid metal and the substrate
material. The weight measurements did not show any change in sample weight
which would be expected should appreciable oxidation occur. Furthermore,
the photomicrographs of the materials used in the leak-testing experiments
clearly showed evidence of microscopic attack. The X-ray diffraction
pattern of the surface material supports this same observation. The

diffraction pattern appears to be characteristic of a metal-type structure rather than an oxide. Systematic review of previously identified structures relating to any of the possible binary metal compounds or metallic oxides which might have been formed failed to provide an identification.

The pattern and interplanar spacing (D values) are reproduced as Figure 1-6 and Table 1-10. The photomicrographs, Figures 1-7, 1-8, and 1-9, show the results of wetting the test materials with the gallium liquid metal alloy. The marked difference in the rate of attack between a heat treated and untreated sample as shown in Figure 1-7 is probably a result of the surface energy condition, as the composition is identical. While none of the samples shown in the photomicrographs were stressed during the wetting cycle, the previously noted observation of material buildup on the bearing surface would seem to relate to a higher stress condition accelerating the reaction. Shown in Figure 1-10 are photomicrographs of tantalum and porous tungsten before and after wetting. The dominant structure of the tantalum is a result of polishing. Retention of the liquid metal in the recessed areas of both materials after surface removal can be seen.

Wettability - As previously noted, wettability or the apparent achievement of wettability can be enhanced by the application of burnishing, ultrasonic, chemical, or thermal vacuum techniques to produce clean surfaces of the substrate materials. While no special problems were encountered in applying the liquid metals to the materials studied here, it must be recognized that liquid metal attack, although slight, may play a dominant role in the apparent ease with which the large number of materials are wet by both liquid metal systems.

Oxidation of Liquid Metals - While the formation of oxides or complex oxide systems by both liquid metal systems may be advantageous for certain wettability considerations, the presence of an oxide scum on the surface of a thin coating would not appear desirable. Purification of the liquid metal systems to remove such contaminants and coating of the parts to be wetted in inert gas facilities could be easily implemented should a problem area of this nature be identified.

## DYNAMIC SEAL TEST

The first phase of an investigation of the wet seal concept included development of a zero leak seal for static applications by using liquid metal coatings between metal sealing surfaces. Zero leakage is defined to be a leakage of less than $10^{-8}$ atm cc/sec helium. Helium was successfully sealed, at pressures to 2250 psig.

The second phase of this development includes an evaluation of the wet seal when used as a seal in dynamic applications such as a poppet valve seat or a sliding-type closure. Preliminary tests were performed in which a cap rotated against the face of a tube simulating a dynamic sliding type seal. The faces of the cap and tube were lapped together and then wetted with a gallium eutectic and one end of the tube was attached to the outlet hose of a helium mass spectrometer as shown in Figure 1-11. A helium probe was used around the sealed joint to provide a leak media. The simulated valve cap was rotated by hand through random, jerky, and continuous turns. Approximately 50 cycles were tried and no indication of a leak was found.

The base metal used for the cap and tube consisted of tungsten, and after several turning motions, periodic sticking was noticed, although not consistently. After examination of the surfaces, it was concluded that high frictional forces (galling) were developing due to poor lubricity of the reacting gallium.

## CONCLUSIONS

1. It can be concluded that surface finishes for sealing surfaces are a very important condition relating to the ability of liquid metals to produce essentially zero leak seals at both high and low pressures. If nominal state-of-the-art finishes of less than one microinch are utilized and can be maintained, both theory and the static test experimental results confirm that pressures in excess of 2,000 pounds per square inch can be sustained in a leak-free condition.

2.  For both static or dynamic seals, compatibilities between the liquid metal and the sealing surface must be exceptionally good in order that long term sealing ability can be maintained.  As a result of the observations obtained here, tantalum, tungsten, or their alloys would appear the most promising seat materials.

3.  The limited observations to date would indicate seal separation, such as required by poppet action, is detrimental to the seal effectiveness. It is believed that may be overcome through the use of porous media or other reservoir techniques to provide replenishment to the sealing services.  A dynamic valve which does not utilize a poppet-type action would appear to be the next most logical step.  Such a valve using rotational motion, where the majority of the sealing area remains in contact, should not suffer loss of sealing properties in the liquid metal film.

4.  Long term materials compatibility, possible enhancement of diffusion bonding, and long term stability of the seal against pressure, must be evaluated.

## RECOMMENDATIONS

1.  Continue investigation on materials compatibility with liquid metals to advance the wet seal concept to practical applications for static and dynamic seals.

2.  After successful completion of (1) above, manufacture and test a shut-off valve utilizing the wet seal concept.

3.  Investigate the applicability of the reservoir techniques to poppet-like valve closures.

REFERENCES

1. T. P. Goodman, ed., Design Criteria for Zero-Leakage Connectors for Launch Vehicles, Advanced Tech Laboratories, Vol 2, Contr. NAS8-4012, 15 March 1963.

2. H. Udin, E. Funk and J. Wulff, Welding for Engineers, J. Wiley and Sons, New York (1954).

3. W. Rose, "Analytical Study of the Behavior of Fluids in Porous Solid Media," 2nd Quarterly Progress Report, University of Illinois AD 233830, March 1960.

4. D. Buckley and R. L. Johnson, "Gallium Rich Films as Boundary Lubricants in Air and Vacuum to $10^{-9}$ mm Hq," prepared for ASLE-ASME Lubrication Conference, Pittsburgh, Pennsylvania.

5. ALCOA-Chemicals Division, "Gallium and Gallium Compounds," data sheet 13-11692, Aluminum Company of America-Chemicals Division, Pittsburgh 19, Pennsylvania.

6. ALCOA-Chemicals Division, "Gallium as a Sealant for Laboratory Apparatus," Aluminum Company of America-Chemicals Division, Pittsburgh 19, Pennsylvania, March 1960.

7. United Mineral and Chemical Corporation-Metals Department, "Eutectic Alloys of Gallium Metals Fluid at Room Temperature," United Mineral and Chemical Corporation, 16 Hudson Street, New York 13, New York.

8. J. T. Boag, "Mercury Alloy Freezes at -74F," in Materials in Design Engineering, October 1963.

9. N. Irving Sax, Dangerous Properties of Industrial Materials, Reinhold Publishing Corporation, New York (1957).

10. C. Willhelm, "Preventing Corrosion by Liquid Metals," in Materials in Design Engineering, November 1963.

11. W. D. Wilkinson, "A Compendium of Published Data on Gallium Alloys," ANL Report 4109, February 1948.

12. M. Hansen, Constitution of Binary Alloys, Second Edition, McGraw-Hill Book Company (1958).

13. V. P. Gladyshev, "The Solubility of Metals in Mercury," Fiz. Metal, Metallored 9, No. 6, 853-860 (1960) translated by V. Alford.

14. W. Rostoker, J. McCaughey, and H. Markus, Embrittlement by Liquid Metals, Reinhold Publishing Corporation, New York, (1960).

15. C. P. Bacha, "Supplementary Report - Design, Development, and Testing of Advanced Pneumatic Solenoid Valve (Single Passage) Part No. 4683-59302," AFBMD-TR-60-203, September 1960.

Table 1-1.  Temperature $^\circ$C for Good Corrosion Resistance*

| Solid Metal | Gallium | Mercury |
|-------------|---------|---------|
| Graphite | 800 | 300 |
| Beryllium | --- | 300 |
| Silicon | --- | 600 |
| Zirconium | 100 | 100 |
| Columbium | 400 | 600 |
| Iron | 300P | 600 |
| Molybdenum | 400 | 600 |
| Chromium | 600P | 600 |
| Nickel | 600P | 100 |
| Vanadium | --- | 600 |
| Titanium | 400 | 300L |
| Platinum | 100 | 100 |
| Tungsten | 800 | 600 |
| Tantalum | 400 | 600 |
| Cobalt | --- | 600 |

*   Unlettered temperature-corrosion less than 1 mil per
    year, L - 1-10 mpy, P $>$ 10 mpy

Table 1-2.  Pertinent Properties of Liquid Metal Systems

| Liquid Metal System: | Ga-In-Sn (Ref. 5) | Hg-In-Tl (Ref. 8) |
|---|---|---|
| Melting Point: | 50°F | -74°F |
| Surface Tension (Rm. Temp.): | 500+ dynes/cm | 532 dynes/cm |

| Material | Temperature (Degrees C) | Vapor Pressure (Ref. 10) (microns) | Evaporation Rate $gm/cm^2$-sec |
|---|---|---|---|
| Ga | 775 | $10^{-2}$ | $1.52 \times 10^{-7}$ |
| | 842 | $10^{-1}$ | $1.46 \times 10^{-7}$ |
| | 937 | 1 | $1.40 \times 10^{-6}$ |
| In | 670 | $10^{-2}$ | $2.04 \times 10^{-7}$ |
| | 747 | $10^{-1}$ | $1.96 \times 10^{-6}$ |
| | 837 | 1 | $1.88 \times 10^{-5}$ |
| Sn | 882 | $10^{-2}$ | $1.87 \times 10^{-7}$ |
| | 977 | $10^{-1}$ | $1.80 \times 10^{-6}$ |
| | 1092 | 1 | $1.72 \times 10^{-5}$ |
| Hg | -28 | $10^{-2}$ | $5.28 \times 10^{-7}$ |
| | -10 | $10^{-1}$ | $5.08 \times 10^{-6}$ |
| | 16 | 1 | $4.86 \times 10^{-5}$ |
| Tl | 412 | $10^{-2}$ | $3.19 \times 10^{-7}$ |
| | 468 | $10^{-1}$ | $3.06 \times 10^{-6}$ |
| | 535 | --- | $2.93 \times 10^{-5}$ |

Table 1-3.    Materials Tested--High Pressure Test

(BC) Beryllium Copper (Berylco 25) QQ-C-530.  Aged three hrs at 600°F

(440C) 440C Stainless Steel QQ-S-763.  Heat Treated R/C 5560 MIL-H-6875

(HSS) AISI T1 High Speed Steel Heat Treated R/C 63-66  MIL-H-6875

(4340) 4340 Steel Condition C4 MIL-S-5000 Heat Treated R/C 48-52 MIL-H-6875

Table 1-4.    Wetted material couples showing no leakage with helium probe techniques.

| | | |
|---|---|---|
| BC | versus | BC |
| 440C | " | 440C |
| HSS | " | HSS |
| WC | " | HSS |
| WC | " | BC |
| WC | " | WC |

## Table 1-5

TEST 440C   SN1   O-RING   E 515-8
Background $3 \times 10^{-9}$ std cc/sec
(Ga-In-Sn)
Seal Bearing Area = 0.0192 in$^2$

| TIME | MEASURED COMPRESSIVE LOAD LBS. | HELIUM PRESSURE psig | LEAK RATE Std cc/sec |
|---|---|---|---|
| 1025 | 700 | 0 | $3.0 \times 10^{-9}$ |
| 1027 | .700 | 55 | $3.0 \times 10^{-9}$ |
| 1029 | 600 | " | rising |
| 1030 | 900 | " | $1.1 \times 10^{-8}$ |
| 1035 | 1000 | " | 1.5 x " |
| 1036 | 900 | " | 1.7 x " |
| 1037 | 800 | " | 1.95 x " |
| 1038 | 700 | " | 2.3 x " |
| 1039 | 600 | " | 2.55 x " |
| 1040 | 500 | " | 2.95 x " |
| 1041 | 400 | " | 3.2 x " |
| 1042 | 300 | " | 3.55 x " |
| 1043 | 200 | " | 3.95 x " |
| 1044 | 100 | " | 4.1 x " |
| 1045 | 200 | " | 4.25 x " |
| 1046 | 300 | " | 4.35 x " |
| 1047 | 400 | " | 4.45 x " |
| 1048 | 600 | " | 4.5 x " |
| 1049 | 800 | " | 4.5 x " |
| 1050 | 1000 | " | 4.5 x " |
| 1051 | 1000 | 0 | 4.75 x " |
| 1052 | 1000 | 0 | 4.9 x " |

<u>Table 1-6</u>

TEST 440C   SN1 (WET Ga-In-Sn) O-RING E 515-8

Background $2.5 \times 10^{-9}$ std cc/sec

Seal Bearing Area = 0.0192 in$^2$

| TIME | MEASURED COMPRESSIVE LOAD LBS. | HELIUM PRESSURE psig | LEAK RATE Std cc/sec |
|------|------|------|------|
| 1705 | 1000 | 0 | $2.5 \times 10^{-9}$ |
| 1706 | 1000 | 55 | 2.5 x " |
| 1712 | 1000 | " | 1.5 x " |
| 1718 | .900 | " | 1.5 x " |
| 1723 | 800 | " | 1.5 x " |
| 1728 | 700 | " | 1.5 x " |
| 1730 | 600 | " | $2.4 \times 10^{-8}$ |
| 1731 | 650 | " | 1.55 x " |
| 1732 | 700 | " | $4.5 \times 10^{-9}$ |
| 1733 | 650 | " | 9 x " |
| 1734 | 600 | " | $2.45 \times 10^{-8}$ |
| 1735 | 550 | " | 4.5 x " |
| 1736 | 500 | " | $1.8 \times 10^{-7}$ |
| 1737 | 475 | " | 2.25 x " |
| 1738 | 450 | " | 3.5 x " |
| 1739 | 425 | " | 4.4 x " |
| | 400 | " | 7.0 x " |
| 1740 | 375 | " | 9.75 x " |
| | 350 | " | $1.27 \times 10^{-6}$ |
| 1741 | 325 | " | 1.95 x " |
| | 300 | " | 2.9 x " |
| 1742 | 275 | " | 4.0 x " |
| | 250 | " | 6.25 x " |
| 1743 | 225 | " | 9.7 x " |
| | 200 | " | $1.7 \times 10^{-5}$ |
| 1744 | 175 | " | 2.9 x " |
| | 150 | " | 5 x " |
| | 200 | " | 3.35 x " |
| | 300 | " | 1.15 x " |
| | 400 | " | $3.75 \times 10^{-6}$ |

Table 1-6, (Con'd)

TEST 440C    SN1 (WET Ga-In-Sn) O-RING E 515-8
Background $2.5 \times 10^{-9}$ std cc/sec

| TIME | MEASURED COMPRESSIVE LOAD LBS. | HELIUM PRESSURE psig | LEAK RATE Std cc/sec |
|------|--------------------------------|----------------------|----------------------|
| 1745 | 500 | 55 | $1.41 \times 10^{-6}$ |
|      | 600 | " | $5.5 \times 10^{-7}$ |
|      | 700 | " | $2.0 \times$ " |
| 1746 | 800 | " | $9.0 \times 10^{-8}$ |
| 1747 | 900 | " | $5.75 \times$ " |
| 1749 | 1000 | " | $2.5 \times$ " |
| 1750 | 1100 | " | $1.55 \times$ " |
|      | 1300 | " | $1.5 \times$ " |
|      | 1400 | " | $1.5 \times$ " |
| 1751 | 1500 | " | $1.15 \times$ " |
| 1753 | 1500 | " | $1.0 \times$ " |
|      | 1400 | " | $1.0 \times$ " |
|      | 1300 | " | $1.0 \times$ " |
|      | 1200 | " | $1.0 \times$ " |
|      | 1100 | " | $1.2 \times$ " |
| 1754 | 1000 | " | $1.75 \times$ " |
|      | 900 | " | $2.95 \times$ " |
|      | 800 | " | $9.0 \times$ " |
| 1755 | 700 | " | $3.1 \times 10^{-7}$ |
|      | 600 | " | $1.0 \times$ " |
|      | 500 | " | $3.1 \times 10^{-6}$ |
|      | 400 | " | $9.0 \times$ " |
| 1756 | 300 | " | $2.85 \times 10^{-5}$ |

## Table 1-7
### TEST O-RING COMPOUND E 515-8
Background $1 \times 10^{-9}$ std cc/sec

| TIME | MEASURED COMPRESSIVE LOAD LBS. | HELIUM PRESSURE psig | LEAK RATE Std cc/sec |
|------|------|------|------|
| 1412 | 1000 | 0 | 0 |
| 1414 | " | 5 | $1.0 \times 10^{-9}$ |
| 1415 | " | 10 | " |
| 1416 | " | 20 | " |
| 1417 | " | 30 | " |
| 1418 | " | 40 | " |
| 1433 | " | 55 | " |
| 1448 | 900 | " | " |
| 1503 | 800 | " | " |
| 1518 | 700 | " | " |
| 1533 | 600 | " | $1.0 \times$ " |
| 1548 | 500 | " | $3.0 \times$ " |
| 1603 | 400 | " | $6.5 \times$ " |
| 1618 | 300 | " | $1.2 \times 10^{-8}$ |
| 1633 | 200 | " | $2.3 \times$ " |
| 1634 | 1000 | " | $2.0 \times 10^{-9}$ |

## Table 1-8

TEST 4340 vs. BC  SN6  (Hg-In-Tl)

Background $1.3 \times 10^{-8}$ std cc/sec

Seal Bearing Area $= 0.185$ in.$^2$

| Time | Measured Compressive Load Lbs. | Helium Pressure psig | Leak Rate std cc/sec |
|---|---|---|---|
| 1109 | 500 | 0 | $1.25 \times 10^{-8}$ |
| 1110 | 500 | 0 | 1.20 x " |
| 1112 | 500 | 0 | 1.05 x " |
| 1114 | 540 | 500 | 1.0 x " |
| 1115 | 560 | 700 | 1.0 x " |
| 1117 | 595 | 1000 | 1.0 x " |
| 1120 | 595 | 1000 | 1.2 x " |
| 1122 | 640 | 1300 | 1.2 x " |
| 1124 | 675 | 1500 | 1.2 x " |
| 1126 | 805 | 1900 | 1.1 x " |
| 1128 | 940 | 2250 | 1.0 x " |
| 1135 | 945 | 2250 | $9.0 \times 10^{-9}$ |
| 1145 | 930 | 2250 | 9.0 x " |
| 1148 | 930 | 2250 | 9.5 x " |
| 1150 | 595 | 1400 | 9.5 x " |
| 1152 | 420 | 1000 | 9.5 x " |
| 1153 | 205 | 500 | 9.5 x " |
| 1157 | 0 | 0 | $1.45 \times 10^{-8}$ |
| 1309 | 500 | 0 | $6.5 \times 10^{-9}$ |
| 1313 | 935 | 2250 | 6.5 x " |

## Table 1-9

Test 4340 vs. HSS SN1 (Ga-In-Sn)

Background 6.5 x $10^{-9}$ std cc/sec

Seal Bearing Area = 0.185 in.$^2$

| Time | Measured Compressive Load Lbs. | Helium Pressure psig | Leak Rate std cc/sec |
|------|--------------------------------|----------------------|----------------------|
| 1712 | 300 | 0 | 6.5 x $10^{-9}$ |
| 1714 | 360 | 500 | 6.5 x " |
| 1722 | 360 | 500 | 6.5 x " |
| 1735 | 360 | 550 | 5.0 x " |
| 0855 | 370 | 700 | 2.0 x " |
| 0908 | 420 | 900 | " |
| 0911 | 440 | 1000 | " |
| 0920 | 440 | 1000 | " |
| 0925 | 640 | 1000 | " |
| 0926 | 645 | 1100 | " |
| 0927 | 655 | 1200 | " |
| 0928 | 670 | 1300 | " |
| 0936 | 950 | 2250 | " |
| 1050 | 950 | 2250 | " |

Table 1-10. Interplanar Spacing of Unidentified Compound

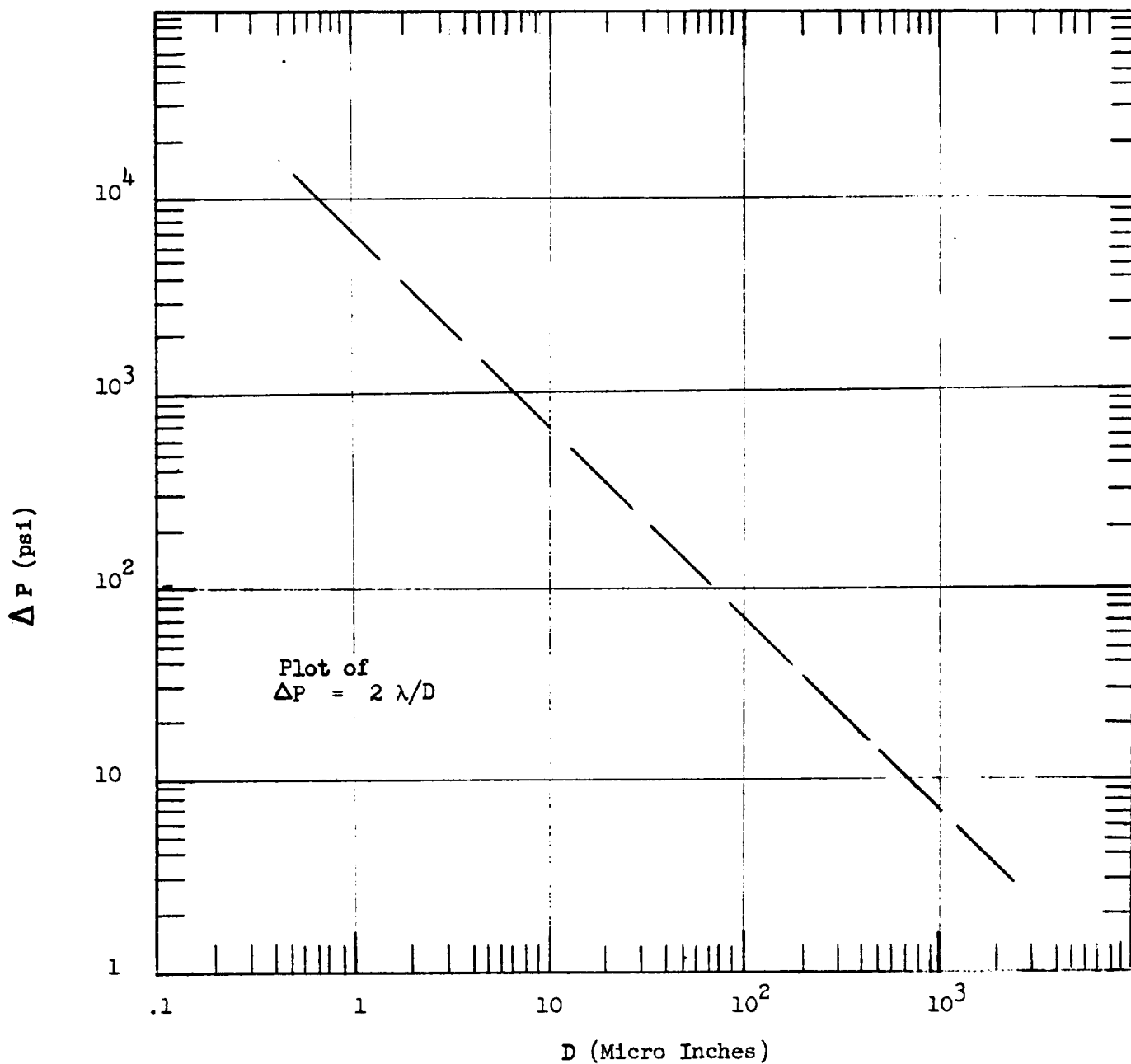| | Intensity | D Value | | | Intensity | D Value |
|---|---|---|---|---|---|---|
| 1. | | 2.8944 | | 16. | S4 | 1.1565 |
| 2. | M | 2.8098 | | 17. | | 1.1410 |
| 3. | | 2.7019 | | 18. | M | 1.0749 |
| 4. | S2 | 2.5311 | | 19. | | 1.0124 |
| 5. | | 2.4472 | | 20. | | .99908 |
| 6. | S1 | 2.0183 | | 21. | | .89579 |
| 7. | S3 | 1.9868 | | 22. | M | .85610 |
| 8. | M | 1.9286 | | 23. | | .78725 |
| 9. | | 1.6431 | | | | |
| 10. | | 1.4507 | | | | |
| 11. | M | 1.4076 | | | | |
| 12. | M | 1.3872 | | | | |
| 13. | | 1.2619 | | | | |
| 14. | | 1.2321 | | | | |
| 15. | | 1.1730 | | | | |

Figure 1-1.  Capillary pressure $\Delta P$ versus spacing D between parallel plates, based on surface tension of $\lambda$ = 500 dynes/cm.

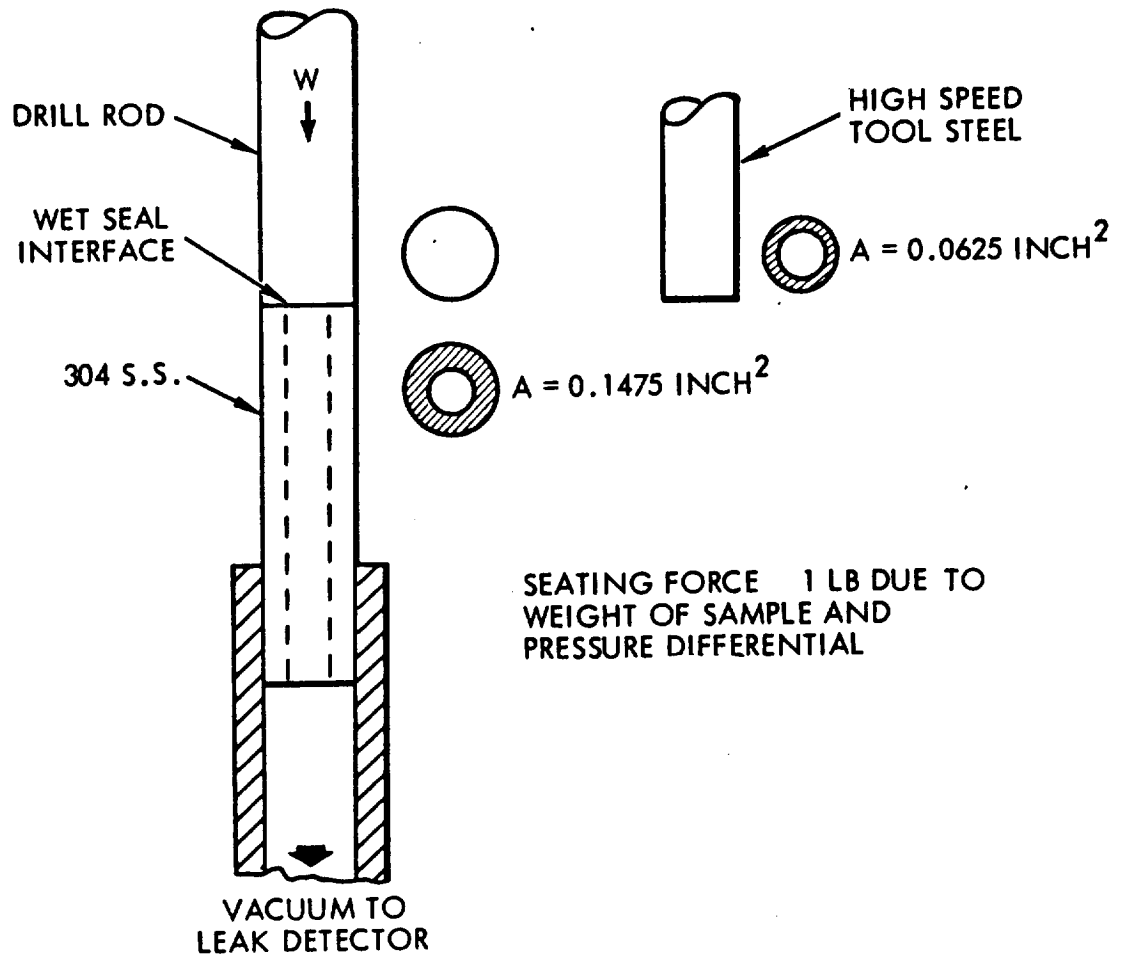Figure 1-2. Preliminary Leak Test Configuration

F(m)

SELF
ALIGNMENT
WASHERS

HIGH
PRESSURE
HELIUM

FLAT
SPECIMEN

LIP
SPECIMEN

WETTED
SURFACES

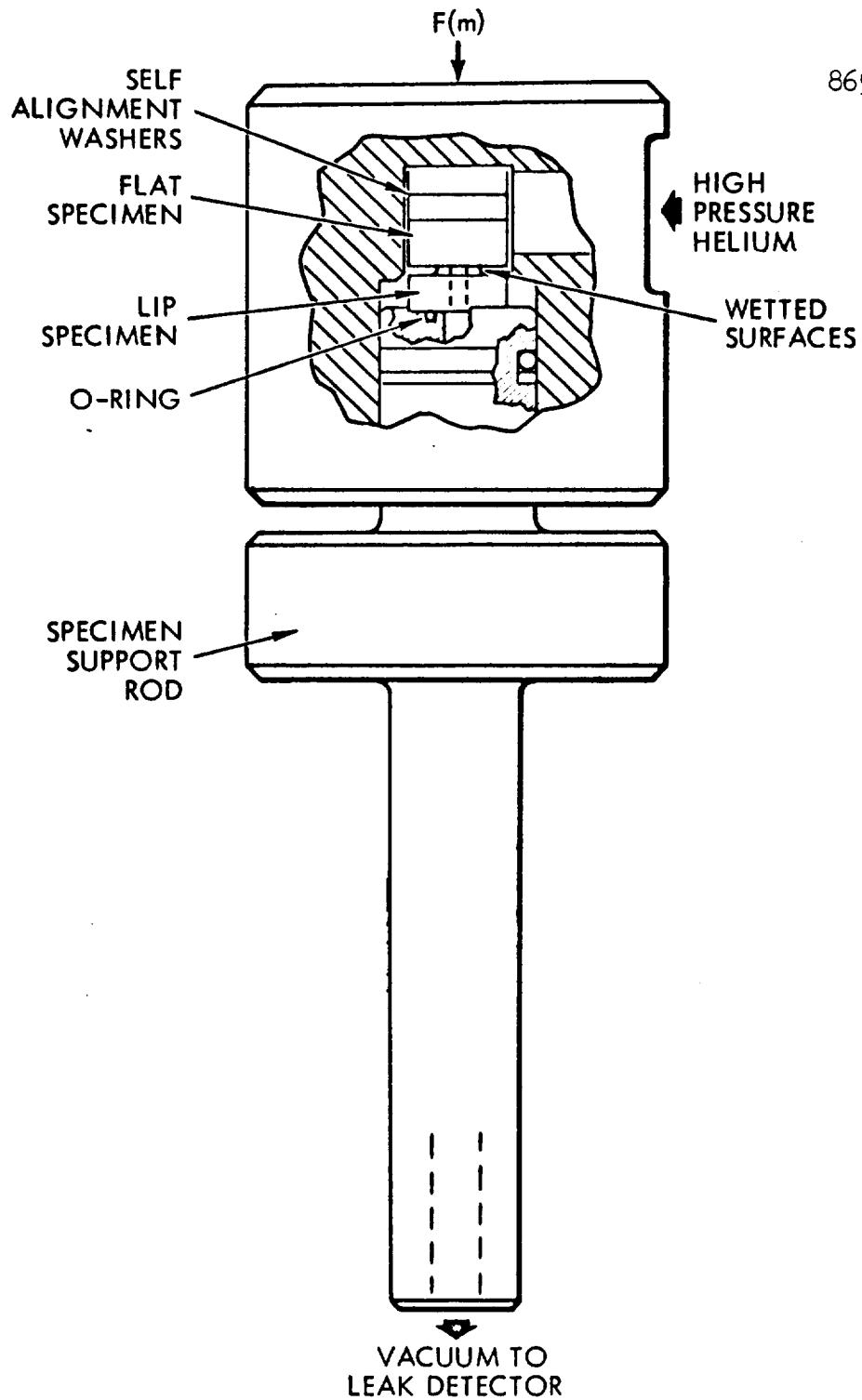O-RING

SPECIMEN
SUPPORT
ROD

VACUUM TO
LEAK DETECTOR

Figure 1-3    High Pressure Cell Assembly
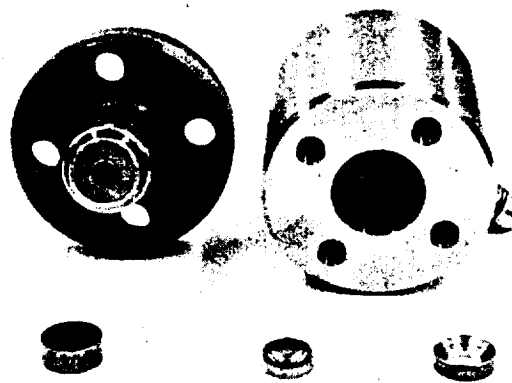
Figure 1-4  Photograph of High Pressure Test Cell
Assembly Showing Lipped Specimen Copper Gasket Mounted,
Flat Specimen and Alignment Washers.
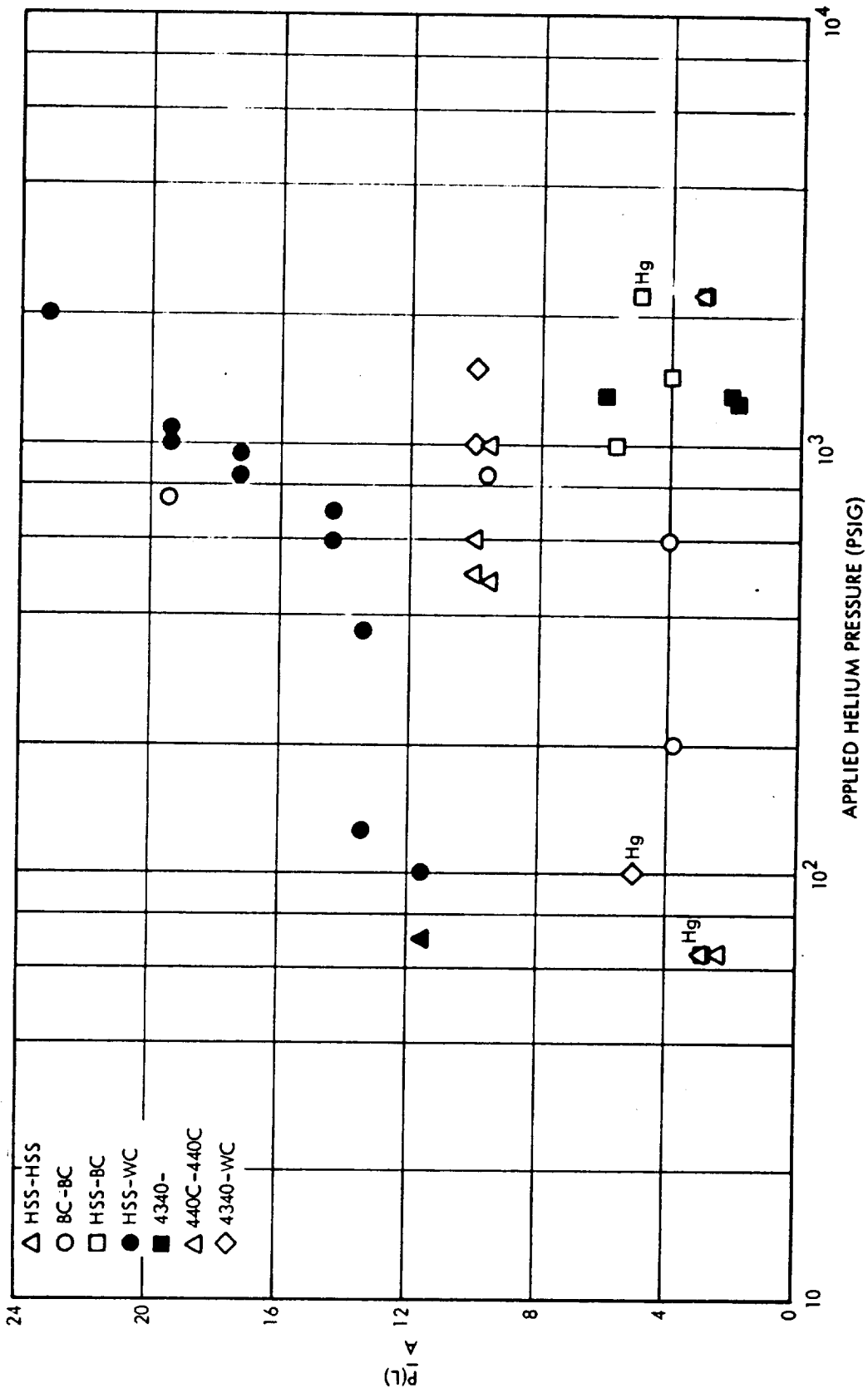
FIGURE 1-5. SUMMARIZATION HIGH PRESSURE TEST
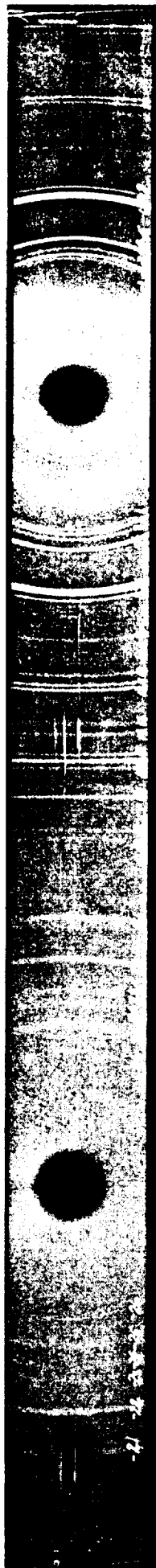
Figure 1-6  Diffraction Pattern of Unknown Compound

a) AISI T1 High Speed Steel X550
Before Wetting
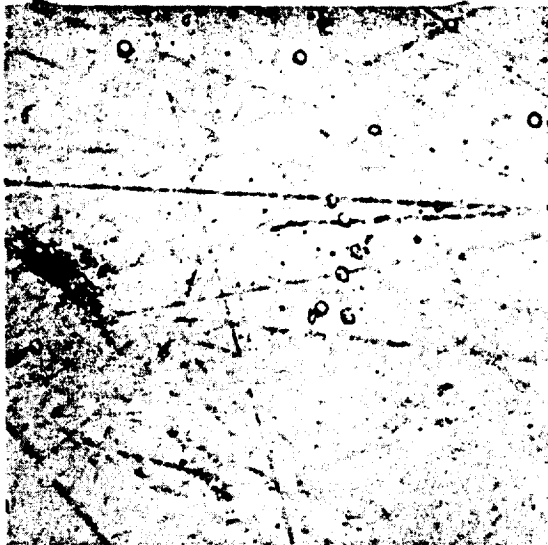


b) Not Heat Treated Sample X550
After 72 Hours in Contact
with Gallium Alloy

c) Heat Treated Sample X550
After 72 Hours in Contact
with Gallium Alloy

Figure 1-7

a) 440C Stainless Steel X550
Before Wetting
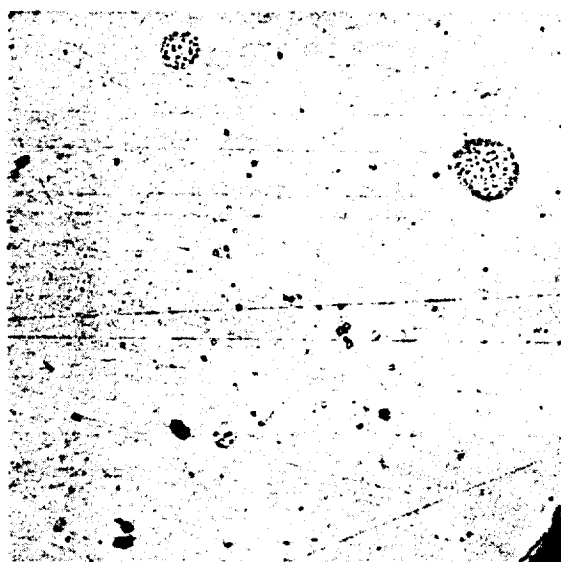
b) After 72 Hours in Contact
with Gallium Alloy  X200

c) After 72 Hours in Contact
with Gallium Alloy  X550

Figure 1-8

a) Beryllium-Copper X550
   Before Wetting
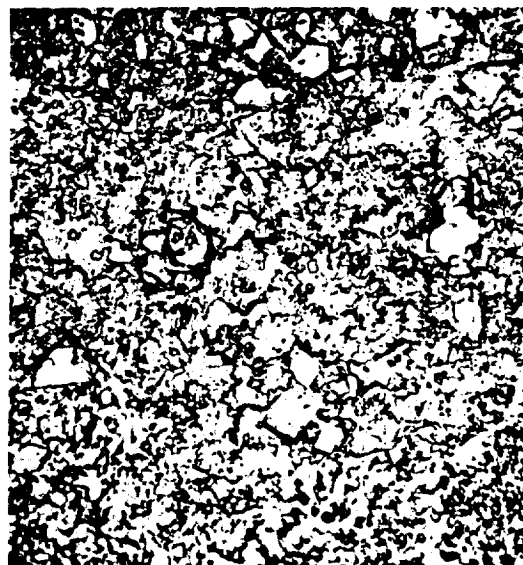
b) Beryllium-Copper X550
   After 72 Hours in Contact
   with Gallium Alloy
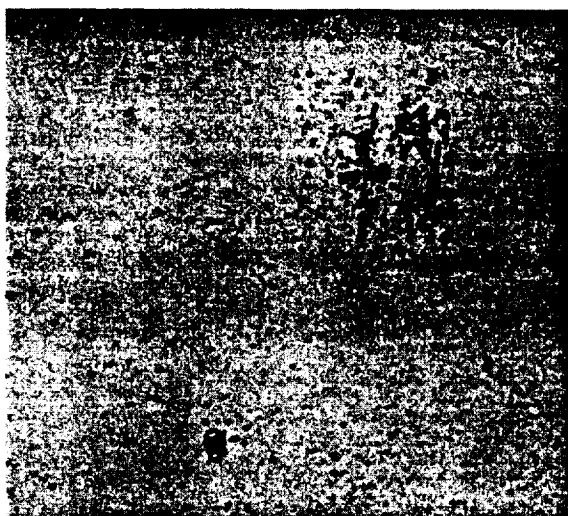
c) Tungsten-Carbide X550
   Before Wetting

d) Tungsten-Carbide X550
   After 72 Hours in Contact
   with Gallium Alloy

Figure 1-9

a) Tantalum X550
   Before Wetting

b) Tantalum X550
   After Wetting

c) Porous Tungsten X550
   Before Wetting

d) Porous Tungsten X550
   After Wetting

Figure 1-10

Figure 1-11   Schematic of Wet Seal Leak Test

## II. ELECTROMAGNETIC ACTUATOR

### INTRODUCTION

This study investigates high-temperature electromagnetic actuators frequently used to control the operation of valves used on spacecraft rocket propulsion engines. Also included in this study is the development of a lightweight high-temperat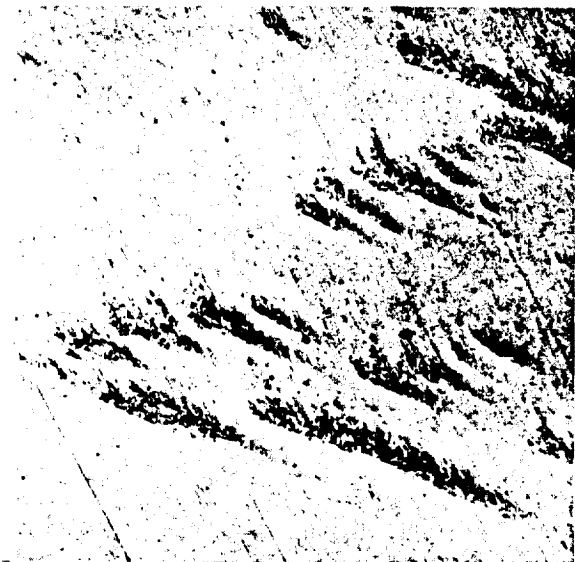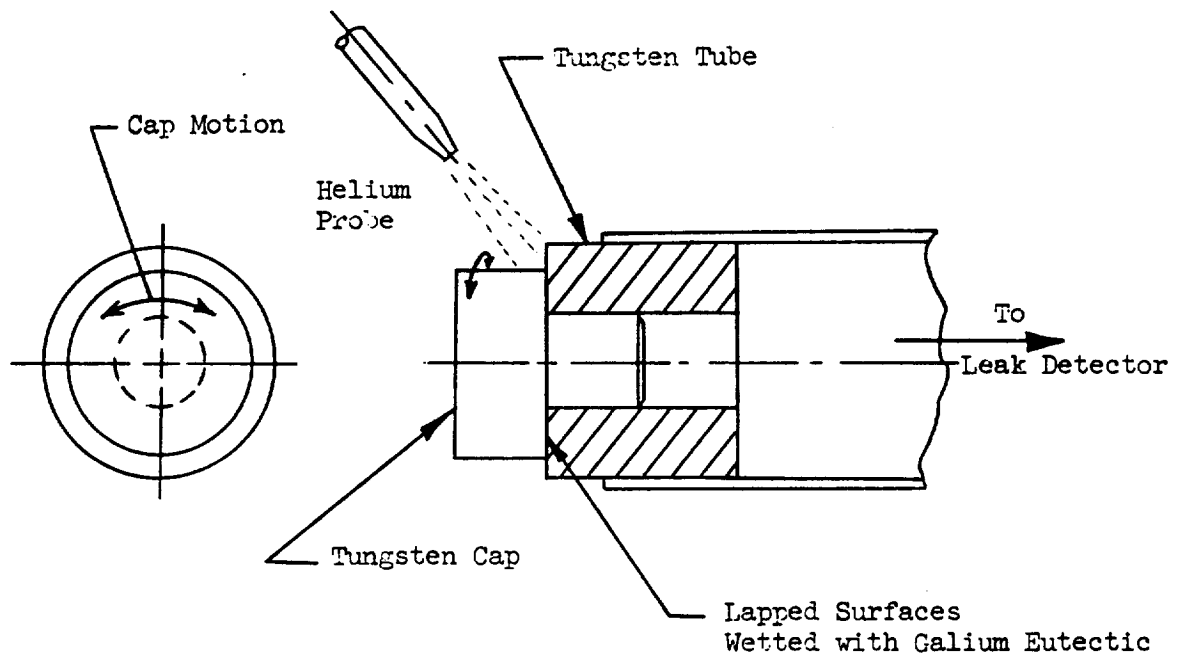ure solenoid. STL Report No. 8651-6016-RU000, "Advanced Valve Technology for Spacecraft Engines," dated March 1963 has given requirements for valves operating at temperatures $200^\circ$ - $1100^\circ$C ($400^\circ$ - $2000^\circ$F). Compact, efficient, low weight electromagnetic actuators for high-temperature valves are considered as a future requirement for spacecraft applications.

Solenoids operating at temperatures up to $250^\circ$C with an operating lifetime exceeding 40,000 hours are possible with available materials. Materials and electromagnetic devices for operating temperatures not exceeding $540^\circ$C are available and a solenoid actuator with a life less than 100 hours at temperatures not exceeding $800^\circ$C is available. The upper temperature limit for presently available efficient magnetic core materials is $1000^\circ$C. A new concept was evolved which shows promise in developing a solenoid operating to $1800^\circ$F.

### SUMMARY

The ultimate performance of high temperature solenoids utilizing available materials and practices is not obtained commercially. This study presents possible performance characteristics and improvements in weight, size, power consumption, efficiency and radiation resistance. The improved performance may be used to define design and development objectives for solenoid actuators. The materials and practices studied here include high temperature magnet wire, insulation, potting, impregnation, effect of temperature and environment on solenoid construction materials, optimum dimensions, weight, force, work, figure of merit for comparisons, magnetizing power, circuits, and selected references.

This study and the references listed can aid in obtaining improved high-temperature solenoid actuator designs and indicate many considerations for continuing development and improvements. A lightweight solenoid capable of operating temperature up to 1800°F was fabricated using beryllium magnet wire.

## HIGH TEMPERATURE MAGNET WIRE AND INSULATION

Recent developments and applications of high temperature organic and inorganic insulating materials provide insulations suitable for an operating temperature of 250°C for as long as 40,000 hours. Copper wire conductors with organic film and fiberglass insulation are not resistant to oxidation for long exposures at temperatures exceeding 180°C. Nickel plating, nickel-clad or aluminum-clad copper wire may be used to obtain resistance to oxidation up to 250°C. Silver, aluminum and anodized aluminum wire are suitable for use with high temperature organic insulations up to 250°C. Above 250°C additional oxidation protection for magnet wire may be required and compatible organic insulations must be used.

## TEMPERATURE AND RADIATION RESISTANCE

The radiation resistance of materials is approximately related to the temperature resistance as follows:

$$\text{Log (Megarads)} = 8.80 - \frac{3200}{°K} \qquad (1)$$

Table 2-1 gives a summary of the temperature and radiation limits for materials used in construction of electromagnetic devices.

Temperature effects such as oxidation, diffusion, or chemical reactions of cladding or insulation, melting point, and grain growth are important in establishing the useful operating range of magnet wire and insulation material combinations (Ref. 1 and 2).

## OXIDATION PROTECTION

Above 200°C insulated copper magnet wire requires protection from oxidation. Four per cent nickel plating is reasonably effective to 400°C and ten per cent nickel plating is more effective. For wires finer than AWG 22 and temperatures exceeding 400°C, nickel clad copper wire is required. Above 500°C the nickel sheath diffuses into the copper base metal increasing the electrical resistance after sustained high temperature operation, although operation at 700°C is not harmful for a short time. The high temperature diffusion of nickel and copper may be avoided by use of a non-diffusing barrier layer such as iron between the copper and nickel sheath. Stainless steel cladding may also be used.

Operation of copper wire at high temperatures causes grain growth which impairs the strength of the wire or may cause surface boundary shifts of the grain boundaries causing failure of the conductor and insulation. Grain growth may be greatly inhibited, with only a slight increase in electrical resistance, by dispersion of a small amount of metallic oxide, aluminum oxide, magnesium oxide, thorium oxide, or beryllium oxide in the base metal. A copper wire dispersion hardened with aluminum oxide has been used at temperatures near its melting point, 1083°C. Commercial clad copper wires are available for operation up to 650°C. Nickel plated anodized aluminum clad copper has a useful life of 2000 hours at 300°C. Nickel or iron-clad copper has a life of about 1500 hours at 400°C.

Aluminum is a good magnet wire material for temperatures above 250°C because of the protective insulating aluminum oxide film which may be formed on its surface. The aluminum oxide film serves to protect the aluminum from oxidation and is used for electrical insulation. Good operating life is obtained with anodized aluminum magnet wire at 500°C. Dispersion hardened anodized aluminum magnet wire is useful at temperatures up to 600°C. Aluminum oxide insulating film is a superior high temperature insulator having an insulation resistance which is at least 100 times greater than available ceramic magnet wire insulations.

The advantage of anodized aluminum combined with the low resistivity of copper or silver may be realized at temperatures above $200^\circ C$ by cladding copper with a silver barrier and an anodized aluminum sheath or anodized aluminum clad silver wire. Pure gold and dispersion-hardened gold are oxidation resistant and may be used for electrical conductors at temperatures approaching the melting point of gold, $1063^\circ C$. The low resistivity and ductility make gold very attractive for magnet wire, but high cost precludes its general use.

Above $1000^\circ C$ to $1500^\circ C$, corrosion resistant alloys such as Inconel X containing nickel are required. These alloys have a high resistivity when compared to copper, silver, gold or aluminum and should be used only when solenoid valve design requirements necessitate solenoid coil operation at temperatures above $1000^\circ C$. Magnetic material performance above $1000^\circ C$ is very inefficient and is a compelling reason for designing electromagnets to operate below $1000^\circ C$.

## OPERATION IN PROTECTIVE ATMOSPHERES AND HIGH VACUUM

In applications where oxidizing or corrosive atmospheres may be excluded, the excellent electrical properties of unclad dispersion-hardened copper and silver may be utilized to temperatures approaching their melting point. The existing ceramic insulating films are not suitable for unclad copper or silver because the thermal expansion coefficients of the available insulation coatings are too low.

High-temperature insulating coatings with expansion coefficients nearly matching silver and copper or possessing sufficient ductility are required. Oxidation and corrosion protective electrical insulating coatings with the necessary mechanical and electrical requirements for temperatures from $180^\circ C$ to $1000^\circ C$ are not available for copper or silver.

The ends of copper, aluminum or silver magnet wire coils must be protected from sublimation at high temperature in space vacuum by a suitable insulating encapsulant or metal sheath. Most brazes or solders used for terminal connections must also be protected.

## RADIOACTIVE ACTIVATION

Table 2-1 shows that high temperature wire, insulation, and magnetic materials are very resistant to space and nuclear radiation; however, if silver is operated in neutron flux densities existing in a reactor pile or neutron shield, it is converted to a radioactive isotope, $Ag^{110}$, with a half-life of 253 days. Cobalt, which is used in magnetic alloys and other high-temperature-resistant alloys, is likewise activated to $Co^{60}$ which has a half-life of 5.25 years. Personnel or sensitive equipment should not be subsequently exposed to silver or cobalt which has been activated by high neutron flux densities.

## HIGH TEMPERATURE IMPREGNATION, ENCAPSULATION, AND POTTING

Insulating impregnation, encapsulation, and/or potting of high temperature magnet wire coils are required to improve shock and vibration resistance, support the coil structure and assembly, improve thermal transfer, reduce sublimation of the magnet wire in high vacuum, prevent oxidation and corrosion, and restrain creep and sag of the coil wire. The materials used must be good electrical insulators which are compatible with the magnet wire and insulation at the highest desired operating temperature.

Coils are usually impregnated by running the magnet wire through a water suspension or slurry of ceramic while the coil is wound. The coil is dried and cured after winding. The coil is cured after drying by heating to a high temperature in vacuum to remove all organic binders and moisture, and to sinter the coil assembly into a solid porous mass. The porous cured impregnating material will absorb moisture if exposed to the atmosphere and should be protected from moisture by a compatible vitreous encapsulating material or hermetic sealing for operation in moist or corrosive atmospheres. Hermetic sealing after vacuum drying is preferable for long life.

A commercially available solenoid coil, with an operating life of less than 100 hours at $800^{\circ}C$, is fabricated by extruding the insulation on the wire before winding the coil with the damp ceramic extrusion

coated wire (green extrusion). The coil is cured at high temperatures to obtain a rigid bonded coil without additional impregnation. The moisture content of the extruded insulation is $14.2 \pm .1\%$. The particle size distribution is selected to obtain maximum cured density and minimum shrinkage.

## EFFECT OF TEMPERATURE ON MAGNETIC MATERIALS

The magnetic properties of materials are affected by temperature. Ferromagnetic materials are magnetic below a critical temperature called the Curie temperature and essentially nonmagnetic above the Curie temperature. The Curie temperature is the upper limit for operation of ferromagnetic materials. Practical applications require a lower operating temperature than the Curie point to obtain useful magnetic induction with useable magnetizing current densities.

The relative saturation magnetization, $I_s/I_o$, of ferromagnetic materials is approximately given by the simplified "Curie-Weiss Law" (Ref. 3).

$$\frac{I_s}{I_o} = \text{Tanh} \left( \frac{I_s/I_o}{T/\Theta} \right) \tag{2}$$

where:

$I_s$ = Saturation magnetization at absolute temperature T

$I_o$ = Saturation magnetization at absolute zero temperature

$T$ = Absolute temperature in same units as $\Theta$

$\Theta$ = Curie temperature (magnetic transition temperature) of the magnetic material

Bloch (Ref. 3) has derived a relation which conforms better to the measured saturation $I_s$ for $T/\Theta \leq 0.4$.

$$\frac{I_s}{I_o} = 1 - AT^{3/2} \tag{3}$$

The "Curie-Weiss Law" and the 3/2 power law give a general behavior
of the magnetic saturation characteristics for all useful ferromagnetic
materials; however, the shape of the magnetization curve and hysteresis
loop cannot be defined analytically. In general, the magnetization curve
of ferromagnetic materials is a variable which is influenced by magnetic,
thermal and mechanical history. Typical experimental magnetization curves
for specific material samples are useful for design purposes and care
must be used to assure the magnetic materials used for construction are
nearly represented by the magnetization curves used for design.

Figure 2-1 illustrates typical relative saturated magnetization curves
for useful magnetic materials. The abrupt magnetic transition of cobalt-
iron alloys at a temperature below the inferred Curie temperature is be-
lieved due to an $\alpha$ to $\gamma$ phase transformation. The $\gamma$ phase is nonmagnetic.

## HIGH VACUUM OPERATION

Available published data on magnetic core materials suitable for high
temperature solenoids indicate the magnetic properties of most magnetic
materials may be improved by high temperature operation in high vacuum
due to gradual sublimation of many entrained impurities such as sulphur,
phosphorous, oxygen, nitrogen, carbon dioxide and carbon monoxide if the
magnetic properties are not otherwise impaired by high temperature
operation. An exception is vacuum purification and annealing of nickel
iron alloys in which the oxygen content is essential for good magnetic
properties (Ref. 4).

## SOLENOID ACTUATORS

## Construction for Minimum System Weight

Electrical solenoid actuators require a power source and power conditioning and control equipment whose specific weight is:

$$\text{sp. wt.} = \frac{\text{Total Power Equipment Weight}}{\text{Kilowatt Power-Output}}$$

which will usually greatly exceed the specific weight of the solenoid; consequently, a solenoid design which will consume minimum power for a given mechanical work or force output will contribute to a near minimum specific weight for the electrical power generating, conditioning, and load equipment. DC solenoids are most efficient and will result in a lower weight than AC solenoids including rectifiers for AC to DC conversion (Ref. 5).

## Optimum Solenoid Dimensions

Direct current solenoids with cylindrical coil and magnet structures are simple and perform well. Alternating current and high speed response DC solenoids require laminated magnetic materials which require a CI or EI shaped magnetic circuit.

Maximum efficiency (Mechanical Power Output/Electrical Power Input) is obtained from a selected magnetic circuit configuration if the dimensions of the magnetic circuit and coil winding space satisfy the following requirements:

$$l_m = l_c \tag{4}$$

$$A_m = A_c = \text{constant} \tag{5}$$

A second independent requirement for maximum performance is:

$$f_m \longrightarrow 1 \tag{6}$$

$$f_c \longrightarrow 1 \tag{7}$$

where:

$l_m$ = mean length of magnetic circuit path

$l_c$ = mean length of current coil turn

$A_m$ = gross cross sectional area of magnetic circuit

$A_c$ = gross cross sectional area of coil winding space

$f_m$ = $\dfrac{\text{Area of useful magnetic material}}{A_m}$

$f_c$ = $\dfrac{\text{Area of useful conductor}}{A_c}$

Optimum dimension for circular cylinder solenoids, illustrated in Figure 2-2 are:

$$D_c = 2.03\,D_p \tag{8}$$

$$D_o = 2.27\,D_p \tag{9}$$

$$h = 1.47\,D_p \tag{10}$$

$$t_1 = \frac{D_p}{4} \tag{11}$$

$$t_x = \frac{D_p^2}{4D_x}\,, \qquad D_p \leq D_x \leq D_o \tag{12}$$

$$t_y = \frac{D_y}{4}\,, \qquad 0 \leq D_y \leq D_p \tag{13}$$

$$l_m = l_c = 4.75\,D_p \tag{14}$$

$$A_m = A_c = \frac{\pi}{4}\,D_p^2 \tag{15}$$

$$V_m = V_c = 3.73\,D_p^3 \tag{16}$$

Where the symbols not defined in Figure 2-2 are:

$A_m$ = gross cross sectional area of magnetic material

$A_c$ = gross cross sectional area of coil space

$V_m$ = gross volume of magnetic material

$V_c$ = gross volume of coil space

$l_m$ = mean length of magnetic circuit

$l_c$ = mean length of coil turn

## Basic Weight

The basic weight of the essential materials of an optimum cylindrical solenoid is obtained from Equation:

$$W = (\sigma m + \sigma c)\ 3.73\ D_p^3 = B_{mc} D_p^3 \qquad (17)$$

Where:

$B_{mc}$ = $(\sigma m + \sigma c)\ 3.73$ (weight coefficient)

$\sigma m$ = average density of the magnetic volume

$\sigma c$ = average density of the coil volume

$D_p$ = plunger diameter

The weight coefficient $B_{mc}$ for typical materials is given in Table 2-2 The weight of additional material used for bearings, mounting, sealing, insulating, shielding, etc. must be added to the basic weight given by Equation (17).

The basic weight of solenoids using several magnetic and electrical conductor materials for a conductor and magnetic material space factor of 1, $f_c = f_m = 1$, are shown in Figure 2-3

## Magnetic Force and Work

A magnetic pressure exists in a magnetic field which may be utilized to obtain a force on the boundaries of rigid magnetic materials. The vector integration of the magnetic pressure on the boundary will produce a net effective total force which is dependent on the shape of the magnetic boundaries. A part of the magnetic pressure on the boundary may produce an available force on the magnetic plunger of a solenoid, for example. All radial components of magnetic pressure on the plunger of a cylindrical

solenoid are balanced out and the axial component of magnetic pressure
will produce a useful force on the plunger.

The magnetic leakage coefficient, $\Upsilon$, is the ratio of total magnetic flux
to the magnetic flux producing a useful plunger force. The approximate
leakage coefficient for a flat face plunger solenoid of optimum dimensions
is given in Figure 2-4. The leakage of magnetic field will reduce the
useful plunger force as the plunger air gap is increased.

The available force on a flat face plunger is:

$$F = \frac{B^2 \pi D_p}{4 \Upsilon^2 \mu} \qquad (18)$$

where B = the magnetic flux density in the magnetic circuit

$\Upsilon$ = magnetic leakage coefficient of plunger and air gap, a
function of $g/D_p$

F = Plunger force

$\mu$ = magnetic permeability of the air gap in a consistent system
of units

$D_p$ = Plunger diameter

The relative available plunger force, $K_F$, as a function of the plunger
gap ratio, $g/D_p$, is given in Figure 2-5.

The available magnetic force is a function of the plunger air gap
although the ferromagnetic circuit may have nearly constant saturated
flux density during the entire stroke due to the variation of magnetic
flux leakage $\gamma$ with $g/D_p$. The total work available from the plunger motion
is the line integral of the available directed force times the differential
stroke. The total work will equal the change of stored magnetic energy
in the volume swept by the plunger motion. The total work is not avail-
able as useful work supplied to an external mechanical load. A loss in
work results from friction, and plunger impact. For most applications
the total available mechanical work is considered to be the product of the

force at the beginning of the stroke times the stroke. The relative work
as a function of the maximum plunger-gap ratio for an optimum solenoid
with a flat face plunger is shown in Figure 2-5. Friction losses must be
subtracted from the work shown in Figure 2-5.

The force and work characteristic for plunger gap ratios $(g/D_p)$
approaching one are not commonly used for low temperature solenoids because
the large electrical power density required for saturation magnetization
would overheat the magnet coil and destroy the insulation. The power
density restriction can be avoided by using high temperature magnetic
materials, magnet wire and electrical insulation. The high power require-
ment is required only during operation of the plunger and may be greatly
reduced by switching the holding current or latching when the plunger is
closed. Figure 2-6 gives the maximum work/solenoid weight for various
magnetic material and coil conductor combinations. The maximum work/weight
ratio is a constant which may be used as a figure of merit to compare
solenoid material combinations. For example these performance character-
istics represent the ultimate which may be obtained from the designated
magnetic materials in a linear motion solenoid of optimum dimensions.
Rotary solenoids of cylindrical construction will give comparable results.

## Magnetizing Current

The maximum force and work obtainable from a solenoid with a nominal
coil magnetizing current and power are obtained when the flux density in
the magnetic circuit is near saturation. The magnetizing current is re-
quired to sustain the required flux density in the magnetic circuit
including the bearing and plunger air gaps. The magnetizing current required
when the plunger is closed is much less than the magnetizing current required
for saturation flux density when the plunger is in the open position. The
large change in required magnetizing current may be obtained with a suitable
power supply circuit.

The magnetizing ampere turns required, NI, is given by

$$NI_{total} = NI_{gap} + NI_{mag.\ mtl.} \tag{19}$$

For a solenoid with dimensions given by Figure 2-2 the magnetizing ampere turn is:

$$NI_{total} = 2.02 \, D_P \left[ \frac{B}{\Upsilon} \left(\frac{g}{D_P}\right) + \left(4.76 \, \frac{g}{D_P}\right) H \right] \tag{20}$$

where:

$\Upsilon$ = plunger gap leakage coefficient, a function of $g/D_p$ given in Figure 2-4

$D_p$ = diameter of plunger in inches

$\frac{g}{D_p}$ = $\frac{\text{plunger gap}}{\text{plunger diameter}}$, plunger gap ratio including an allowance for bearing air gap

$B$ = desired magnetic circuit flux density in gauss

$H$ = magnetizing force in oersteds required to sustain the flux density B in the magnetic material. This is obtained from a manufacturer's representative D. C. magnetization curve for the magnetic core material used in the solenoid.

## Magnetizing Power

After steady magnetic fields are established by application of the magnetizing current, the steady D.C. power must supply the Joule heating, ($I^2R$ losses) in the coil for the required magnetizing current. The required steady magnetizing power, $P_m$ is:

$$P_m = \frac{2.39 \, (NI_t)^2 \rho_c}{f_c \, D_p} \tag{21}$$

where:

$NI_t$ = total ampere turns given by Equation (20)

$\rho_c$ = resistivity of the magnet coil wire in ohm cm (see Fig. 2-7)

$f_c$ = gross space factor of coil winding

The stored energy in the magnetic field is proportional to $D_p^3$; however, Equations (20) and (21) show the power required to sustain the steady magnetic field is proportional to $D_p$. Equation (21) shows the steady magnetizing power is proportional to coil material resistivity and inversely proportional to coil winding space factor; therefore, for minimum power the coil construction should maximize space factor $f_c$ and use a material of minimum resistivity, $\rho_c$, consistent with requirements for temperature, insulation, life, thermal capacity, weight, etc.

Figure 2-8 gives the power requirements for Supermendur with silver and beryllium magnet wire coils.

## Oxidation and Corrosion Protection of High Temperature Solenoid Actuators

Magnetic materials are selected for the desired magnetic properties and may not possess the required corrosion and oxidation resistance at high temperatures. High temperature magnet wire insulation and impregnating materials are porous allowing the ingress and attack of moisture and corrosive materials if they are present in the environment. The protective methods should not impair the proper functioning of the magnetic material, coil and insulation. Magnetic materials operating at high temperature are readily impaired by the reaction with and/or absorption of many materials such as oxygen, nitrogen, hydrocarbons, carbon, silicon, sulphur, nickel, phosphorous, etc. (Ref. 3).

Diffused chromium may improve the magnetic properties of magnetic iron by removing some of the undesired carbon to form chromium carbide. Diffused chromium coatings (Ref. 6) on low-carbon iron, nickel-iron and cobalt-iron allows have a corrosion resistance comparable to 400 series stainless steel. Diffused chromium coating on low-carbon iron is very resistant to hot nitric acid and oxides of nitrogen. The diffused chromium coating has a secure bond and is less porous than plated coatings. The coating should not be used at temperatures greater than $400^\circ$C because chromium diffusion into the bulk of the magnetic material decreases surface protection and may impair the magnetic properties. The magnetic properties of Supermendur are very sensitive to oxidation at $400^\circ$C (Ref. 7, 8 and 9)

and a diffused chromium coating may be insufficient protection in oxidizing atmospheres.

A hermetically-sealed construction with high temperature ceramic metal seals for the electrical connections and a laminated diaphragm or bellows for transmission of mechanical motion provide good protection and prevent the ingress of materials which may impair mechanical motion. The enclosure material may be selected to provide good protection for the intended environment. The magnetic material should be fastened to the enclosure with a material which will prevent diffusion of undesired contaminants into the magnetic material; for example, the magnetic properties of cobalt-iron alloys are impaired by traces of nickel, which is used in many oxidation- and corrosion-resistant alloys.

Vacuum melted and purified materials are recommended for construction of hermetically-sealed solenoids because volatile impurities such as sulphur, phosphorus, etc. sublime at high temperatures, depositing at lower temperature locations within the hermetic enclosure. The transporting and depositing of impurities may impair mechanical and insulation properties. If vacuum melted and purified materials are not used, the components may be thoroughly outgassed by baking out in a high vacuum at temperatures above the highest processing or operating temperature. Caution must be used in selection of baking temperatures for some magnetic materials because the magnetic properties may be irreversibly impaired by high temperatures.

## Material Selection

Material data similar to Figures 2-6, 2-7, 2-8, 2-9, and Tables 2-1 and 2-3 may be used to determine the best materials for an application. The following combinations are typical:

(a) For light weight, lowest cost, and good performance to 400°C, use pure magnetic ingot iron with an anodized aluminum wire coil.

(b) Same as for (a) except for lower power consumption; however, with an increase in weight, use ingot iron with a ceramic insulated nickel clad copper coil.

(c) For lowest power consumption and best performance to 500°C, use high purity cobalt iron alloys with hermetic sealing and a ceramic insulated silver wire coil.

(d) For future applications requiring the best available performance to 1000°C with low weight, use high purity 49 Co, 49 Fe, 2 Va magnetic material with anodized beryllium wire coil in a hermetically sealed cage.

(e) For applications at temperatures from 500°C to 1000°C, improvements are required in the cobalt iron alloys presently used for core materials. Ceramic insulated nickel clad silver wire may be used to 750°C.

Residual Magnetism and External Forces
Due to Planetary Magnetic Field

Solenoid actuators will exert a magnetic torque on the mounting frame when immersed in an external magnetic field such as the Earth's magnetic field. These torques may influence the spacecraft orientation in a planetary magnetic field. The external torque depends on the angle between the external magnetic field and the solenoid axis, solenoid construction, materials, number of cycles of operation, temperature, plunger position, and magnetizing current. The cylindrical construction with constant magnetic material cross-section shown in Figure 2-2 will produce a minimum external magnetic field in the closed position because the outer and inner cylinders and the end discs produce nearly equal and opposing external magnetic moments due to internal magnetization. The low external field is enhanced by careful construction to assure constant magnetic cross-section for all magnetic parts of the solenoid.

The use of the highest quality soft magnetic materials, properly annealed after fabrication, will minimize external fields from the solenoid. This is especially true of fields due to residual magnetism in unenergized solenoids when the magnetic moment of the plunger is not cancelled by the magnetic moment of the outer cylinder. The external magnetic field may be greatly reduced by enclosing all magnetic components within a completely enclosing high permeability magnetic box or shield. Compensating external magnets to balance the external magnetic moments of the solenoid may switch compensation to correspond to the normally open or closed position of the solenoid.

## Transient Mechanical Impulse

If the plunger and the solenoid body are coupled to a common mounting frame, no net impulse external to the frame will exist; however, the center of gravity of the solenoid will shift during plunger motion. A transient impulse may exist during the free travel of the solenoid plunger before it impacts the stop. This transient impulse will produce a slight jerk in the spacecraft, however, returning to its normal position after the plunger motion is completed.

## Solenoid Magnetizing Circuits

High temperature solenoids are capable of operating with high power surges during the plunger motion time without exceeding the operating temperature limit. The ability to withstand high magnetizing power surges during the operating cycle enables the maximum possible force, stroke, and work. The operating temperature limit restricts the available work of solenoids constructed with low temperature materials.

The short impulse, high power demand required of optimum design solenoids may be obtained directly from the power supply; or, in cases where the power supply surge capability is insufficient, an auxiliary impulse-energy storage capacitor or battery may be used. Circuits for supplying the magnetizing current of DC solenoids are shown in Figure 2-10. The method used for short stroke low temperature solenoids with a low useful work/weight ratio is shown in Figure 2-10(A). The power demand for the circuit of Figure 2-10(A) is nearly constant for plunger pull-in and holding positions and is suitable for short stroke solenoids. Figure 2-10(B) may be used for long stroke applications $g/D_p \leq 1$, where the ratio of required pull-in power to holding power is large. $R_s$ is selected to limit the power surge from the power source and to provide the proper holding current. $C_s$ is required to store sufficient energy for solenoid actuation. Figure 2-10(C) may be used for N number of equal resistance solenoid coil sections which are switched from parallel aiding to series aiding by a set of contacts which are actuated by the solenoid plunger closing. The ratio of pull in power to holding power by switching N equal resistance coil sections is $N^2$.

A four times power reduction obtained with two coil sections requires a simple, single pole, double throw, back contact set on the solenoid. Figure 2-10(C) is a combination of the methods used in Figure 2-10(A) and (B); it reduces the power in the current limiting resistor four times and requires less switch contacts than a coil having more than two sections. The circuit of Figure 2-10(E) may be used for excitation of DC solenoids from AC power supplies. The circuit provides impulse energy storage by $C_e$ and optimum pull-in and holding current by proper selection of the AC supply voltage, $E_s$. The current limiting inductance $L_i$ may be included as leakage inductance in the transformer for $E_s$. The curcuit of Figure 2-10(C) provides proper pull-in and holding current without switching solenoid coils or current limiting resistors.

## Recommendations for Future Investigation

### Magnet Wire

1. Investigate the use of pure and dispersion hardened beryllium wire for magnetic coils at temperatures up to $1000^\circ C$.

2. Continue experimental evaluation and development of dispersion hardened copper, silver, and aluminum magnet wire for operation near the wire melting temperature.

3. Investigate wire cladding and diffusion barriers with improved electrical properties and long life for temperatures near the base conductor melting temperature.

### Magnet Wire Insulation

1. Investigate possible magnet wire insulation films suitable for direct application to copper and silver wire for operation at temperatures up to $1000^\circ C$.

2. Investigate magnet wire insulation films which will protect the magnet wire from corrosion in corrosive atmospheres where temperatures reach $1000^\circ C$.

3. Investigate the use of an anodized film electrical insulation on beryllium magnet wire up to $1000^\circ$C.

## Magnet Coil Impregnation and Potting

1. Investigate coil impregnation and potting materials with the following improved properties:

   (a) Compatibility with coil wire and insulation for a wide temperature range up to $1000^\circ$C.

   (b) High insulation resistance up to $1000^\circ$C.

   (c) Greater thermal conductivity.

   (d) Improved thermal shock resistance with coil materials.

   (e) Reduced permeability of corrosive liquids and gases.

   (f) Impregnation or potting with a suitable liquid system which may be cured to a 100% dense solid material suitable for temperatures up to $1000^\circ$C.

## Magnetic Materials

1. Develop cobalt-free magnetic alloys with high temperature properties equal to or better than existing cobalt iron alloys for applications prohibiting long time radioactive activation from neutron exposure.

2. Investigate and develop high flux density magnetic alloys without a non-magnetic phase transition below the inferred Curie temperature of $1200^\circ$C or higher.

3. Develop high flux density soft magnetic alloys which may be assembled by arc welding, brazing, or other fabrication processes at temperatures above $1200^\circ$C without permanently impairing their magnetic properties below $1000^\circ$C.

Solenoid Assemblies

1. Construct solenoid assemblies, utilizing existing design, material, and fabrication methods given in this study to demonstrate performance near the ultimate capabilities shown in this study.

2. Evaluate the external magnetic field produced by solenoids in applications where it may have adverse effects.

3. Demonstrate plunger bearing and lubricant materials which have long life up to $1000^{\circ}C$ and do not impair the desired properties of solenoid contruction materials.

4. Construct and demonstrate performance of a solenoid actuator suitable for operation for long periods in corrosive atmospheres at temperatures above $400^{\circ}C$. This capability may be obtained by installing the solenoid in a high temperature corrosion resistant enclosure utilizing a laminated corrugated diaphragm or bellows for sealing the mechanical motion.

5. Construct and evaluate a solenoid with an anodized beryllium wire coil suitable for continuous operation at $1000^{\circ}C$.

NEW CONCEPT:  LIGHTWEIGHT SOLENOID ACTUATOR

## Introduction

The solenoid actuator study suggests beryllium magnet wire with an
anodized film for insulation will permit construction of solenoids
with approximately one-half the weight of presently designed solenoid
actuators using copper or nickel magnet wire.  Anodized beryllium wire
may operate at temperatures up to and exceeding $600^\circ$C in air and up to
$1000^\circ$C in high vacuum or protective atmospheres.  The use of anodized
beryllium magnet wire has not been exploited, and the experimental use
and evaluation of this wire in the construction of a lightweight
solenoid actuator is progressing as a part of the new concepts evalua-
tion of the Advanced Valve Technology Program.  The work pertaining
to the experimental evaluation of the beryllium wirewound lightweight
solenoid actuator is described in this report.  A patent disclosure
of this concept was submitted to the TRW/STL Patent Office.

## Beryllium Wire Study and Evaluation

Possible sources and properties of economically available beryllium wire
were investigated.  Number 14 A.W.G. square wire (.064 in. square) was
considered attractive for high space factor and ease of winding without
random embedding into the turns of adjacent layers; however, no supplier
considered was originally able to supply square wire with acceptable price
and delivery.  Manufacturing technology for square beryllium wire is not
well established and the manufacture of useful lengths of square wire is
generally considered to be very difficult and expensive.  Number 14 A.W.G.
round wire was selected as a reasonable compromise between manufacturing
cost and fabrication and performance characteristics.  Two types of bery-
llium wire were considered for use:  (1) a commercially pure dispersion-
hardened wire with 1.5 to 2 percent beryllium oxide (BeO) content and (2)
a high-purity, low BeO content wire.  The dispersion-hardened and low BeO
content wire have nearly the same electrical conductivity (Ref. 10).  The
dispersion-hardened wire is expected to have superior mechanical properties
at high temperatures while the high purity wire is expected to have greater

notch resistance and ductility. The cost and delivery of the high-purity
wire were not acceptable; consequently, the dispersion-hardened 1.5 to
2 per cent BeO wire obtained from Brush Beryllium Corporation will be
used for evaluation and construction of the solenoid.

Late in the report period Nuclear Metals, Incorporated, was found to
have developed a manufacturing process for round or square beryllium
wire which is capable of a large amount of elongation in bending
without significant springback or fracture (Ref. 11): 3/8 inch
diameter coils of No. 14 wire may easily be wound by hand at room
temperature. The high elongation beryllium wire is most suited for
magnet wire coil fabrication and should be used if schedule and cost
will permit.

Ductile, square beryllium wire may be obtained from Nuclear Metals
Corporation. The use of ductile square wire will enable winding of
beryllium coils at room temperature with approximately 20% improve-
ment in winding space factor. The winding irregularities caused by
interlayer embedding of multilayer round wire coils are also eliminated.
The interlayer contact between square wire windings is much greater
than obtained with round wire: consequently, the interlayer thermal
resistance is greatly reduced by use of square wire. The reduced
interlayer thermal resistance will permit a proportionate increase
in thermal dissipation density and current density within the coil
winding. The increased current density of square wire coils will
permit the use of smaller coils to obtain a specified magnetizing
ampere turn.

Previous sections of this report have mentioned the conspicuous
qualities of beryllium oxide coated beryllium magnet wire which led
to the interest and experimental work with solenoid actuator coils
of beryllium wire. Data on beryllium metal and other metals used
for electrical conductors are given in Table 2-3. Table 2-3 also
shows corresponding data on two good high-temperature ceramic insulating
materials, pure aluminum oxide and beryllium oxide. Table 2-4 gives a
comparison of copper and beryllium, and Table 2-5 gives a comparison

of alumina and beryllia ceramic insulation.

An investigation of available beryllium anodize coatings suitable for electrical insulation was made; the earlier simple chromic acid anodize process described by Lockheed (Ref. 12) did not have the desired mechanical, protective, and electrical insulation properties.

Atomics International has reported an anodize coating have protective, mechanical, and electrical insulation properties superior to other sources of anodizing considered (Ref. 12, 13, 14, 15). Four different samples of anodized wire were obtained from Brush Beryllium Corporation for evaluation. Room temperature voltage current tests were made on the Brush Beryllium anodize samples.

## Experimental Evaluation of Insulating Film

The voltage-current test results conducted at ambient conditions for the four samples of Brush Beryllium anodized wire are shown in Figure 2-11. This test is a modification of the standard twist test (Ref. 16) for magnet wire insulation in which the wires are held in intimate contact by a tight wrapping of Teflon tape instead of a loose spiral twist of the wires. Twisting is difficult to accomplish with ordinary beryllium wire due to its stiffness and low elongation compared to copper or aluminum wire. The tests were taken with a four inch element contact length between a pair of anodized beryllium wires as shown in Figure 2-12. The current shown in Figure 2-11 corresponds to the current per inch length through the wire insulation to four adjacent wires with the voltage applied between the center wire and the adjacent wires.

Tests of the same samples in moderate vacuum indicated a great improvement in electrical insulation properties, probably due to removal of most of the moisture entrained in the anodize insulating film. The measured leakage current on all samples for all voltages up to 100 volts was less than $6 \times 10^{-10}$ amperes. The small leakage current indicated on the vacuum tube millimicroammeter used was independent of applied voltage on the wire insulation and was probably due to residual leakage current and zero error in the measuring instrument.

The leakage current through the anodized insulation on beryllium wire does not follow Ohm's law ($E = IR$); i.e., the current is not proportional to voltage.

The leakage current in the beryllium anodized test samples follows an exponential law, Equation (22)

$$I = K(E_a - E_b + V)^n \qquad (22)$$

Where:

$I$ = Electric current.

$E_a$ = The electrochemical or contact potential between beryllium base metal and a contact on the outside surface of the anodize.

$E_b$ = A similar but different electrochemical contact potential for wire b.

$V$ = The applied voltage between wire a and wire b.

$K$ = Perveance depending on geometry, temperature, processing, history, humidity, and other factors.

$n$ = An exponent required to fit the observed current voltage relationship.

The exponent $n$ is $3/2$ for the samples tested, corresponding to the exponent obtained for space-charge-limited thermionic diodes and some semiconductor diodes.

The observed current voltage relationships for the anodize coating on the beryllium wire samples tested suggest that the anodize film may be a poorly conducting solid electrolyte or a semiconductor due to the impurities in the beryllium oxide coating. Low moisture content and an anodize process which greatly reduces the impurities such as iron, free beryllium, chromium, nitrogen, etc., may produce an insulating film which approaches the excellent electrical properties of high-purity beryllium oxide insulation.

The observed potentials $E_a$ and $E_b$ are of the order of one volt for the samples tested, with a typical difference of .04 to .06 volts. These potentials do not have an important effect on the leakage currents for applied voltages exceeding one volt.

The leakage current through the anodize films may result in electro-
lytic erosion of the base metal wire in cases where direct current
is applied to the conductor. Electrolytic corrosion for direct
current applications may be minimized by using high-current low-voltage
coils and selecting an anodize film which will have a minimum leakage
current for the range of operating conditions selected. The life
of properly constructed power solenoid actuators may not be affected
by the anodize insulation leakage current in many applications;
however, the life of fine wire sensitive actuators, or relays would be
limited by the anodize insulation leakage current.

## Design and Fabrication of Solenoid Components

All components for a high-temperature solenoid were fabricated. Figure
2-13 illustrates a breakdown of all the components used for the solenoid
assembly. The geometry and design are given in Figure 2-2 of this
report. Covandur alloy was used for the magnetic components (49 Co
49 Fe, 2 Va) because small stock quantities were available. High-purity
aluminum oxide ceramic (99.5% $Al_2O_3$) was used for all bearings and
insulators. The plunger sleeve bearing was made from small sectors
of a cylindrical ring of alumina ceramic to eliminate the dimensional
variation problems which would be caused by the differential in the
temperature coefficient of expansion between Covandur and alumina.
The magnetizing coil was a 32-turn bifilar wound coil of No. 14
A. W. G. anodized commercially pure, round, beryllium wire. A wire
temperature of approximately $600^\circ C$ at the point where the coil
radius is formed will permit maximum strain of the beryllium wire
without damage to the wire (Ref. 17, 18, 19, 20). The protective
quantities of a good beryllium oxide electrical insulation film are
expected to protect the wire from progressive corrosion during the
winding operation. Anodized beryllium has operated with good oxidation
protection for 5 hours at $1200^\circ C$ in oxygen and 1750 hours at $800^\circ C$ in
air containing 1 per cent moisture (Ref. 21, 22, 23).

Construction details of the solenoid actuator are given on the following STL drawings:

| Figure Number | Drawing Number | Description |
|---|---|---|
| 2-14 | X-216474 | Solenoid Housing |
| 2-15 | X-216475 | Solenoid End Plate and Bearing |
| 2-16 | X-216476 | Solenoid Plunger and Insulator |

## Construction of Special Protective and Handling Facilities

A modified dry box with an exhaust fan and filter was used to contain the beryllium coil winding operation as shown in Figure 2-17. A simple hand-driven coil winder with an electrical resistance heater surrounding the wire just before entry on the winding mandrel was tried for heating the wire for winding. The rapid cooling of the wire when first contacting the winding mandrel prevented satisfactory winding with this electrical heater. A winding heater utilizing a flat-shaped gas flame shown in Figure 2-18 produced acceptable winding results when the flame point was placed on the mandrel about 3/16 inch after initial entry of the wire on the mandrel.

The extent of the protective installation required to prevent excessive exposure to beryllium will depend on the particular operation. A completely enclosed glove box may be required for protection involving the handling of fine powders, an open fume hood may be suitable for less hazardous materials, and a high-velocity exhaust orifice and hood mounted at the work position with a flexible hose is used for many machine and fabrication processes. Continuous air sampling and wipe tests must be used to establish the safety of all beryllium operations.

The dry box installation for beryllium wire coil winding shown in Figure 2-17 resulted in personnel exposure levels during coil winding which were not detectable by the most sensitive methods of analyses. The observed beryllium concentrations were:

1.  Air sample near operators head $< 10^{-9}$ grams/cubic meter hour.

2.  Wipe test on coil fixture before scrubbing with water $1.5 \times 10^{-6}$ grams.

3.  Wipe test on coil fixture after scrubbing with water $< 2 \times 10^{-8}$ grams.

4.  Wipe test on dry box interior near workers eye level after operations but before scrubbing with water $9.2 \times 10^{-7}$ grams.

A high-velocity exhaust shroud installed at the coil winding work position may provide adequate protection and should be considered due to its convenience and simplicity. The effectiveness of all beryllium handling  facilities must be established in accord with approved standards (Ref. 10, 24, 25, 26), in general, the simplest arrangement consistent with  safety is best.

The safety from toxic exposure of beryllium in completed electrical assemblies should be considered for all operating conditions which are subject to personnel exposure. Protective provisions for applications of complete electrical units do not appear to be difficult and may be realized by most assemblies which meet the desired functional requirements. For example, the vapor pressure of beryllium is less than $2 \times 10^{-8}$ grams per cubic meter at a temperature of $885^{\circ}C$, and attempts to ignite or cause rapid erosion of the Number 14 beryllium wire used in the coil winding with the propane torch were unsuccessful. The transport and continuous sublimation of beryllium and beryllium compounds on the cold walls of an enclosure which enclose beryllium assemblies operating for long periods of time at high temperatures should be recognized.

Clinical experience during the past 20 years has established the toxic effects of certain forms of beryllium and its compounds. The U. S. Atomic Energy Commission has adopted standards which have prevented new cases of beryllium toxemia related to routine exposure since its adoption. The recommended exposure limits are as follows (Ref. 10):

"1.   The in-plant atmospheric concentration of beryllium should not exceed 2 $\mu g/m^3$ averaged over an 8 h day. This is an arbitrary value since the levels causing the chronic disease are in doubt.

"2.   The concentration should never exceed 25 $\mu g/m^3$ for any period of time, however short. This is aimed at preventing the acute disease; the figure is partly based on the incident reported in Section 12.1.1.

"3.   In the neighbourhood of a plant handling beryllium compounds, the average monthly concentration should not exceed 0.01 $\mu g/m^3$. This is derived from the mean concentrations at the outer limit of the neighbourhood cases.

"4.   If the average in-plant concentration over three months is $> 2$ but $< 5$ $\mu g/m^3$, or if a single, short-term sample is $> 25$ but $< 100$ $\mu g/m^3$ work can continue if the operators wear approved respiratory equipment, but corrective action must begin at once. If the three-monthly in-plant concentration exceeds 5 $\mu g/m^3$ or the single sample exceeds 100 $\mu g/m^3$ work must cease until corrective action is completed."

Assembly and Test of Solenoid

The solenoid was assembled; however, testing of the solenoid assembly could not be accomplished because of the defective insulation on the anodized beryllium coil. The anodize film specified for the beryllium wire coils was selected on the basis of the sample tests; however, similar room environment and vacuum insulation tests on the wire used for the magnetizing coil indicate the insulation leakage current was too great to utilize the wire for magnetizing coils. The leakage current observed on the coil wire was at least $10^{12}$ times greater than the corresponding sample. The supplier of the beryllium anodized wire

believes the poor insulation quality on the long anodized wires was caused by anodizing the wire in coils of approximately 1 foot diameter instead of a long straight continuous length enclosed by a concentric circular cylinder cathode. The throwing power of the beryllium anodize is known to be poor and anodizing for electrical insulation must allow for this.

## Summary

A summary of important advantages of beryllium-oxide-insulated beryllium magnet wire in electromagnetic device coils obtained from Tables 2-3, 2-4, and 2-5 are:

1. Lighter weight

   1/5 the weight of typical magnet wire materials.

2. High-temperature operation to $1000^{\circ}C$

   Be melts at $1283^{\circ}C$

   BeO melts at $2550^{\circ}C$

   BeO insulation is adherent, protective and compatible with Be metal to $1000^{\circ}C$.

3. Good Electrical Conductivity

   Be has 40% the volume electrical conductivity of copper at $25^{\circ}C$.

   Be has 2.07 times the electrical conductivity of copper on a weight basis at $25^{\circ}C$.

4. Good thermal conductivity

   Be and BeO have superior thermal conductivity assuring cool operation at high power densities.

5. Superior mechanical properties for rotating machine applications

   The low density, high Young's modulus, and high tensile strength provide a combination of mechanical properties which improve the high-speed performance. Up to 15 times the power rating may be obtained when compared to the usual conductor materials used in high-speed rotating machines in cases where the peripheral speed limit of the rotor windings limits the power rating.

Methods of applying a beryllium oxide coating to beryllium wire which may be suitable for electrical insulation are:

1. Deposition and curing a film from a beryllium oxide slurry.

2. Extrusion and curing of a wet plastic beryllium oxide film.

3. Direct surface boundary oxidation by using a controlled atmosphere and temperature.

4. Deposition by electrophoresis from a colloidal beryllium oxide suspension.

5. Vacuum vapor deposition.

6. Spray coating of molten beryllium oxide.

7. Application of an anodized film by an electrochemical process.

## Recommendations

1. Continue investigation on the cause of unsatisfactory electrical insulation of the anodize coatings on beryllium wire and obtain beryllium wire having satisfactory electrical insulation.

2. Construct an anodized beryllium wire coil which is operational and assemble and test the solenoid actuator.

3. Procure sufficient ductile, square, anodized beryllium wire to wind a good solenoid actuator coil and evaluate the performance of the coil.

4. Extend the investigation of insulation methods for beryllium magnet wire with improved mechanical and electrical properties.

5. Extend the application and investigation of beryllium magnet wire to include motor driven actuators and servo devices and other space applications.

REFERENCES

1.  W. W. Pendleton. "Advanced Magnet Wire Systems," Electro-Technology, October 1963.

2.  "Thin Film Aluminum Oxide Wire and Strip," Permaluster, Inc., 1844 North Keystone Avenue, Burbank, California.

3.  R. M. Bozorth. "Ferromagnetism," Van Nostrand Company, Inc., New York, New York.

4.  E. A. Nesbitt, R. D. Heidenreich and A. J. Williams. "A Necessary Factor for Heat Treatment of the Permalloys in a Magnetic Materials - Supplement to the Journal of Applied Physics, Vol. 31, pp. 228S - 229S, McGraw-Hill, New York, 1960.

5.  Massachusetts Institute of Technology Staff. "Magnetic Circuits and Transformers," John Wiley and Sons, Inc., New York, N. Y.

6.  J. Huminik, Jr. "High Temperature Inorganic Coatings," Reinhold Publishing Corporation, New York, N. Y.

7.  M. Pasnak and R. Lundsten. "Effects of Ultrahigh Temperature on Magnetic Properties of Core Materials," A.I.E.E. Transactions, Part I, January 1960, pp. 1033 - 1039.

8.  M. Pasnak and R. H. Lundsten. "Effects of High Temperature on Magnetic Properties of Core Materials," Proceedings of the Fourth Symposium on Magnetism and Magnetic Materials - Supplement to the Journal of Applied Physics, Volume 30, pp. 107S - 108S, McGraw Hill, New York, N. Y., 1959.

9.  M. Lauriente and G. E. Lynn. "Characteristics of Supermendur at $500^{\circ}$C," Proceedings of the Fifth Symposium on Magnetism and Magnetic Materials - Supplement to the Journal of Applied Physics, Vol. 31, McGraw Hill, New York, N. Y., 1960.

10. Darwin and Buddery. Beryllium, Academic Press (1960).

11. S. Helles, V. Nerses and J. Siergiej. "Beryllium as a Structural Material, How Great a Deterrent Is Its Lack of Ductibility?" Journal of Metals, (November 1963).

12. E. Gower, D. J. Levy and L. Whitley. "Chromic Acid Anodizing of Beryllium Process Variables," LMSD-895064, 10 January 1961, Lockheed Missiles and Space Division, Sunnyvale, California.

13. "Black Anodizing of Beryllium as an Oxidation Barrier Using the B.B.C-257 Process," Brush Beryllium Corporation, Cleveland, Ohio, April, 1963.

14. J. Roush. "Oxidation Protection of Beryllium at High Temperatures," Armour Report No. I.I.T.R.I.-B251-15, July 1963, Armour Research Foundation, Chicago, Illinois.

15. "Work Pertaining to Protective Coatings for Beryllium," United States Atomic Energy Commission, AEC Contract No. AT-11-1-Gen-8 to North American Aviation, Inc.

16. "Test Procedure for Evaluation of the Thermal Stability of Enameled Wire in Air," A.I.E.E., No. 57, January 1959.

17. R. F. Crawford and A. B. Burns. "Strength, Efficiency, and Design Data for Beryllium Structure," ASD Technical Report 61-692, Contract AF 33(616)-6905, Project 1368, Task 13928, Lockheed Missiles and Space Company, Sunnyvale, California, February 1962.

18. "Beryllium in Aerospace Structures," The Brush Beryllium Company, Cleveland, Ohio.

19. "Products and Applications of Beryllium," Bulletin 2120, The Beryllium Corporation, Reading, Pennsylvania.

20. "Forming Beryllium," Bulletin 2140, The Beryllium Corporation, Reading, Pennsylvania.

21. T. S. Nakae, J. J. Rausch, and A. J. Stonehouse. "Anodized Films as Oxidation Protection for Beryllium Metal," 12th Annual Atomic Energy Commission Corrosion Symposium, Pleasanton, California, May 20-22, 1963.

22. W. W. Beaver and A. J. Stonehouse. "Beryllium: Surface Treatment and Coatings," Seminar at the University of California, Los Angeles, March 4-8, 1963, The Brush Beryllium Company, Cleveland, Ohio.

23. A. J. Stonehouse and W. W. Beaver. "Corrosion and Protection of Beryllium Metal," Aerospace Metals Symposium, March 9-13, 1964, Chicago, Illinois, Brush Beryllium Corporation Report No. BBC-2R-335.

24. "Plain Talk on Beryllium," March 1959, The Brush Beryllium Corporation, P. O. Box 1462, Reading, Pennsylvania.

25. A. J. Breslin and W. B. Harris. "health Protection in Beryllium Facility," (HASL-36), (May 1959), Office of Technical Services, U. S. Department of Commerce, Washington 25, D. C.

26. "Conference on Beryllium Disease and Its Control," M.I.T. September 30 - October 1, 1958, Vol. 19, No.2, A.M.A. Archives of Industrial Health, February 1959.

TABLE 2-1

Radiation Exposure and Temperature Limits for Electromagnetic Materials

| 100 hr Radiation Exposure | Total Dose 100 Megarads at $10^5$ to $10^6$ rads/hr | Total Dose 1000 Megarads at $10^6$ to $10^7$ rads/hr | Total Dose to $10^4$ Megarads at $10^7$ to $10^8$ rads/hr | Total Dose $10^5$ Megarads at $10^8$ to $10^9$ rads/hr | Total Dose $10^6$ Megarads at $10^9$ to $10^{10}$ rads/hr | Total Dose $10^7$ Megarads at $10^{10}$ to $10^{11}$ rads/hr |
|---|---|---|---|---|---|---|
| Material Class Temperature Limit | 180° C Max. | 250° C Max. | 400° C Max. | 650° C | 1000° C | 1500° C |
| Electrical Insulation | Silicones, glass mica, asbestos, polyesters, epoxys and combinations | Polyimide film and varnish, silicone varnish, composites, glass, mica, asbestos, ceramic | Ceramic Coatings and embedding, special fiberglass, glass, glass enamel, glass bonded mica, mica, paper, asbesto anodic films | Glass bonded fibers, glass + ceramic, glass bonded mica, glass enamel ceramic embedding and extrusions, anodic films, vapor deposited films | Special glasses, ceramics, quartz, ceramic and glass fibers, ceramic embedding ≠ extrusions, vapor deposited films | Oxide ceramics, alumina, beryllia, magnesia, sapphire |
| Conductors | copper, aluminum, silver, beryllium | nickel plated copper, aluminum clad copper, silver, beryllium, aluminum, anodized aluminum, anodized beryllium | nickel plated copper, nickel clad copper, aluminum, silver, beryllium, nickel clad silver, anodized aluminum, anodized beryllium | nickel clad copper stainless steel clad copper, nickel + iron clad copper, nickel clad copper, nickel clad silver, dispersion hardened anodized aluminum, anodized beryllium | Inconel + barrier on dispersion hardened copper, Inconel on silver, Inconel on dispersion hardened silver, anodized dispersion hardened beryllium in protective atmosphere | platinum |
| Magnetic Materials | Ingot iron, silicon iron, silicon-aluminum iron, nickel iron, cobalt iron | Ingot iron, silicon irons, silicon-aluminum iron, nickel iron, cobalt iron | Ingot iron, silicon iron, silicon-aluminum iron, nickel iron, cobalt iron | Ingot iron to 500° C, cobalt iron | Cobalt iron, cobalt | none |

WEIGHT COEFFICIENT $B_{mc}$ FOR OPTIMUM DIMENSION D.C SOLENOID

| $B_{mc}$ | Magnetic Material $(3.73\sigma_m)$ | Conductor Material $(3.73\sigma_c)$ |
|---|---|---|
| 1.41 | 50 Fe + 50 Co | Al |
| 2.21 | 50 Fe + 50 Co | Cu or Cu + Ni |
| 2.42 | 50 Fe + 50 Co | Ag |
| 1.30 | 50 Fe + 50 Co | Be |
| 1.37 | Fe | Al |
| 2.17 | Fe | Cu or Cu + Ni |
| 2.66 | Fe | Ag |
| 2.38 | Co | Cu or Cu + Ni |
| 1.39 | Co | Be |
| 2.43 | 50 Fe + 50 Ni | Ag |

TABLE 2-3

DATA ON ELECTRICAL CONDUCTORS AND CERAMIC INSULATORS

| MATERIAL | | DENSITY LBS/CU IN. | MELTING TEMPERATURE °C | SPECIFIC HEAT CAL/GM | | ELECTRICAL RESISTIVITY µΩ CM | | THERMAL CONDUCTIVITY GM CAL/SEC CM² °C | | YOUNG'S MODULUS PSI X $10^{-6}$ | | ULTIMATE TENSILE STRENGTH PSI X $10^{-3}$ | |
|---|---|---|---|---|---|---|---|---|---|---|---|---|---|
| | | | | @25°C | @1000°C | @25°C | @1000°C | @25°C | @1000°C | @25°C | @1000°C | @25°C | @1000°C |
| ALUMINUM | Al | 0.100 | 653 | 0.214 | | 2.824 | | 0.504 | | 10.1 | 0 | 30 | 0 |
| BERYLLIUM | Be | 0.066 | 1283 | 0.425 | 0.79 | 4 | 40 | 0.45 | 0.15 | 44 | LOW | 50-70 | 2.5 |
| COBALT | Co | 0.321 | 1480 | 0.100 | 0.187 | 6.24 | 77.4 | 0.165 | | 30 | | 30-100 | 12 |
| COPPER | Cu | 0.323 | 1083 | 0.092 | | 1.724 | 9.42 | 0.918 | | 15 | | 30 | |
| GOLD | Au | 0.698 | 1063 | 0.031 | | 2.44 | 12.52 | 0.700 | | 11.3 | | 20-46 | |
| NICKEL | Ni | 0.321 | 1452 | 0.105 | | 6.8 | 48 | 0.206 | | 30 | | 120 | 5.2 |
| SILVER | Ag | 0.379 | 960 | 0.0558 | | 1.59 | | 1.00 | | 11.2 | 0 | 42 | 0 |
| IRON | Fe | 0.27 | 1539 | 0.107 | | 10 | 116 | 0.161 | 0.191 | 30 | | 25 | |
| ALUMINA | $Al_2O_3$ | 0.1395 | 2050 | 0.18 | 0.28 | $>10^{20}$ | $2 \times 10^{12}$ | 0.88 | 0.25 | 50 | | 35 | 21+ |
| BERYLLIA | BeO | 0.109 | 2550 | 0.240 | 0.5+ | $>10^{21}$ | $8 \times 10^{19}$ | 0.63 | $>0.07$ | 50 | 37 | 21 | 13.5 |

TABLE 2-4    COMPARISON OF BERYLLIUM AND COPPER

| | | |
|---|---|---|
| DENSITY RATIO $\rho_{Be}/\rho_{Cu}$ | | 0.204 |
| SPECIFIC HEAT RATIO $C_{P_{Be}}/C_{P_{Cu}}$ | | 4.62 |
| VOLUME RESISTIVITY RATIO $R_{Be}/R_{Cu}$ | @ 25°C | 2.32 |
| | @ 1000°C | 4.25 |
| THERMAL CONDUCTIVITY RATIO $G_{Be}/G_{Cu}$ | | 0.49 |
| TENSILE MODULUS RATIO $E_{Be}/E_{Cu}$ | | 2.93 |
| TENSILE STRENGTH RATIO $S_{Be}/S_{Cu}$ | | $\cong 2$ |
| RESISTIVITY RATIO × DENSITY RATIO $R_{Be}/R_{Cu} \times \rho_{Be}/\rho_{Cu}$ | @ 25°C | 0.483 |
| | @ 1000°C | 0.868 |
| THERMAL CONDUCTIVITY RATIO ÷ DENSITY RATIO $G_{Be}/G_{Cu} \div \rho_{Be}/\rho_{Cu}$ | | 2.4 |
| MODULUS RATIO ÷ DENSITY RATIO $E_{Be}/E_{Cu} \div \rho_{Be}/\rho_{Cu}$ | | 14.36 |
| TENSILE STRENGTH RATIO ÷ DENSITY RATIO $S_{Be}/S_{Cu} \div \rho_{Be}/\rho_{Cu}$ | | $\cong 9.8$ |
| YIELD STRENGTH RATIO ÷ DENSITY RATIO $G_{Be}/G_{Cu} \div \rho_{Be}/\rho_{Cu}$ | | $\cong 26$ |

TABLE 2-5  COMPARISON OF BERYLLIA AND ALUMINA

| | | |
|---|---|---|
| DENSITY RATIO $BeO/Al_2O_3$ | | 0.778 |
| SPECIFIC HEAT RATIO $C_{P_{BeO}}/C_{P_{Al_2O_3}}$ | @ 25°C | 1.333 |
| | @ 1000°C | 1.788 |
| VOLUME RESISTIVITY RATIO $R_{BeO}/R_{Al_2O_3}$ | @ 25°C | 10 |
| | @ 1000°C | $4 \times 10^7$ |
| THERMAL CONDUCTIVITY RATIO $G_{BeO}/G_{Al_2O_3}$ | @ 25°C | 7.1 |
| | @ 1000°C | $>2.8$ |
| TENSILE MODULUS RATIO $E_{BeO}/E_{Al_2O_3}$ | | 1 |
| TENSILE STRENGTH RATIO $S_{BeO}/S_{Al_2O_3}$ | | 0.6 |
| RESISTIVITY RATIO ÷ DENSITY RATIO $R_{BeO}/R_{Al_2O_3} \div \rho_{BeO}/\rho_{Al_2O_3}$ | @ 25°C | 12.86 |
| | @ 1000°C | $5.14 \times 10^7$ |
| THERMAL CONDUCTIVITY RATIO ÷ DENSITY RATIO $G_{BeO}/G_{Al_2O_3} \div \rho_{BeO}/\rho_{Al_2O_3}$ | @ 25°C | 9.03 |
| | @ 1000°C | $>3.6$ |
| MODULUS RATIO ÷ DENSITY RATIO $E_{BeO}/E_{Al_2O_3} \div \rho_{BeO}/\rho_{Al_2O_3}$ | | 3.77 |
| TENSILE STRENGTH RATIO ÷ DENSITY RATIO $S_{BeO}/S_{Al_2O_3} \div \rho_{BeO}/\rho_{Al_2O_3}$ | | 0.77 |
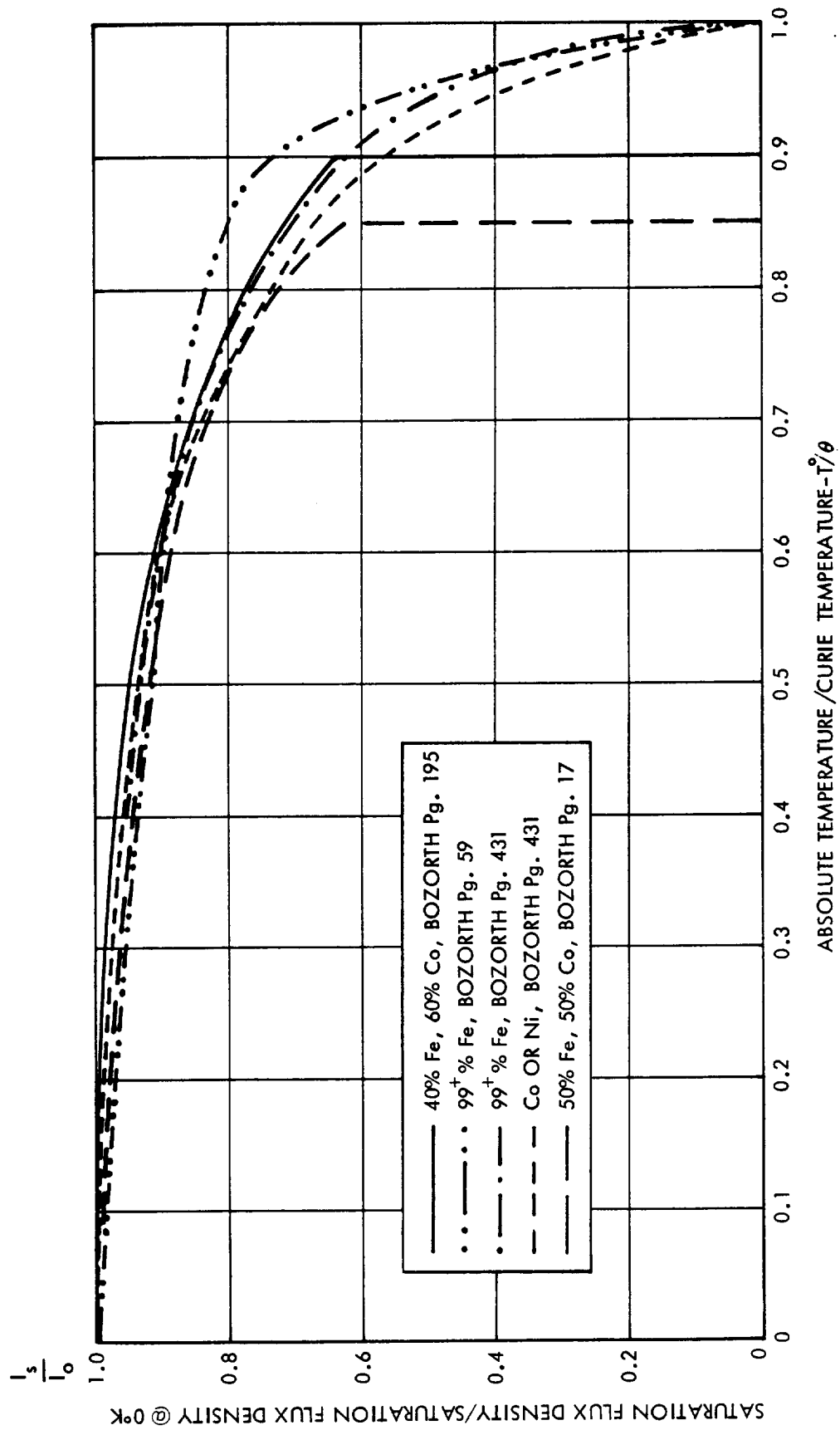
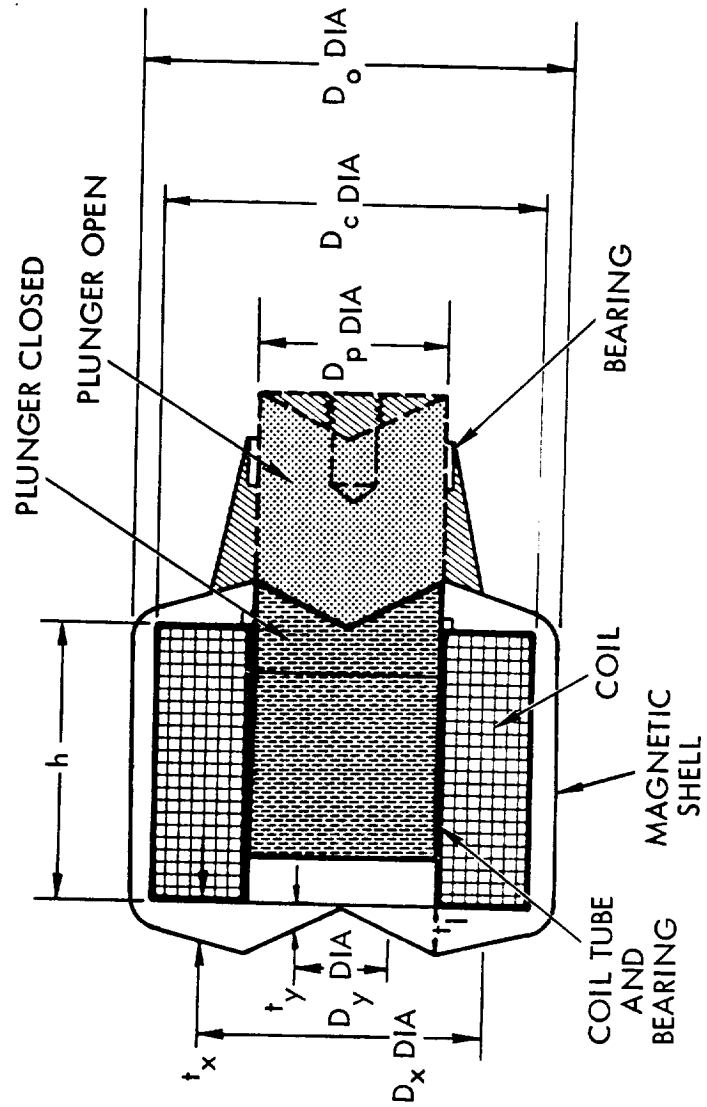Figure 2-1. Saturation Flux Density Ratio vs Temperature for Ferromagnetic Materials
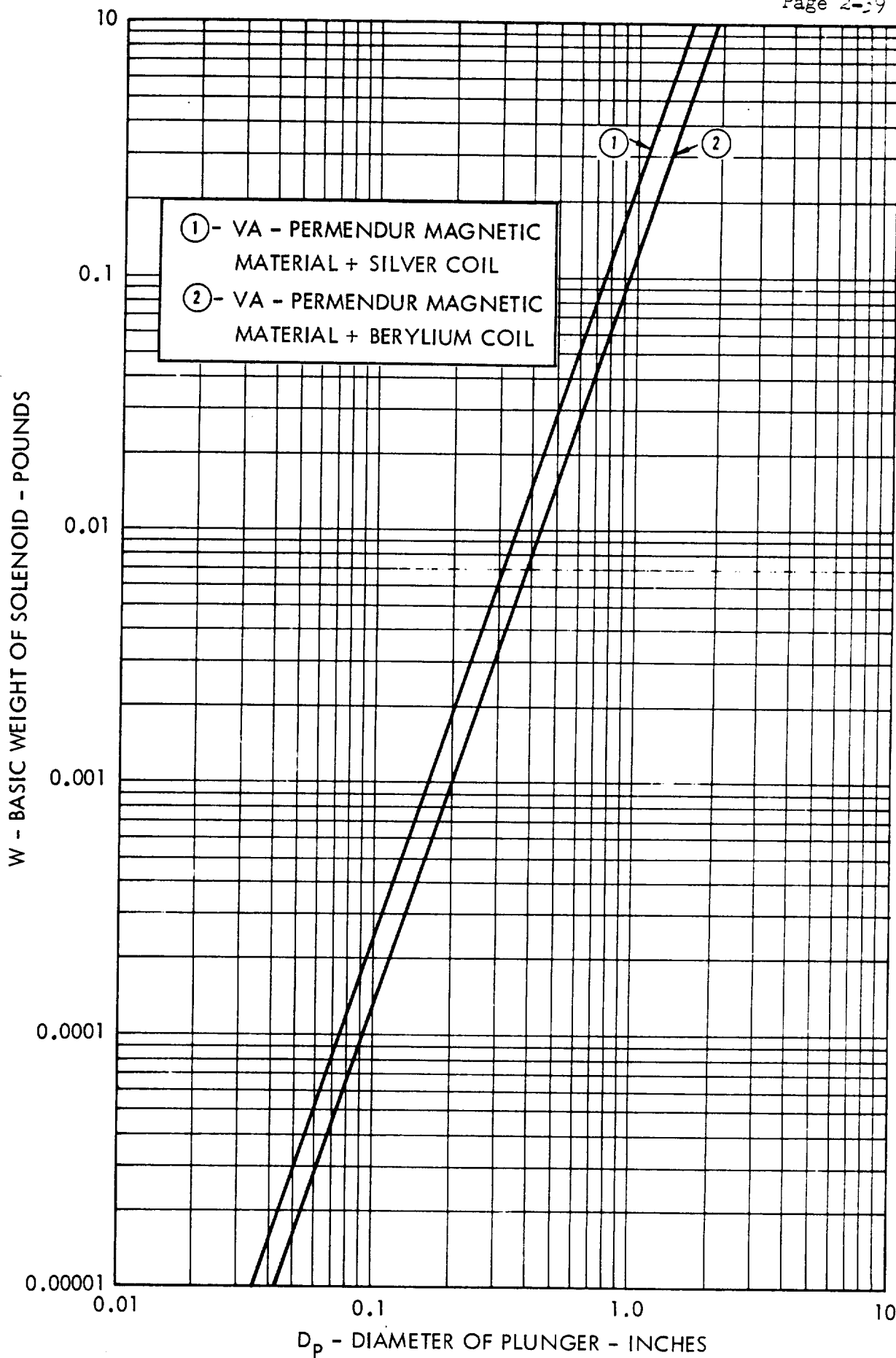
Figure 2-2. Cylindrical DC Solenoid Dimensions

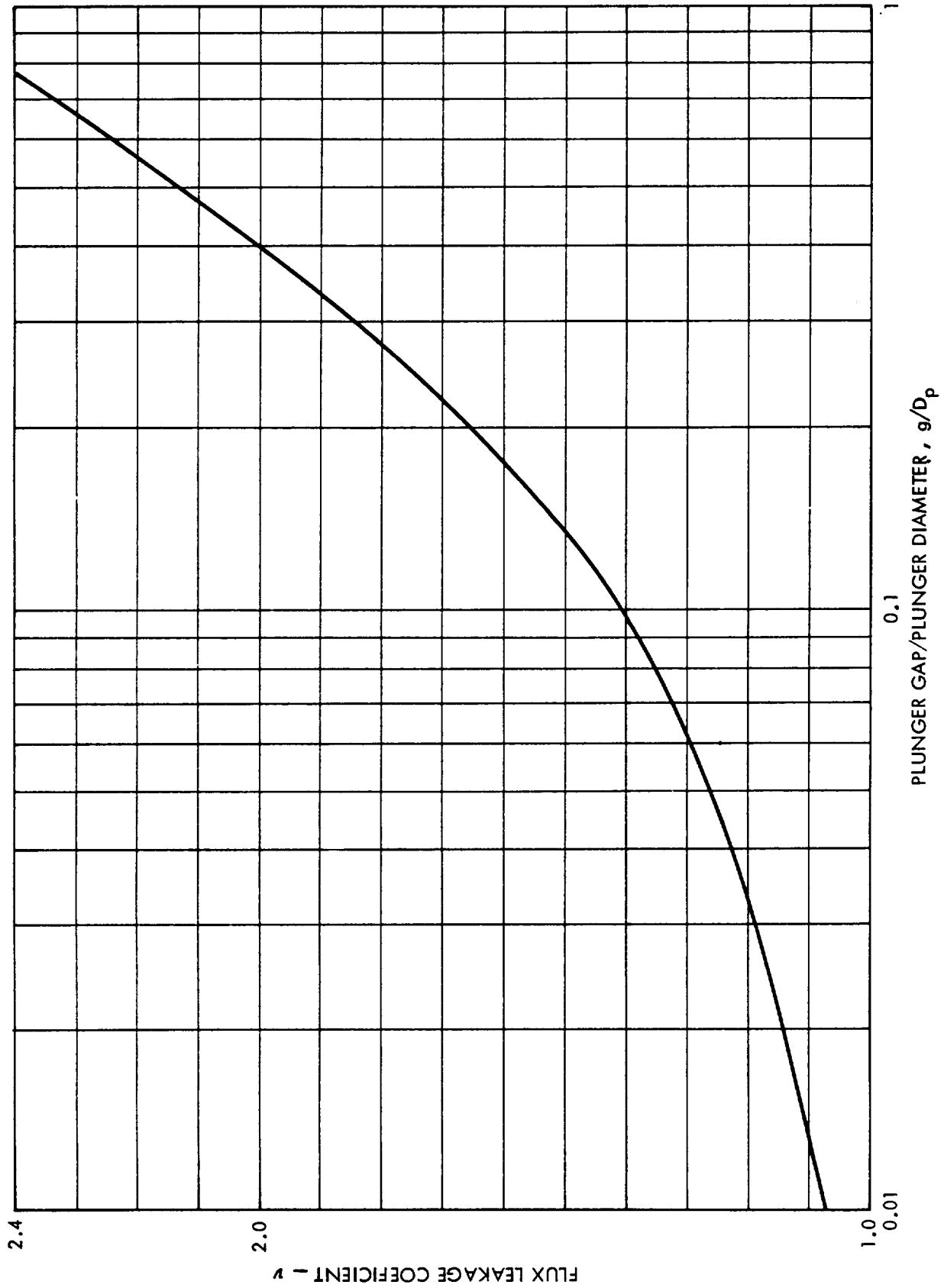Figure 2-3. Basic Weight of Optimum Cylindrical Solenoid Actuators

Legend within figure:

① - VA - PERMENDUR MAGNETIC
MATERIAL + SILVER COIL

② - VA - PERMENDUR MAGNETIC
MATERIAL + BERYLIUM COIL

W - BASIC WEIGHT OF SOLENOID - POUNDS

$D_p$ - DIAMETER OF PLUNGER - INCHES

Figure 2-4. Plunger Gap Flux Leakage Coefficient vs Plunger Gap Ratio
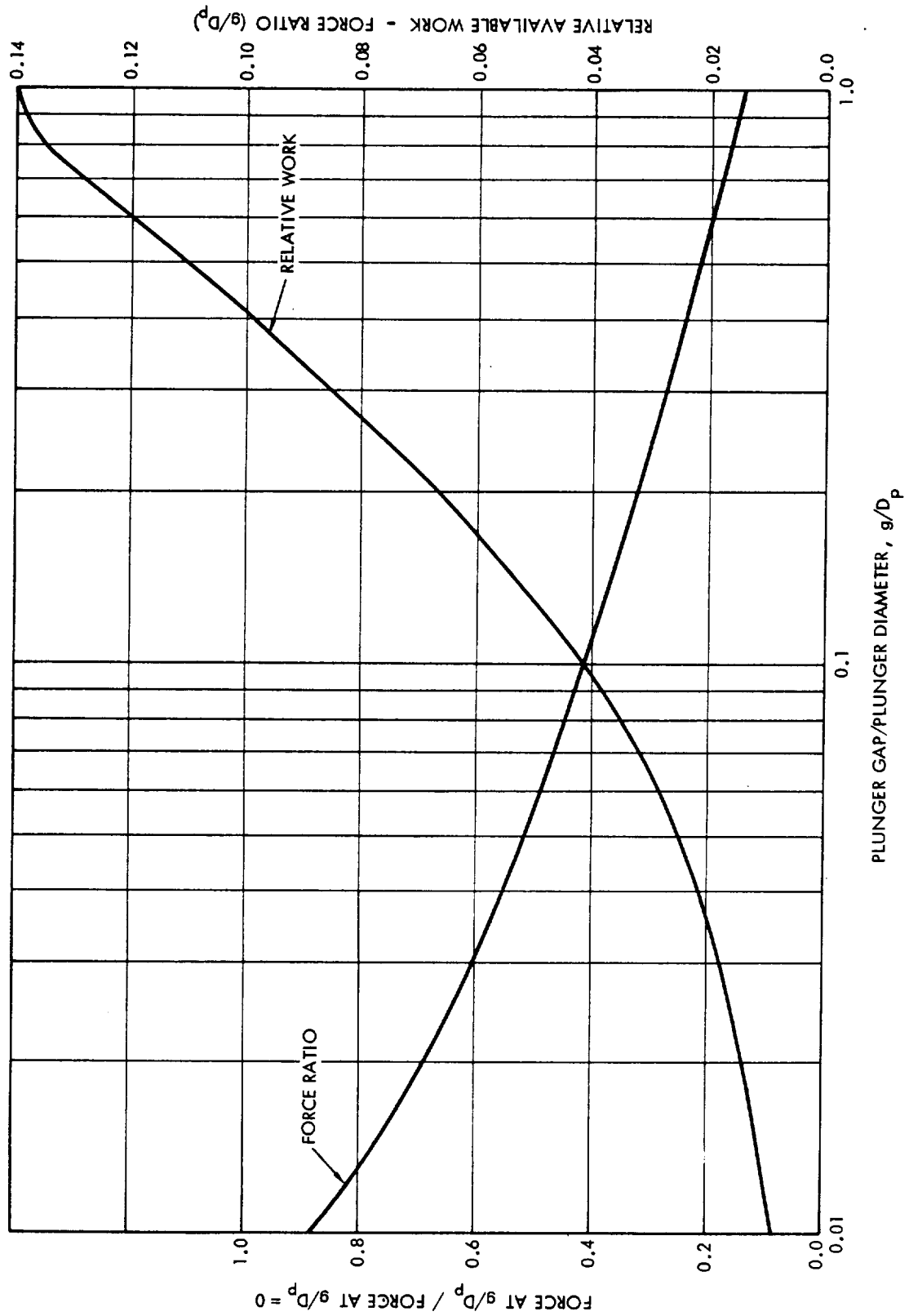
Figure 2-5.   Relative Saturated Plunger Force and Work vs Plunger Stroke/Diameter
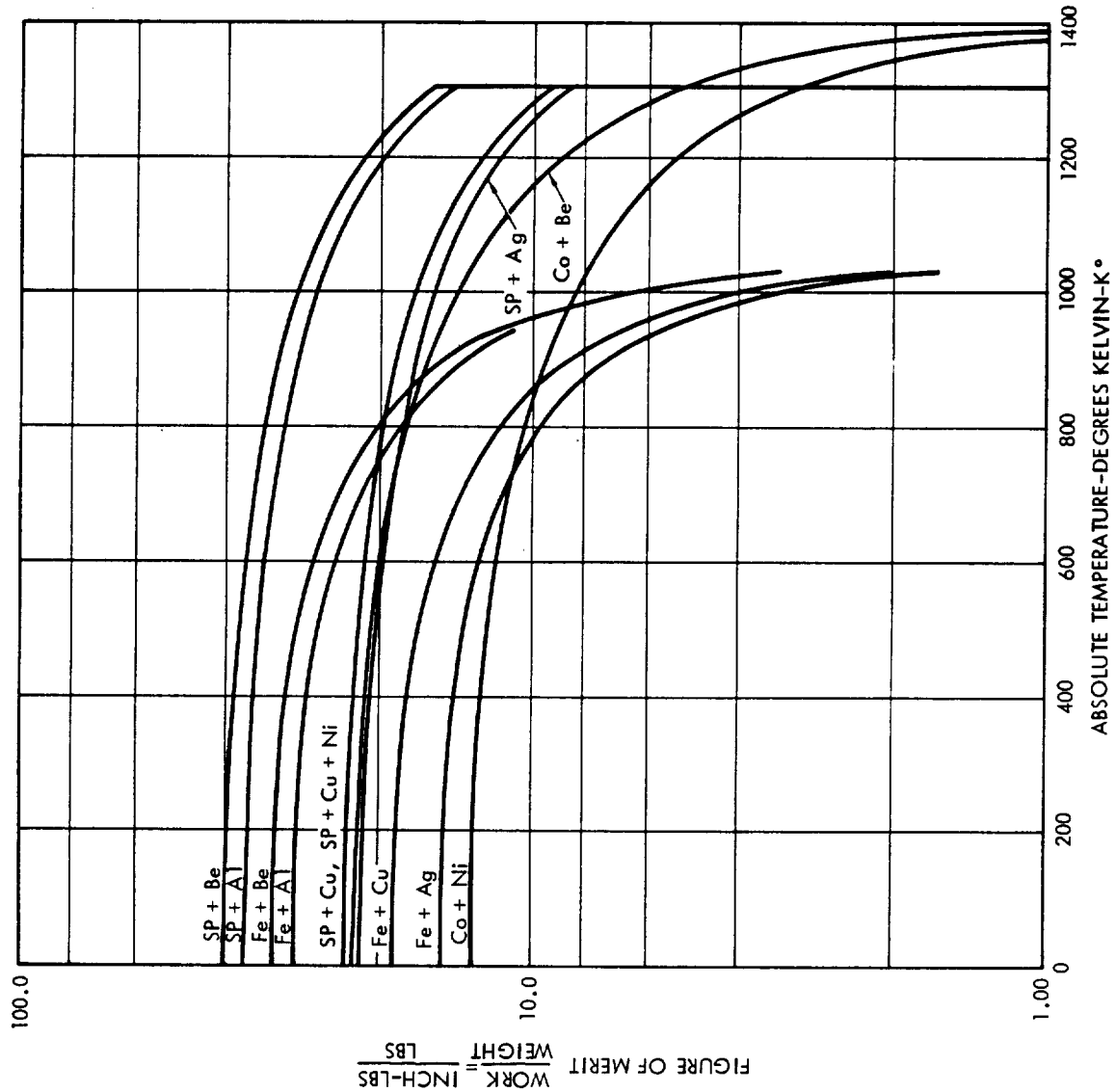
Figure 2-6. Work/Weight Figure of Merit for D.C. Solenoids of Various Magnetic and Conductor Materials

TEMPERATURE – DEGREES KELVIN-K°

ρ RESISTIVITY – MICROHM CM
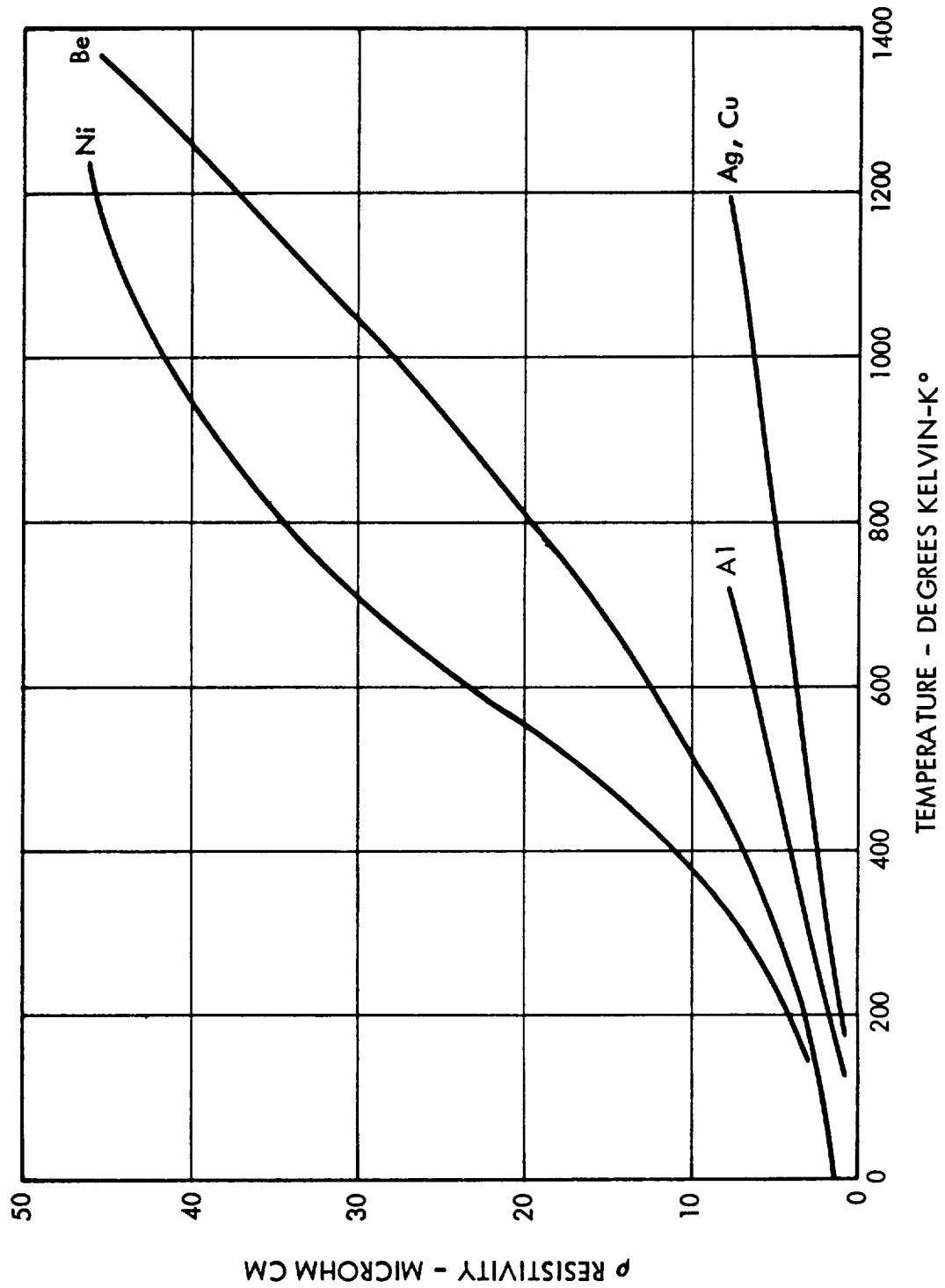
Figure 2-7. Electrical Resistivity vs Temperature

Scale A  —  Pull in Power Watts for $g/D_p = 1$
Scale B  —  Holding Power Watts for $g/D_p = 0.002$
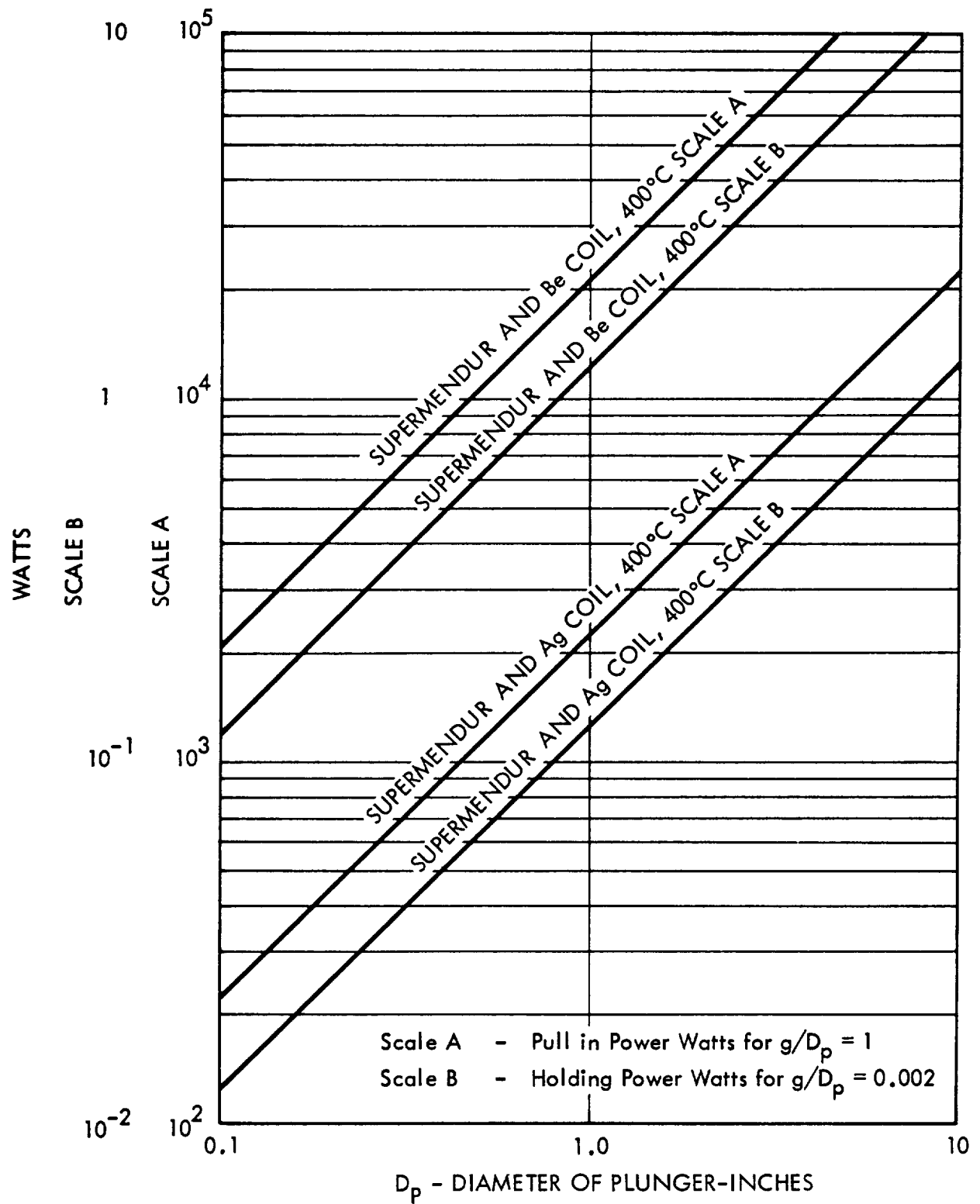
Figure 2-8.  Minimum Solenoid Exciting Power for Optimum Cylindrical Solenoids
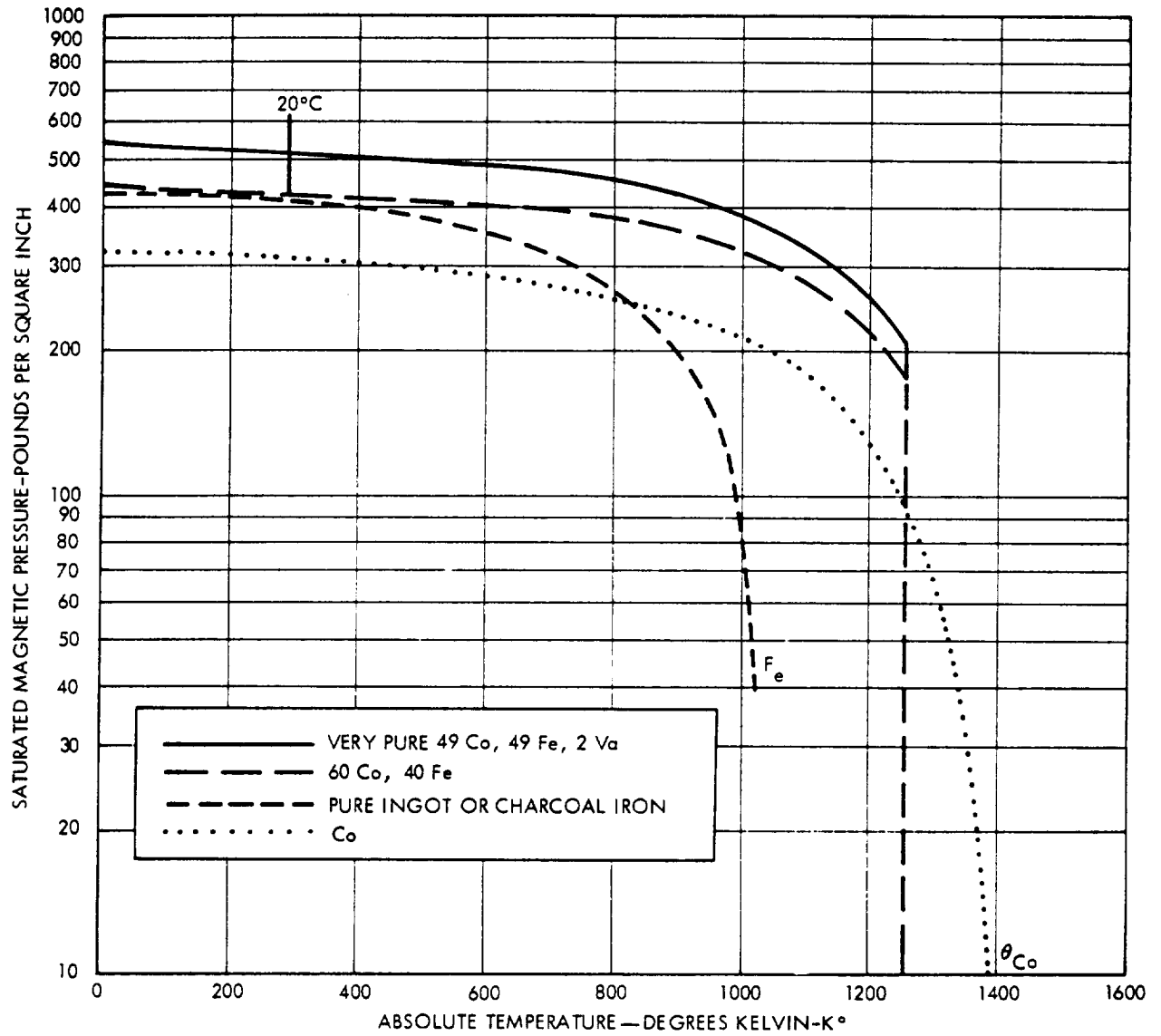
Figure 2-9. Saturated Magnetic Pressure of Ferromagnetic Materials vs Temperature

Figure 2-10. DC Solenoid Power Supply Circuits

$C_c$ – CONTACT PROTECTION CAPACITOR

$C_s$ – ENERGY STORAGE CAPACITOR

$D_1$ – POWER RECTIFIER

$L_i$ – CURRENT LIMITING INDUCTANCE

$L_s$ – SOLENOID COIL INDUCTANCE

$R_\ell$ – SOLENOID COIL RESISTANCE

SW – SOLENOID ON-OFF SWITCH

A. SIMPLE DC SUPPLY SOURCE

B. DC SUPPLY WITH HOLDING CURRENT LIMITING RESISTOR, $R_s$, AND ENERGY STORAGE CAPACITOR, $C_s$

C. SOLENOID WITH 2 EQUAL COIL SECTIONS AND BACK-CONTACTS TO REDUCE HOLDING CURRENT
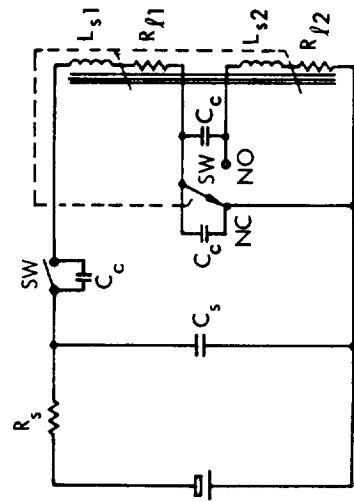
D. DC SUPPLY WITH CURRENT LIMITING RESISTOR, $R_s$, ENERGY STORAGE CAPACITOR, $C_s$, AND 2 SECTION SOLENOID COIL WITH BACK-CONTACT COIL SWITCHING
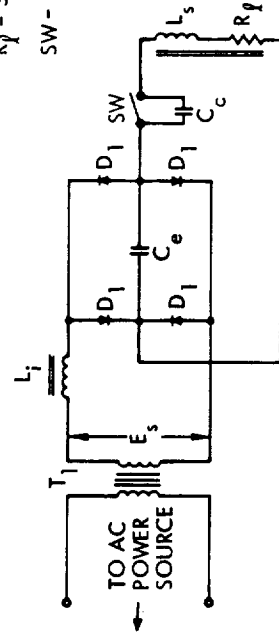
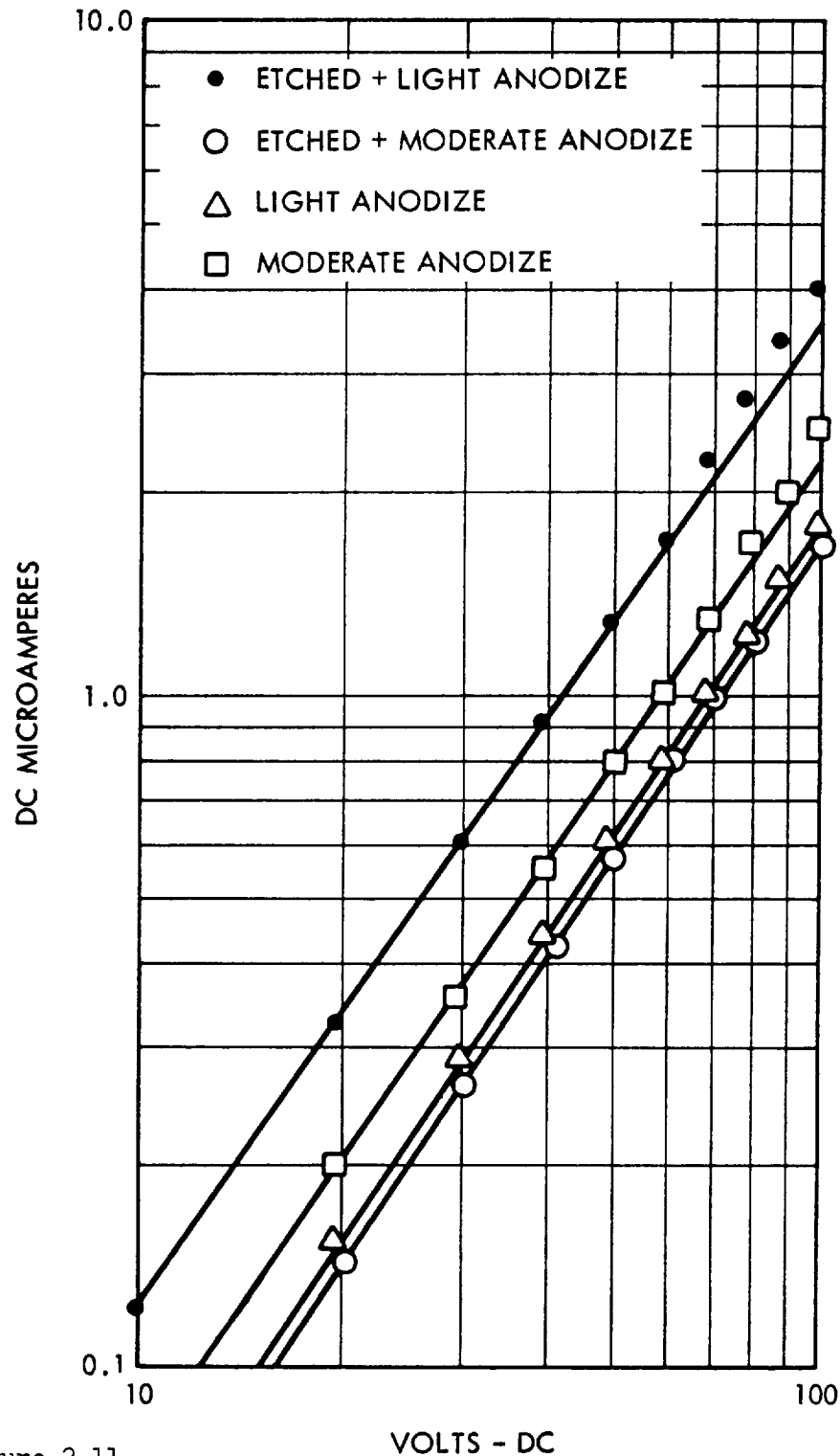E. AC SUPPLY WITH CURRENT LIMITING INDUCTANCE, $L_i$, AND ENERGY STORAGE CAPACITOR, $C_e$

Figure 2-11.

Insulation Voltage-Current Characteristics of sample pairs of
.064 inch diameter beryllium anodized wire coating.  Length of
anodized contact = 4 inches (see Fig. 2-12).  Test conducted at
ambient conditions.

Figure 2-12.   Test sample for low temperature evaluation
of beryllium anodized insulation.

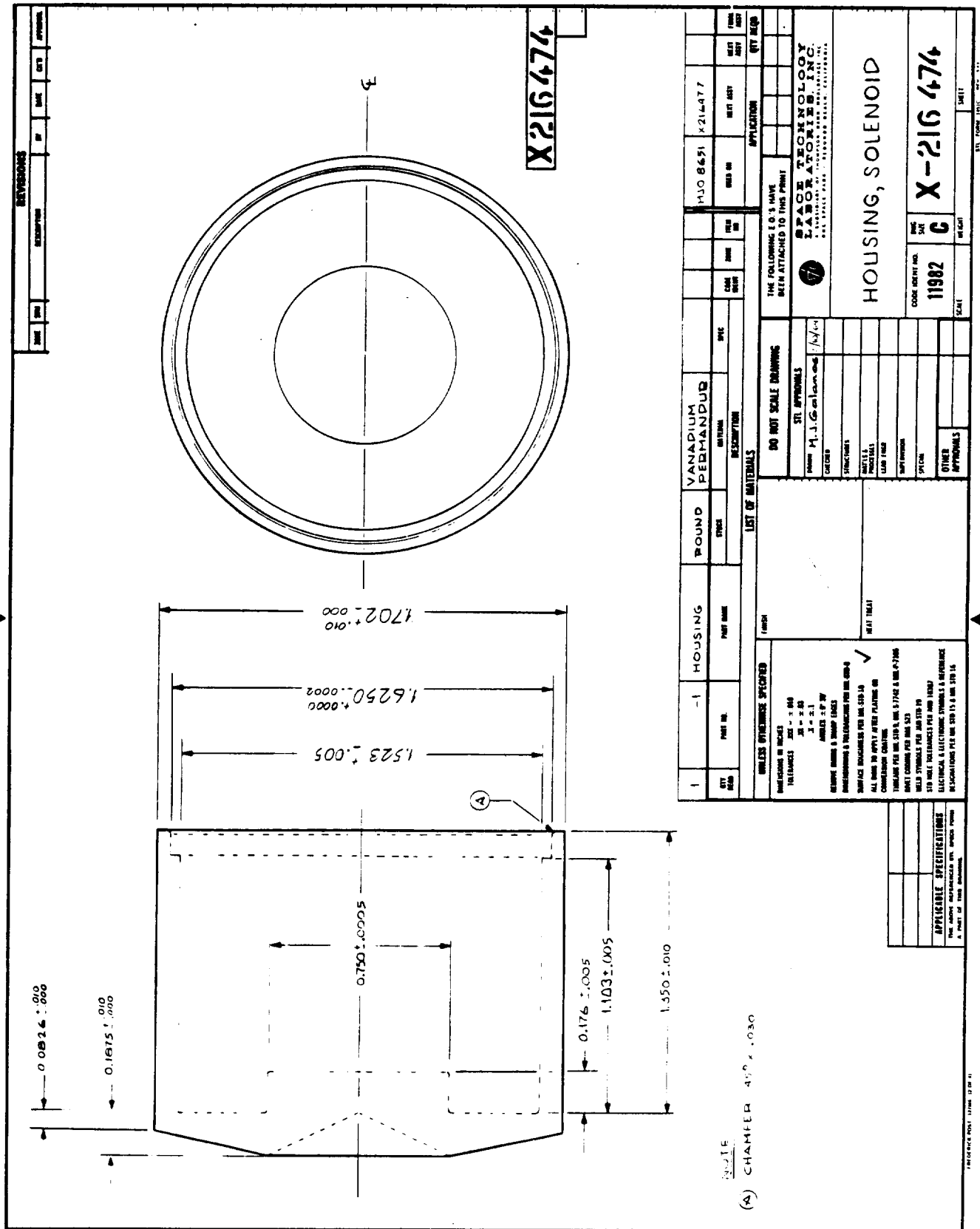Figure 2-13.  Lightweight High-Temperature
Solenoid Before Assembly

X216474

X216474

HJO 8651 | X216477

THE FOLLOWING E.O.'S HAVE
BEEN ATTACHED TO THIS PRINT

APPLICATION

STR APPROVALS

DO NOT SCALE DRAWING

H.J.Galanes

HOUSING, SOLENOID

SPACE TECHNOLOGY
LABORATORIES, INC.

CODE IDENT NO. 11982

X-216 474

LIST OF MATERIALS

VANADIUM
PERMANDUR

ROUND

HOUSING

NOTE

(A) CHAMFER 45° x .030

1.702 ± .010

1.6250 +.0000 / -.0002

1.523 ± .005

0.750 ± .005

0.176 ± .005

1.103 ± .005

1.350 ± .010

0.0826 + .010 / -.000

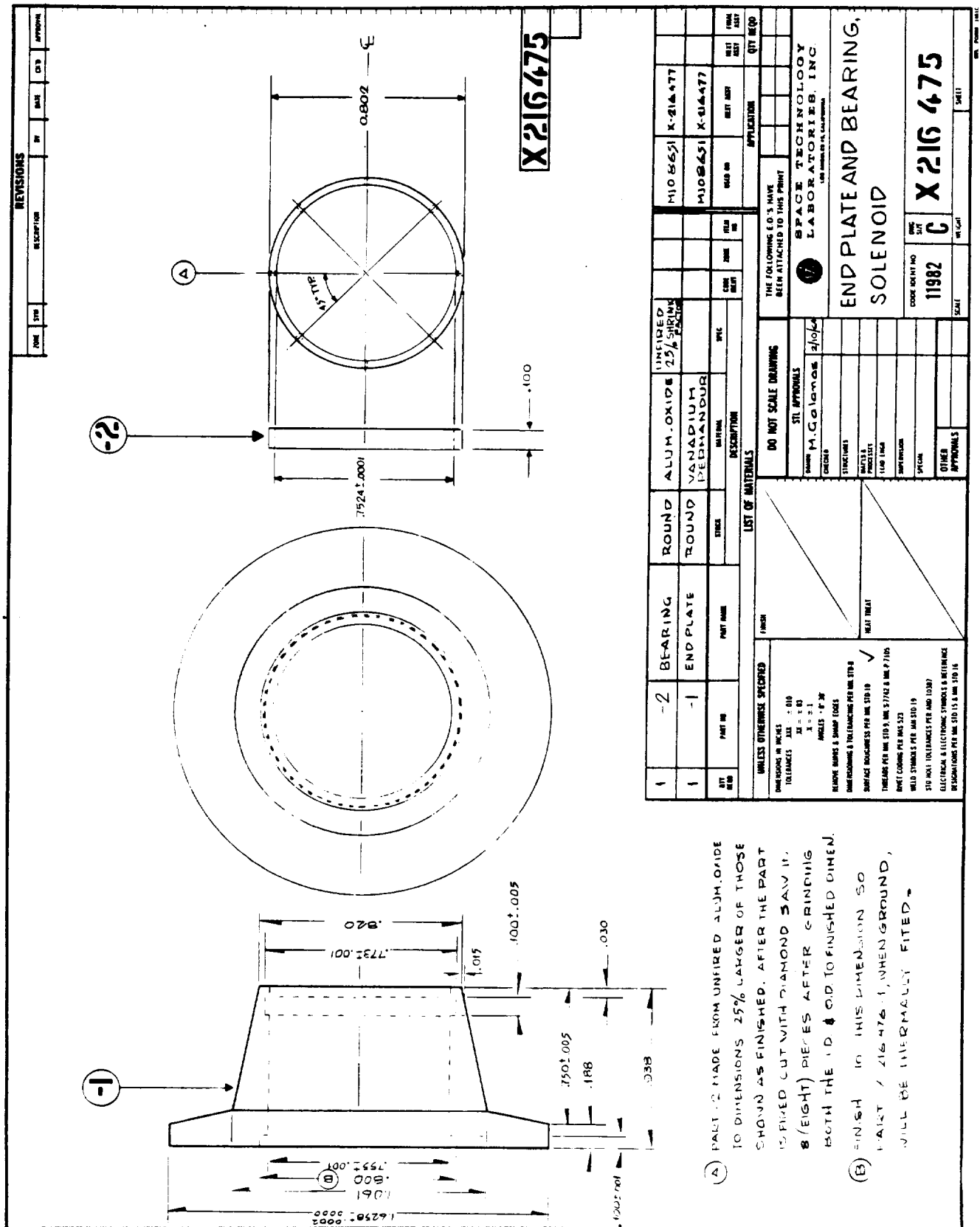0.1615 + .010 / -.000

Figure 2-14.   Solenoid Housing

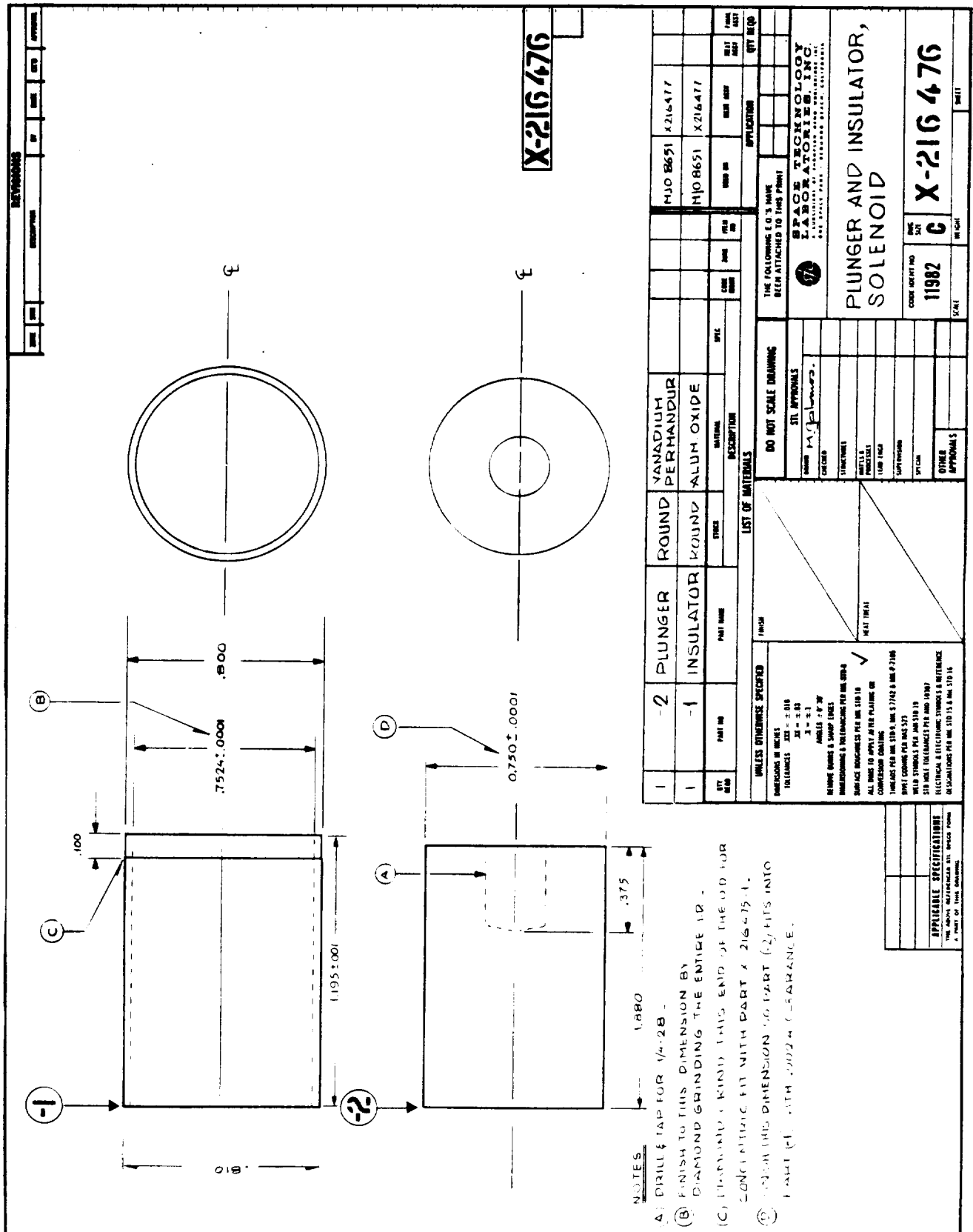Figure 2-15. Solenoid End Plate and Bearing
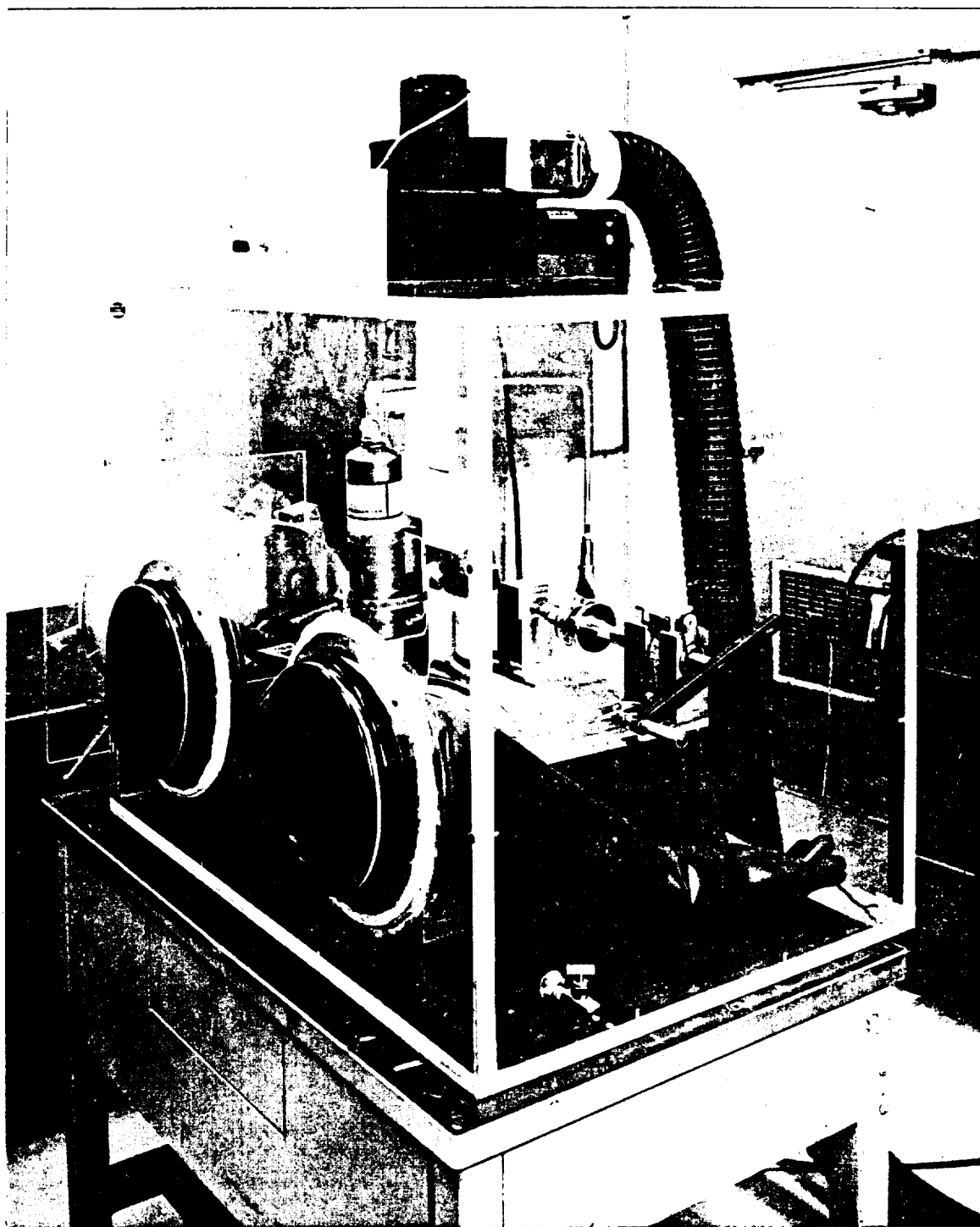
Figure 2-16.   Solenoid Plunger and Insulator

Figure 2-17. Coil Winding Machine and Dry Box
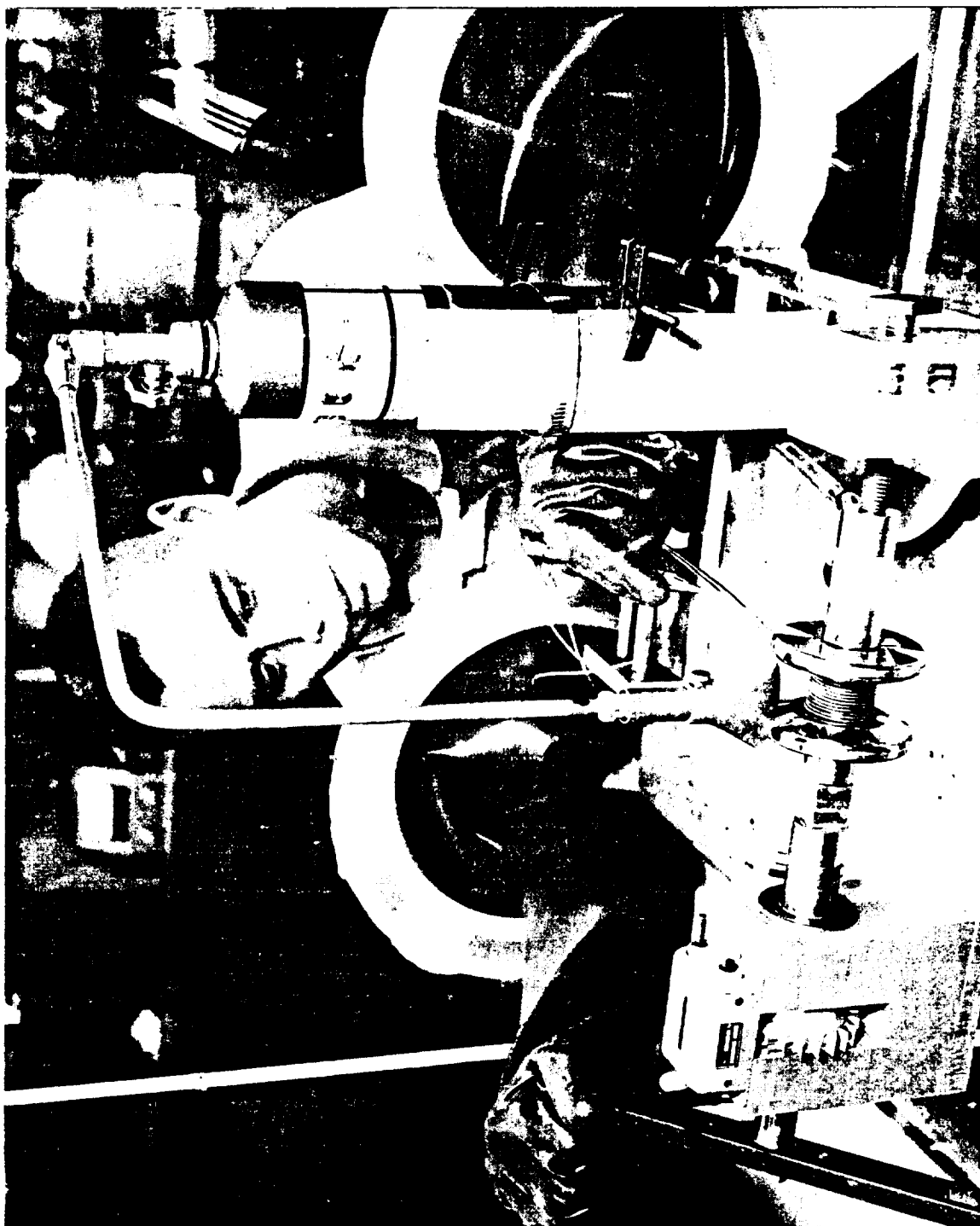for Winding Beryllium Wire

Figure 2-18.  Beryllium Winding Operation Utilizing
Flat-shaped Gas Flame Heating

III.   ZERO-G VENT VALVE

Cryogenic propellants contained within space vehicles usually accept or give off heat to the environment.  Cases where heat is absorbed and converted to support propellant evaporation will result in increasing tank pressure.  Without some control of heat flow into the tank, it is necessary to return the heat absorbed to the outside of the tank, preferably by means of venting gas.  Like most systems, efficiency is important in the operation; therefore, the heat must be removed as cheaply as possible.

Conventional venting methods depend on the availability of gas or vapor to carry off energy to the outside.  Conventional vents are effective only when the vapor/liquid interface location is defined and can be consistently positioned by applying acceleration to the tank in the same direction.  With the absence of gravity, acceleration must be applied with the settling rocket or other means which lowers the efficiency of the process.  Without the use of acceleration to settle, the probability of venting liquid is high.  Venting may be considered effective if the heat absorbed by the propellant is released with saturated or superheated vapor instead of liquid, or if a favorable balance of flow exists between the heat leaving the tank and that entering the tank.

Several thermodynamic processes of heat exchange or possible compression and expansion can be employed to provide an effective transfer of energy from the tank.  The use of the compression/expansion cycle depends on a secondary heat transport system for operation, as will be described later.  However, for most cryogenics it is theoretically feasible to depend on constant enthalpy expansion process and heat exchange between the venting fluid and the bulk propellant to achieve efficient venting.  Figure 3-1 is a simplified schematic of a vent valve and in-line heat exchanger arrangement.  Inlets are shown in both the liquid and vapor, only to show that the system is indifferent to the fluid phase entering the vent valve. The pressurized fluid at $T_1$, $P_1$, pressure and temperature, respectively, expands across the expansion valve at constant enthalpy, thus discharging

at a lower temperature and pressure $(T_2, P_2)$. With good heat exchange and distribution, it is possible to extract heat from the propellant faster than it is transferred through the tank wall from the outside.

A more complex system, further advancing the above technique, is shown in Figures 3-2 and 3-3. Liquid or gaseous propellant enters the system at point (1) and is expanded to a lower pressure passing through the expansion valve. Joule-Thompson cooling from expansion causes a lowering of temperature at point (2), then expanded propellant passes through a low pressure heat exchanger, thus extracting energy from the bulk propellant remaining in the tank. It may be desirable to continue venting fluid flow through the throttle valve actuator for thermal control purposes at point (3) where throttle control "C" varies the throttle position such as to increase or decrease flow, thus maintaining constant temperature through the actuator. The venting fluid further expands isentropically across the centripetal turbine and then is discharged to the atmosphere. The turbine, if necessary, provides torque for the circulation fan which enhances heat transfer in the heat exchanger.

Since the steady-flow, throttling process is isenthalpic, enthalpy of the fluid follows the relation

$$h_2 = h_1, \text{ and } (h_3 - h_2) = (h_3 - h_1)$$

Venting fluid flowing through the heat exchanger contributes to a coefficient designated by the symbol U and is defined by Newton's differential equation of heat transfer.

$$dq = U \Delta T \, dA = (h_3 - h_2) \, dW/dt$$

where dq is the element of heat transfer with respect to time across an element of area dA when the temperature difference between the venting and remaining bulk fluid is $\Delta T$.

$h_1$ = Specific enthalpy of high pressure propellant within the tank, Btu/lb.

$h_2$ = Specific enthalpy of the venting fluid after throttling, Btu/lb.

$h_3$ = Specific enthalpy of the low-pressure fluid leaving the heat exchanger, Btu/lb.

$h_4$ = Specific enthalpy of the venting fluid after turbine expansion to space, Btu/lb.

$Q_T$ = Heat flow rate, Btu/hr.

If saturated liquid is vented, the heat extracted by the heat exchanger plus the heat required to increase the gas volume within the tank must be equal to the total heat flow into the tank.

$$Q_T = \dot{W}(h_3 - h_2) + \dot{W} \frac{\rho_g}{\rho_L} H_L$$

where

$\dot{W}$ = Venting rate = $dW/dt$, lb/sec

$\rho_g$ = Density of saturated vapor, lb/ft$^3$

$\rho_L$ = Density of saturated liquid, lb/ft$^3$

$H_L$ = Heat of vaporization, Btu/lb

$$(h_3 - h_2) = \frac{Q_T - \dot{W}\rho_g/\rho_L H_L}{\dot{W}} = U\triangle T \int dA$$

The pressure drop across the heat exchanger accompanying the turbulent flow of a gas in the tube is given by

$$P_1^2 - P_2^2 = 2RT_m G^2 \left[ \ln \frac{V_2}{V_1} + \frac{f_m L}{2r_h} \right]$$

the symbols are:

$P$ = Absolute pressure, $lb/ft^2$

$R$ = Universal gas constant, ft $lb/lb°R$

$T_m$ = Mean temperature, $°R$

$G$ = Mass velocity, $lb/sec-ft^2$

$V$ = Specific volume, $ft^3/lb$

$f_m$ = Mean value of friction factor

$L$ = Equivalent length of straight tube, ft

$r_h$ = Hydraulic radius, ft

The final stage of thermal reaction is work extracted by the expansion turbine.

$$W_K = \dot{W}(h_3 - h_4) = \dot{W}V^2/2g$$
$$V = 2\pi r\omega$$

where

$V$ = Turbine exit velocity, ft/sec

$\omega$ = Turbine rotor angular velocity, radians/sec

$r$ = rotor radius, ft

$$\dot{W}(h_3 - h_4) = \frac{2\dot{W}(\pi r\omega)^2}{g}$$

Approximate rotor radius is,

$$r = \sqrt{\frac{g(h_3 - h_4)}{2(\pi\omega)^2}}$$

Turbine weight is a function of rotor radius. From the above analytical expressions an understanding of the Btu/hr rating of the process can be established, as can some imagination of system weight and effectiveness.

It is a temperature entropy plot of the reaction of such a system containing hydrogen. Let's assume liquid hydrogen is vented from the tank beginning at point (1) $42^{\circ}R$ and 30 psia. The liquid expands via constant enthalpy to point (2) at 2 psia and $27^{\circ}R$. If effective heat transfer takes place by approaching point (3), the heat extraction from the remaining liquid is

$$\Delta h_{ex} = h_3 - h_1 = 330 - 130 = 200 \text{ BTU/lb}$$

where h is enthalpy. Heat extraction with respect to time is a function of venting rate.

$$H_{ex} = \dot{w} (h_3 - h_1)$$

where $\dot{w}$ is venting gas flow rate in pounds per second. Heat extraction rate can vary with throttle valve actuation.

If the same process is applied by beginning at point (1'), the heat extraction potential is still the same. Venting vapor without the heat exchanger results in a lower energy venting rate if saturated vapor is vented; that is,

$$\Delta H_{ex} = h_{1'} - h_1 = 313 - 130 = 183 \text{ Btu/lb}$$

It can be seen that venting with the heat exchanger can be 8.5% more efficient than venting with saturated vapor.

A similar, but still more complex zero-g venting process is designed as shown in Figures 3-4 and 3-5. This concept employs a secondary technique which by means of compression/expansion, the venting gases can be further superheated. The fluid in the secondary system used for transporting heat must be either a liquid or gas whose boiling point is near that of the propellant being vented. For this example, helium gas is used as the secondary fluid, and hydrogen liquid or gas is the propellant under consideration.

In Figure 3-5 the process began at the helium tank, which is submerged in

hydrogen at $42^\circ$R, at which temperature the thermal properties at point (1) are obtained. The venting fluid in the first system expands via constant enthalpy from point (5) to (6) to $27^\circ$R. While both fluids are flowing through the external heat exchanger, the helium is cooled to $27^\circ$R at point (3), thus producing a T of $15^\circ$ between the helium and the remaining propellant. The heated hydrogen at $72^\circ$R discharging from the heat exchanger at point (7), and by reversible adiabatic expansion across the turbine thus providing compressor torque. The motor shown supplements the compressor during start and for make-up.

The heat absorption potential from point (6) to (7) as shown on Figure 3-4 is

$$\Delta H_{6-7} = h_7 - h_6 = 397.0 - 130 = 267 \text{ Btu/lb}$$

Thus, this system is theoretically 46% more effective than venting saturated vapor. However, the efficiency of such a system is likely to degrade the theoretical value.

Therefore, it can be concluded that heat can be removed from the tank by discharging liquid, thus making it possible to disregard the need for liquid/vapor separation and location during zero-g venting.

## DEVELOPMENT AND TESTING OF A CRYOGENIC ZERO-G VENT SYSTEM  DRAWING NO. LD-2028-1

### Introduction and Objective

This development and test program was initiated in support of the Advanced Valve Technology study. The primary objective of this program was to demonstrate the feasibility of equally efficient and effective liquid or vapor venting. The secondary object was to utilize the vent process for the purpose of extracting from the bulk propellant, heat which entered through the tank wall.

The program involved the following three basic tasks:

    a.  Design and fabrication of experimental
          hardware unit

b. A test program to demonstrate the effective-
ness of the vent process

c. Correlation between concept analysis and a
reduction to practice.

## Conclusion and Recommendation

An experimental zero-g thermal vent system was designed, fabricated, and
tested. The test unit operated directly as planned without a need for
modifications. Although vapor and liquid vented through the system was
under the influence of earth's gravity, the test results were instructive
and revealing.

Data obtained from the test indicate that the development of a lightweight
prototype unit is entirely feasible. One main design consideration is
properly sizing the heat exchanger to effect heat transfer not less than
the maximum heat flow into the propellant. Circulation of gas or liquid
past the heat exchanger is necessary to effect heat transfer throughout
the propellant.

## Discussion

Design. The test was conducted using a heavy-duty workhorse type fixture
designed for personnel safety, and to make possible testing under a vari-
ety of test conditions. Concepts and parts are shown schematically in
Figure 3-6 and by photographs, Figures 3-7 through 3-11. The unit con-
sists of two valves for flow selection either through the heat exchanger
or directly overboard. The pressure gages shown monitor tank pressure
and throttle valve discharge pressure. The burst diaphragm mounted on
top of the unit is rated to rupture at 150 psi. A 1000 Btu/hr Max. heater
is attached at the base of the tank. The heat input was variable from 10%
to 100% by the heat control unit.

Fabrication. An experimental unit was fabricated using simple off-the-
shelf parts. As can be seen from the photographs, the fittings are
standard AN tube fittings. The heater (heat supply unit) and weight

scale was equipment borrowed from other programs. The section of tubing downstream of the throttle valve is shown covered with insulation to reduce test fluid boiloff during liquid expansion. The tank vent outlet was installed near the inner wall to allow venting gas or liquid by simply rotating the tank mounted in the horizontal.

Test Procedure. The test equipment and setup were prepared first for liquid nitrogen cooldown. For this application an adapter was installed between the $LN_2$ bottle and the test fixture vent outlet (see Figure 3-7). The two vent valves were placed in the full open position, permitting cold gas or liquid to pass by reverse flow through the heat exchanger and the tank. When the tank outside wall temperature decreases below -30°F, cooldown is complete. A typical cooldown test setup, Figure 3-7, is shown with cooldown gas discharging out through the fill connection. It was necessary to mount the test fixture on its side to duplicate test conditions. In this position the heat input was repeatable for liquid or gas venting. The tank outlet as indicated above is conveniently installed off center near the inside wall. By rotating the tank 180° with the outlet in a vertical plane, liquid or gas can be discharged from the tank. Liquid is removed with the outlet at the bottom as shown on Figure 3-10.

At the completion of cooldown, with temperature at -30°F, the tank was filled with Freon-12 through the vent outlet with the throttle valve in the closed position. The tank has a 40-lb capacity which was registered by the weight scale. The filling operation took place with the tank vented to atmospheric pressure. Liquid Freon-12 entered at -20°F. After filling, the fluid and tank were reheated to 90°F and 100 psig, then test began. The liquid or gas energy extraction process continued until fluid weight decreased to approximately 5 pounds. The data were recorded as shown on the test data and analysis sheets.

Test Results. The constant test parameters were tank pressure at 100 psig and heat input setting at 1000 Btu/hr. Data listed in Tables 3-1 and 3-2 are tabulated with respect to time in irregular intervals. Table 3-1 is the result of the gas vent test bypassing the heat exchanger, and Table 3-2 is

the result of the liquid vent test through the heat exchanger. These data are summarized by Figure 3-12, which is a plot of measured weight versus venting time.

It can be seen that the curves are linear and do not superimpose because of different starting weights. However, equation for each curve is as follows:

Gas Venting: $W_T = 99 - 0.241t$

$d\ W_T/dt = 0.241\ \text{lb/min}$

Liquid Venting: $W_T = 101 - 0.238t$

$d\ W_T/dt = 0.238\ \text{lb/min}$

The slope of each curve represents the respective venting rates. As indicated, tank pressure was maintained at a constant value of 100 psig with a slightly lower fluid loss rate during the liquid venting process.

The fluid heat absorption is equal to the difference of enthalpy between the gas leaving the vent and saturated liquid.

$$h = h_g - h_f$$

### Gas Venting

| | Temperature | Pressure | Enthalpy |
|---|---|---|---|
| Saturated Liquid | $90^\circ$F | 114.7 psia | 28 Btu/lb |
| Gas | $70^\circ$F | 14.7 psia | 87.5 " |

$h_g = 87.5 - 28 = 59.5\ \text{Btu/lb}$

$Q = (dW_T/dt)\ \Delta h_g \times 60$

$Q_g = .241 \times 59.5 \times 60 = 860\ \text{Btu/hr.}$

### Liquid Venting

| | Temperature | Pressure | Enthalpy |
|---|---|---|---|
| Saturated Liquid | $90^\circ$F | 114.7 psia | 28.0 Btu/lb |
| Gas | $84^\circ$F | 14.7 psia | 91.0 Btu/lb |

$$\Delta h_L = 91 - .28 = 63 \text{ Btu/lb}$$

$$Q_L = .238 \times 63 \times 60 = 900 \text{ Btu/hr}$$

From the above analysis it is evident that the heat absorption rate during liquid venting was higher, and a comparison of the slope of each curve indicates a saving of propellant by venting liquid or gas through the heat exchanger. This is a net gain over a process which vents gas or saturated vapor directly from the tank.

TABLE 3-1

## ZERO-G VENT SYSTEM TEST DATA AND ANALYSIS

PURPOSE: TO DETERMINE THE FEASIBILITY OF EFFICIENT MIXED PHASE VENTING          DATE: 3/4/64

APPARATUS: 1000 BTU/HR THERMAL VENT SYSTEM

VENTING FLUID: ULLAGE GAS FREON-12

| HEATER POWER SETTING | TIME | TANK PRESSURE | APPARATUS GROSS WEIGHT | HEAT EXCHANGER INLET TEMP | TANK VENT OUTLET TEMP | FLUID WEIGHT LOSS ΔWt | TOTAL VENT TIME | ΔWT/Δt |
|---|---|---|---|---|---|---|---|---|
| BTU/HR | HR:MIN-SEC | PSIG | LBS | °F | °F | LBS | MIN | LB/MIN |
| 1000 | 11:08-15 | 100 | 99.700 | | 60 | | | |
| 1000 | 11:18-00 | 100 | 96.800 | | 64 | 2.900 | 9.75 | 0.298 |
| 1000 | 11:24-25 | 94 | 95.010 | | 69 | 1.790 | 16.17 | 0.279 |
| 1000 | 11:27-40 | 97 | 94.085 | | 69 | 0.925 | 19.42 | 0.284 |
| 1000 | 11:32-45 | 99 | 92.875 | | 70 | 1.210 | 24.54 | 0.236 |
| 1000 | 11:36-00 | 99 | 92.255 | | 70 | 0.620 | 28.79 | 0.146 |
| 1000 | 11:40-25 | 100 | 91.085 | | 70 | 1.170 | 33.21 | 0.265 |
| 1000 | 11:47-20 | 100 | 89.675 | | 72 | 1.410 | 40.128 | 0.204 |
| 1000 | 11:56-15 | 100 | 87.574 | | 75 | 2.101 | 49.046 | 0.236 |
| | | | | | | | | |
| | | | | | | | | |
| | | | | | | | | |
| | | | | | | | | |
| | | | | | | | | |
| | | | | | | | | |
| | | | | | | | | |

DATA RECORDER   B. HAYES                    DATA APPROVED  _L. D. Young_

TABLE 3-2

## ZERO-G VENT SYSTEM TEST DATA

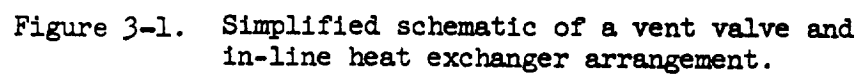PURPOSE: TO DETERMINE THE FEASIBILITY OF EFFICIENT MIXED PHASE VENTING     DATE: 3/4/64

APPARATUS: 1000 BTU/HR THERMAL VENT SYSTEM

VENTING FLUID: LIQUID FREON-12

| HEAT | TIME | TANK PRESSURE | APPARATUS GROSS WEIGHT | HEAT EXCHANGER INLET TEMP | TANK VENT OUTLET TEMP | FLUID WEIGHT LOSS ΔWt | TOTAL VENT TIME | ΔWt/Δt |
|------|------|------|------|------|------|------|------|------|
| BTU/HR | HR:MIN-SEC | PSIG | LBS | °F | °F | LBS | MIN | LB/MIN |
| 1000 | 2:36-05 | 100 | 101.0 | -14 | 78 | 0 | 0 | 0 |
| 1000 | 2:40-55 | 100 | 97.8 | -13 | 81 | 1.2 | 4.833 | 0.248 |
| 1000 | 2:44-30 | 100 | 98.9 | -8 | 83 | 0.9 | 3.75 | 0.240 |
| 1000 | 2:47-50 | 100 | 97.8 | -5 | 83 | 1.1 | 3.33 | 0.330 |
| 1000 | 2:52-25 | 105 | 96.8 | -4 | 84 | 1.0 | 4.60 | 0.218 |
| 1000 | 2:55-40 | 101 | 95.8 | -7 | 85 | 1.0 | 3.25 | 0.308 |
| 1000 | 2:59-55 | 100 | 94.8 | -5 | 85 | 1.0 | 4.25 | 0.236 |
| 1000 | 3:04-10 | 102 | 93.8 | -5 | 86 | 1.0 | 4.25 | 0.236 |
| 1000 | 3:08-50 | 100 | 92.8 | -7 | 86 | 1.0 | 4.66 | 0.215 |
| 1000 | 3:12-55 | 100 | 91.8 | -4 | 86 | 1.0 | 4.12 | 0.243 |
| 1000 | 3:16-55 | 100 | 90.8 | -7 | 85 | 1.0 | 4.00 | 0.250 |
| 1000 | 3:20-55 | 101 | 89.8 | -6 | 86 | 1.0 | 4.00 | 0.250 |
| 1000 | 3.25-30 | 100 | 88.8 | -8 | 86 | 1.0 | 4.60 | 0.218 |
| 1000 | 3:30-30 | 98 | 87.8 | -8 | 87 | 1.0 | 5.00 | 0.200 |
| | | | | | | | | |

DATA RECORDER  B. HAYES          DATA APPROVED  _LOYoung_

Figure 3-1.  Simplified schematic of a vent valve and
in-line heat exchanger arrangement.

Figure 3-3. Block diagram of arrangement and in-line heat exchanger arrangement.

| POINT | TEMP ~ °R | ENTHALPY BTU/16 | PRESS PSIA |
|-------|-----------|-----------------|------------|
| 1 | 42 | 130 | 30.0 |
| 2 | 27 | 130 | 2.0 |
| 3 | 42 | 330 | 2.0 |
| 4 | 27 | 295 | SPACE |

Figure 3-2. Schematic of a more complex vent valve and in-line heat exchanger arrangement.
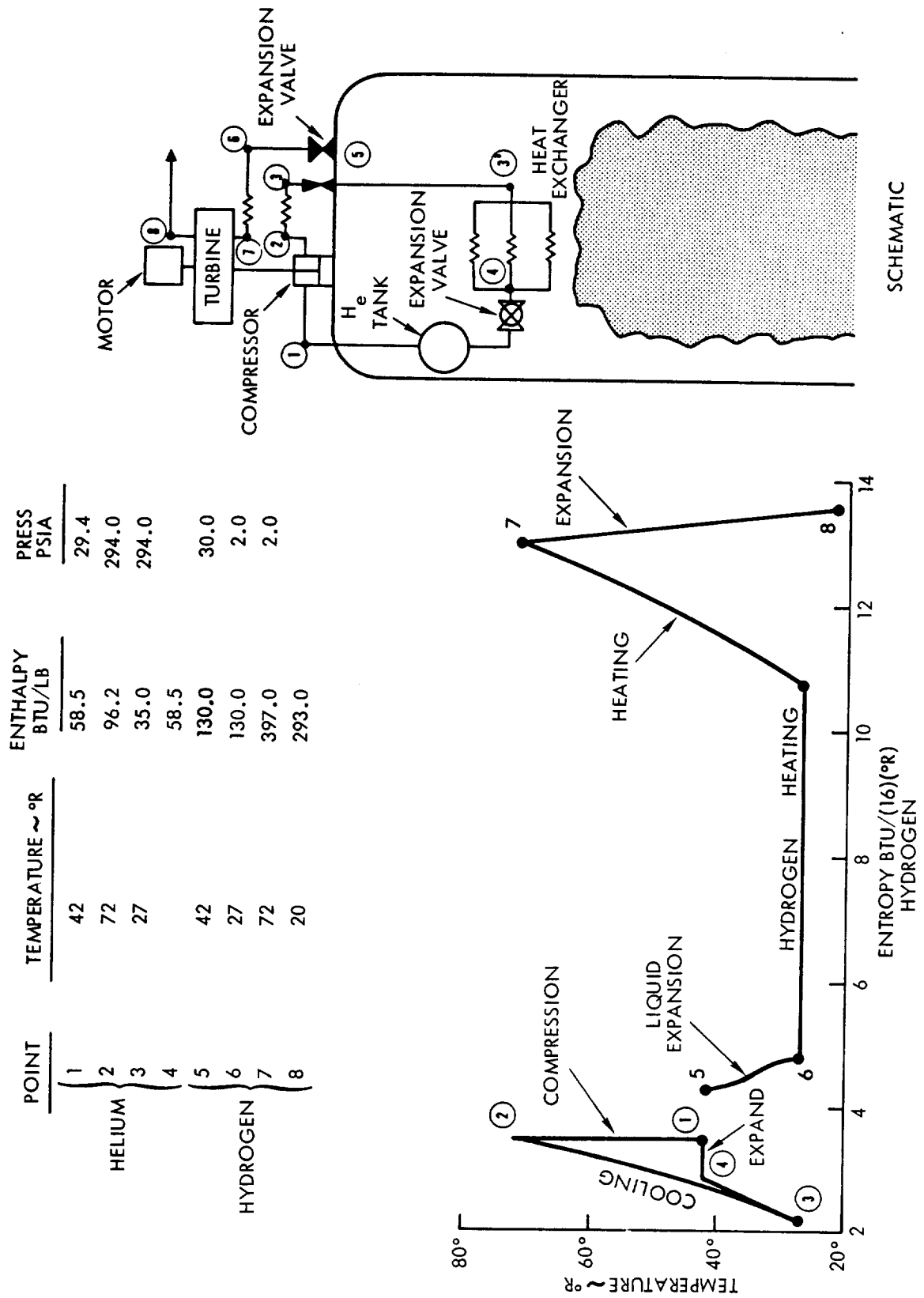
Figure 3-5. Block diagram of venting process shown in Fig. 3-4.

| POINT | | TEMPERATURE ~ °R | ENTHALPY BTU/LB | PRESS PSIA |
|---|---|---|---|---|
| HELIUM | 1 | 42 | 58.5 | 29.4 |
| | 2 | 72 | 96.2 | 294.0 |
| | 3 | 27 | 35.0 | 294.0 |
| | 4 | | 58.5 | |
| HYDROGEN | 5 | 42 | 130.0 | 30.0 |
| | 6 | 27 | 130.0 | 2.0 |
| | 7 | 72 | 397.0 | 2.0 |
| | 8 | 20 | 293.0 | |



Figure 3-4. A zero-g venting process employing a second system which by means of the compression/expansion cycle releases heat to the venting fluid and extracts heat from the remaining propellant.
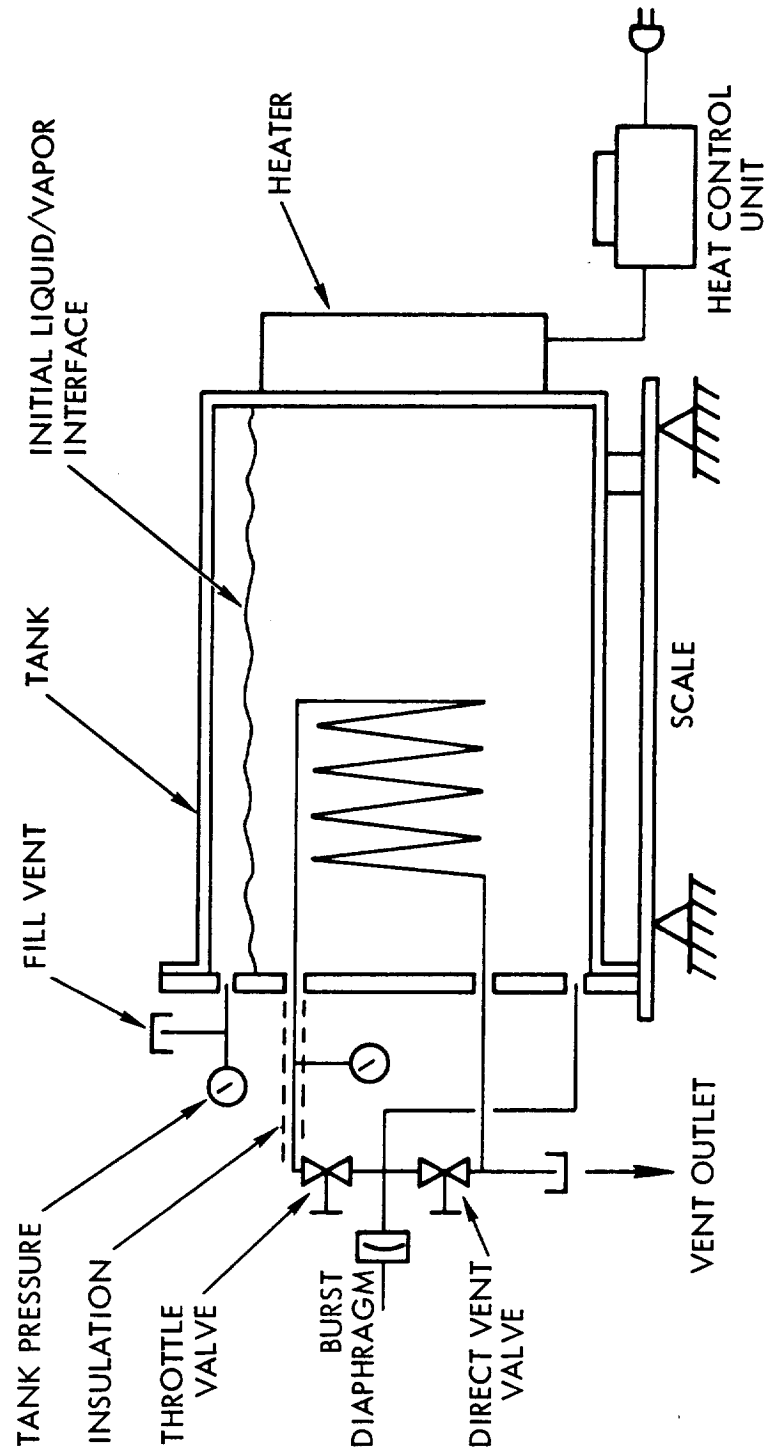
Figure 3-6. Cryogenic Zero-g Thermal Vent Test Fixture Schematic
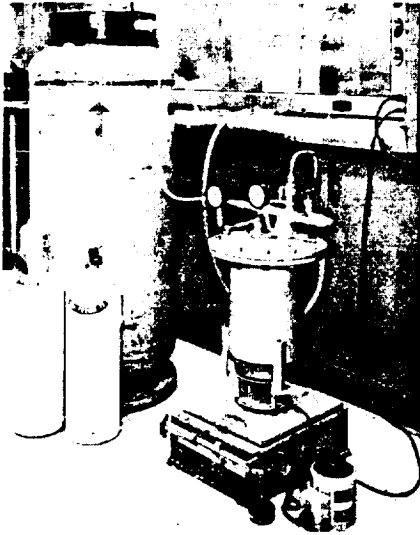
Figure 3-7.    LN$_2$ Cooldown
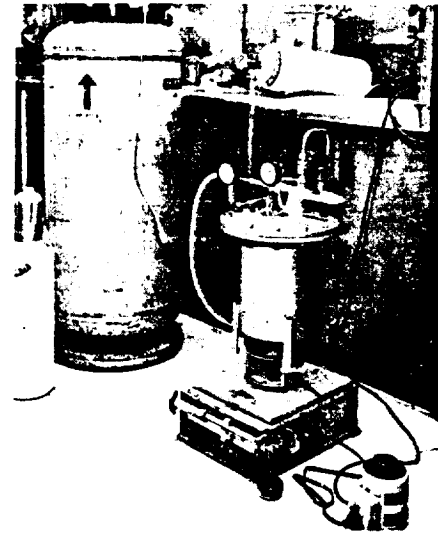


Figure 3-8.    Freon-12 Fill
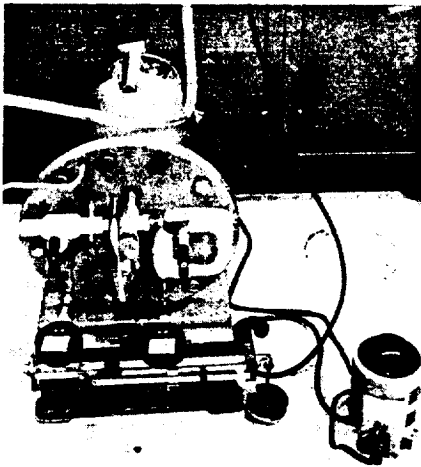


Figure 3-9.    Gas Vent
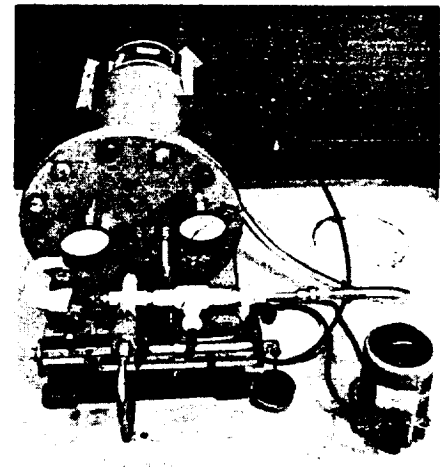


Figure 3-10.  Liquid Vent

THERMAL VENT TEST POSITIONS
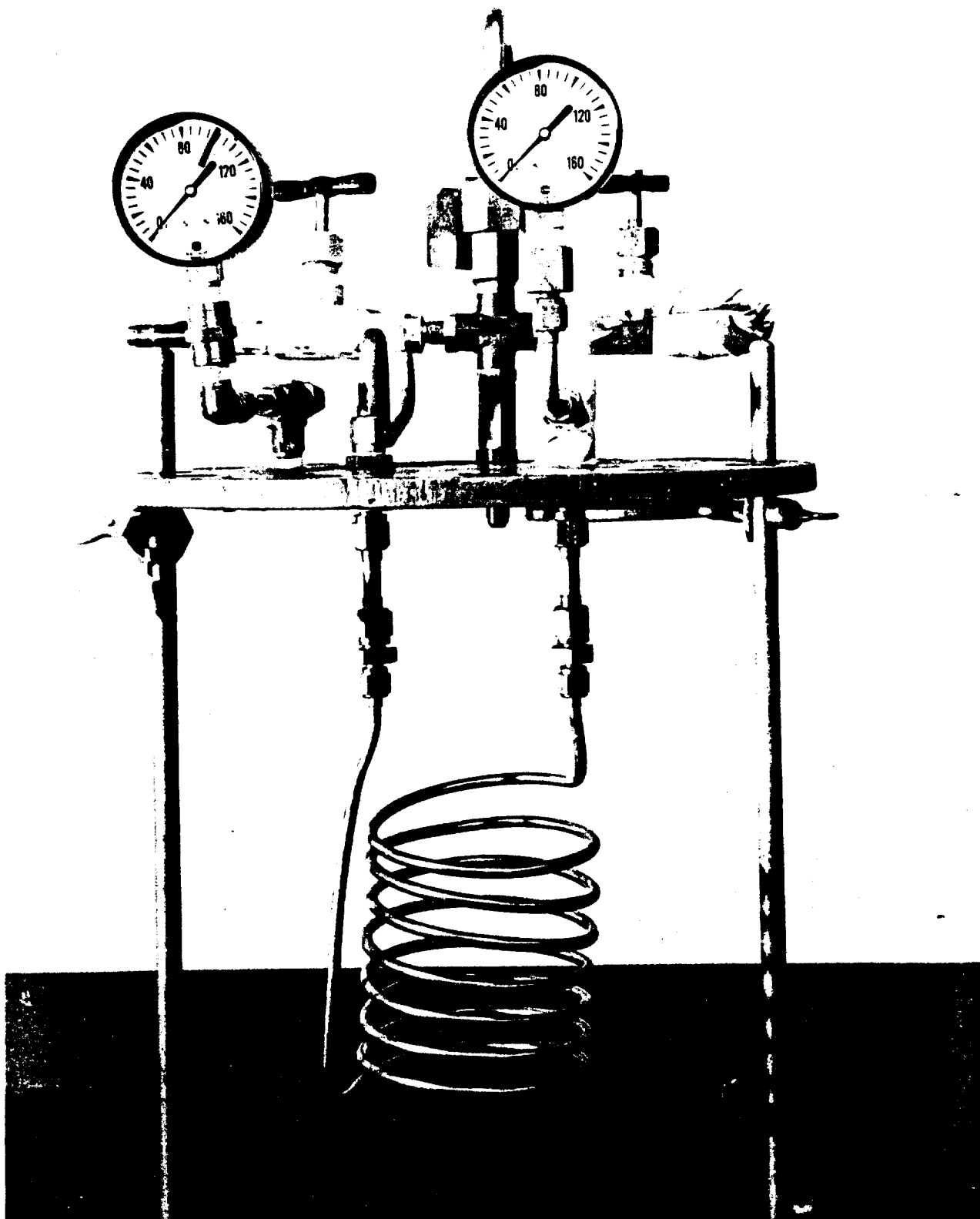
Figure 3-11.  Thermal Vent System

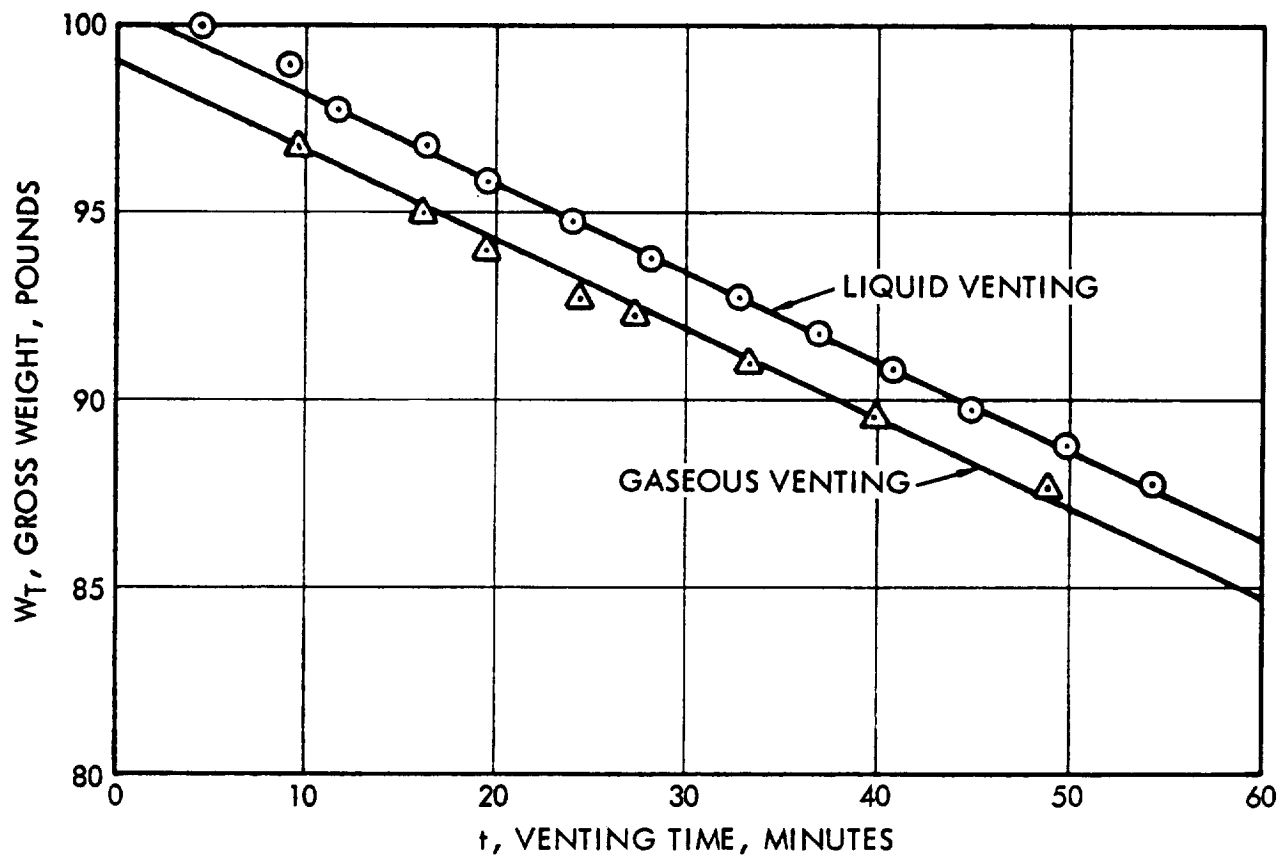ZERO-G VENT SYSTEM TEST DATA

LIQUID FREON-12



Figure 3-12.   Container Gross Weight versus Time

## IV.   RADIOACTIVE PROXIMETER

INTRODUCTION

In view of the fact that a radioactive source may be made small and lightweight and that no contact is required between the radioactive source and the detector to obtain a meaningful output, it was felt that the employment of a radioisotope in a valve position indicating device would provide significant advantages over more conventional techniques.  In concept, valve position would be measured by a source-detector system in which the radioisotope is the particle source: the number of particles striking the particle detector per unit time becomes a measure of the relative displacement between the source and the detector.  Configurations involving both angular and linear displacement between source and detector have been considered.

To demonstrate the feasibility of the use of a radioisotope in a valve position indicating system, the valve actuator of the Lunar Excursion Module (LEM) descent engine was selected as a specific case for analysis.  The requirements associated with the present position measuring device, which utilizes potentiometers, provide a realistic basis for analysis of a positioning device employing a radiating source.

SUMMARY

Three source/detector arrangements were investigated: one involved the change in the solid angle subtended by a point source on a detector with a change in source-to-detector separation distance, and the other two involved a relative change in angular displacement between source and detector.  It was found that, for the LEM valve

actuator, the source sizes (power or rate of energy output) required
for the change in solid angle approach were a factor of 50 or more
larger than the source sizes required for the angular displacement
approach for equivalent particle flux. Small source size is desir-
able, since the larger the source the greater is the radiation
hazard and required shielding.

A device incorporating a split-detector and rotational radioisotope
emitter was found to compare most favorably with the present LEM
potentiometer system. Comparing the present and alternate systems
on a unit-for-unit basis (i.e., one potentiometer versus one proxi-
meter), the power requirements would be slightly decreased for the
proximeter, but the volume and weight of the circuitry required to
back up any one radioisotope positioning device may be somewhat
larger than comparable values for a single potentiometer-based posi-
tioning device. Circuitry volume associated with each radioisotope
device was estimated prior to any attempt at system refinement, to
be within 15 and 25 cubic inches, while the weight was similarly
estimated to be in the range of from one to one-and-a-half pounds.
The weight of circuitry presently associated with each potentiometer
is of the order of one-quarter pound and the volume approximately
7 cubic inches.

The volume of circuitry is important from the standpoint of system
reliability, since the addition of components normally is detrimental.
On a one-for-one basis, assuming validity in estimated weights and
volumes, this would show the proximeter to be inferior. However,
because of the relative insensitivity of the proximeter to vibration,
temperature, fluid environment, etc., it is anticipated that one,
or at most, only two proximeters and their associated electronics

would be required to replace the four potentiometers (and associated electronics) now used. The net effect here, and in most systems so constituted, is expected to be a reduction in total circuitry.

The curves derived in Appendices A, B, and C expand on the analysis of the several source/detector configurations considered for the LEM valve actuator and are applicable to valves in general.

Technical Discussion

As noted in the summary, three general approaches to methods of positioning utilizing a radioisotope were considered. Each of the methods will be discussed in detail here and in the Appendices. The first approach was based upon results published in an Aerojet-General Corporation document (Ref. 1), in which a point source of alpha particles and a beryllium target were used to measure linear displacement between a target and a source. Figure 4-1 shows the general arrangement of source, target, and electronic devices required to analyze the output. Alpha particles from the source, S, travel to the target, T, where they react with the beryllium and produce carbon-12 and a neutron. About 70 percent of the carbon-12 atoms produced are in an excited state and return to the stable or ground state by emitting a 4.4 mev gamma ray. A certain portion of these gammas striking the detector result in voltage pulses which are amplified and then counted by the count rate meter. Thus, the count rate is directly proportional to the number of alphas striking the beryllium target per unit time. The number of alphas, in turn, striking the beryllium target per unit time is proportional to the solid angle subtended by the source on the target. This is a function of

the target radius, r, and the source-to-target distance, d. Thus
for a fixed target radius the change in count rate measured by the
count rate meter is proportional to the change in d. A plot of
solid angle (i.e., alpha particle flux at the target) versus d/r
is given in Figure A-1 of Appendix A.

The major advantage of the above system is the fact that a meaning-
ful detector output may be obtained even though some material is
interposed between the target and detector. The conversion of an
alpha particle flux to a gamma flux through the use of a beryllium
target allows one to place the detector farther from the source
because the interaction probability of a gamma ray with extraneous
matter is much lower than that for an alpha particle. The same
results could be obtained by eliminating the beryllium target and
using a straight gamma source, but this is undesirable, since the
shielding requirements for a gamma source are relatively high.

The major disadvantage of the alpha source/beryllium target approach
is the large quantity of alpha source required to give reasonable
accuracy in the position measurement: the radiation hazard is a
direct function of source quantity. Large source quantities are
a result of the low probability that an alpha particle will produce
a 4.4 mev gamma. There are several ways in which the alpha particle
may lose energy upon entering the beryllium target, only one of
which is production of an activated carbon-12 atom. The cross sec-
tion for the reaction which produces the carbon-12 atom is relatively
low ( - 0.4 barn), and only 70 percent of the carbon-12 atoms produced
are in the excited state (i.e., produce a gamma ray); so alpha sources
must be large to obtain reasonable gamma fluxes at the detector.
Another disadvantage of this approach is the fact that more shielding

would be required to shield the detector from extraneous gamma rays than would be required to shield a detector which detected charged particles such as alphas or betas.

Using the LEM valve actuator design as a test bed, source quantity calculations were performed for the alpha source, beryllium target, and detector arrangement as shown in Figure 4-2. Source size is proportional to the product of the inverse square of the specified resolution (i.e., tolerable uncertainty in the position measurement) and the reciprocal of the counting time. The counting time is governed by the time required for the valve to traverse the resolution distance while moving at maximum velocity, and the statistical error in the count rate is proportional to the square root of the ratio of the count rate to the counting time. Thus, for very fine resolution and relatively high velocity, the counting time is necessarily small, making count rates high to produce good statistical accuracy. Source size is also a function of source to detector distance, since the solid angle subtended by the target decreases with an increase in source to target distance. Source size is plotted versus percent resolution for three counting times and two values of d/r in Figures A-2 and A-3 of Appendix A. Figure A-2 shows that an alpha source size of about one megacurie is required to meet the LEM valve total resolution requirement of 0.6 percent of full stroke. Megacurie source sizes are much too large to consider from a practical handling standpoint. Based upon the AEC tolerable dose rate of 2.5 millirem/hr and considering a distance of 6 inches from the point source, the upper limit on a Polonium-210 alpha source with about 6 millimeters of tungsten shielding is about 15 curies. In view of this fact the alpha source, beryllium target configuration was not considered feasible for use with the LEM valve actuator.

Before abandoning the solid angle approach, source size calculations were performed for a source-detector arrangement in which the source particles are detected directly. Source size requirements for this arrangement are shown in Figures A-4 and A-5 of Appendix A. Figure A-4 shows that a source size of about one curie is required to obtain the specified LEM resolution. A one curie source size, although not completely impractical from a radiation hazards standpoint--assuming a Polonium-210 alpha source could be used--produces count rates of the order of $10^9$ counts per second. Count rates exceeding $10^6$ counts per second are very difficult to analyze electronically so this approach was considered unfeasible for the LEM valve actuator from an electronic standpoint.

It should be pointed out here that for a valve stroke less than that specified for the LEM valve (0.8 inch), the change in solid angle approach may permit smaller source sizes because of the lower $d/r$ ratio which results. A comparison of the source size requirements for two $d/r$ ratios may be made by referring to Figures A-4 and A-5 of Appendix A. The comparison shows that as the $d/r$ ratio is reduced from 5 to 1, the source size is reduced by about a factor of 10. The value of $d/r = 1$ corresponds to the LEM valve at the zero position while the value of 5 corresponds to the LEM valve at 100 percent stroke. Maximum sensitivity (i.e, the greatest change in count rate per unit change in separation distance) occurs at a $d/r$ value of 0.706.

Since the change in solid angle approach did not appear attractive for use with the LEM valve actuator, an alternate approach was sought which would result in smaller source requirements. The result was the source detector arrangement shown in Figure 4-3. In concept, the rotating shaft has a quadrant of its surface coated with a

radioisotope. The shaft is surrounded by a four-quadrant detector which has four outputs: plus x, plus y, minus x and minus y. The X-Y output from the detector defines the angle, θ, through which the shaft has rotated from a zero position. Appendix B contains the development of the relationship between the source size, the resolution, and the counting time.

Figure B-3 in Appendix B shows that a source of about one millicurie is required to attain the LEM specified resolution if the counting efficiency of a solid state detector is assumed to be unity and a geometry factor of 0.5 is used; i.e., half of the particles leaving the source are counted. Thus, source sizes are down by a factor of about $10^3$ from the source sizes required for the solid angle approach. There are two reasons why the source sizes are so greatly reduced. One is the fact that the geometry factor for the rotational approach is about a factor of 50 times the geometry factor for the solid angle device. The other is the fact that the sensitivity of the rotational device is much greater; i.e., small changes in valve motion result in large changes in the output signal from the detector. Figure 4-4 shows the location of the device in the LEM valve actuator. A source size of one millicurie does not represent a radiation hazard: Based on a dose rate of 2.5 millirem/hr, a distance of 6 inches and a typical shield thickness of 6 millimeters of tungsten, the tolerable curie levels for representative alpha, beta and gamma sources are, respectively, about 15 curies of Polonium-210, about 45 millicuries of Strontium-90, and about 60 microcuries of Cobalt-60.

Although the four-quadrant detector is attractive from the standpoint of source size, the development in Appendix B shows that the output signal from the detector is non-linear. A non-linear signal must be linearized for use in feedback control. The circuitry required to provide a signal useful for feedback control to the LEM valve actuator motors adds complexity to the system and decreases the reliability of the system.

Realizing the desirability of a linear output for feedback control, source-detector configurations were investigated which would yield a linear output. Figure 4-5 shows a concept which yields a detector output which is directly proportional to angular shaft motion. Half of the circumference of the shaft is coated with a radioisotope, and the difference between the outputs from the two detectors yields a linear response. The development of the relationship between source size, resolution, and counting time is presented in Appendix C. Figures C-1 and C-2 in Appendix C show the detector response as a function of angular shaft displacement, $\theta$, and the obtainable resolution in shaft motion as a function of $\theta$, respectively. Figure C-3 shows the source size as a function of total resolution requirement, and shows that a source size of about 50 millicuries is required for the LEM valve actuator. This source size is reasonable from a radiation hazard standpoint, although the count rate at the detector is relatively high.

Since the divided detector yields a reasonable source size and a linear response, a particular system based upon its use was considered for the LEM valve actuator. It appears that the circuitry required for the proximeter approach will be more complex than the

circuitry required for each potentiometer of the system presently employed in the LEM valve actuator. The power requirements for the two systems would be quite similar. Since the anticipated reliability of a developed source and detector will be high, the total circuitry is expected to be reduced by the need for fewer source/detector units. A pictorial representation of the system required for the proximeter, utilizing a detector with a linear output, is shown in Figure 4-6. Estimates of the weights and volume of the electronic components are one to one-and-a-half pounds and 25 cubic inches, respectively. The weight of the present LEM valve potentiometer circuitry is of the order of one-quarter pound. Consideration of the count rate circuitry of the two systems on a one-to-one basis would, therefore, appear to present a possible reduction in reliability for the proximeter configuration; i.e., the mean time to failure for the radioisotope system would be lower. The smaller number of proximeters expected to be required, however, should be more than compensative in reduced circuitry on a total system basis. A gain in overall reliability is anticipated. Additional advantages of the radio-isotope device lie in the fact that no contact between source and detector must be made and the inertia effects attributable to the measuring device are very small: the weight of a 50 millicurie beta source is of the order of $10^{-3}$ gm.

Conclusions and Recommendations
----

It appears that a positioning device based upon the use of a radio-isotope is feasible. However, since the circuitry required to productively use the output from the source/detector combination is relatively complex, carte blanche approval of the concept cannot

be stated. The following qualifications must be made:

1. For non-critical missions where the environment will permit a single potentiometer to operate continuously with high reliability, a radio-isotope-based position indicator would appear to add complexity and weight to circuitry.

2. When environmental, physical, and/or thermal factors dictate the use of redundant potentiometers to achieve desired system reliability, the radioactive proximeter technique appears to provide a method for increasing overall reliability.

3. An additional area of potential usage for this concept is one in which no contact is permitted with the device whose position is to be detected and no detectable loading of that device can be tolerated. Although available test components based on the use of magnetic fields fulfill the first of these needs, they generally impose objectionable inertia loads.

In general, it appears that a source-detector device based upon the change in solid angle approach may be used to indicate valve position for valves which move in a linear manner at moderate speeds. Either the four-quadrant detector or the divided detector may be used to indicate valve position for valves which move in a rotary manner.

The two major problems associated with a radioisotope position indicator are the counting time required to obtain good statistical accuracy and the circuitry required to analyze the detector output. If feedback control is required, an additional burden is placed on the source-detector system in that a linear detector output becomes desirable. Laboratory scale testing of the devices shown in Figures 4-3 and 4-5 would be desirable for the purpose of obtaining practical knowledge with respect to the fabrication and testing of such devices. Also desirable would be a detailed analysis of the electrical circuits required to obtain an output from the four-quadrant detector.
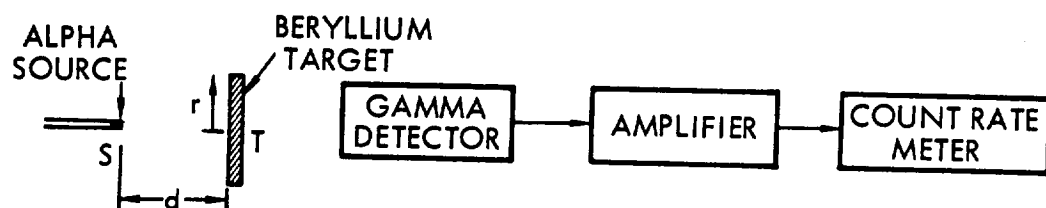
Figure 4-1.  Alpha Source, Beryllium Target Positioner
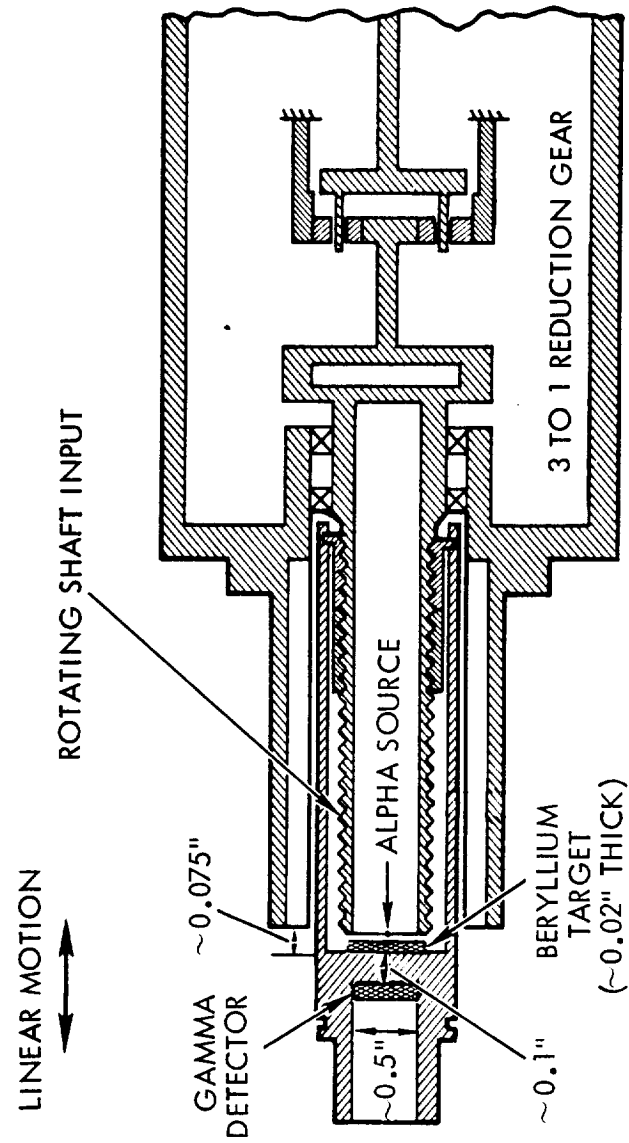
Figure 4-2. LEM Valve Actuator Geometry
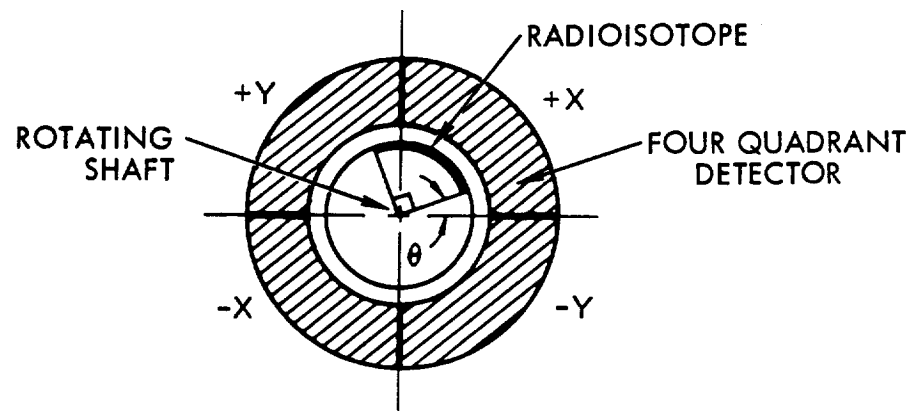
Figure 4-3.  Four Quadrant Position Indicator
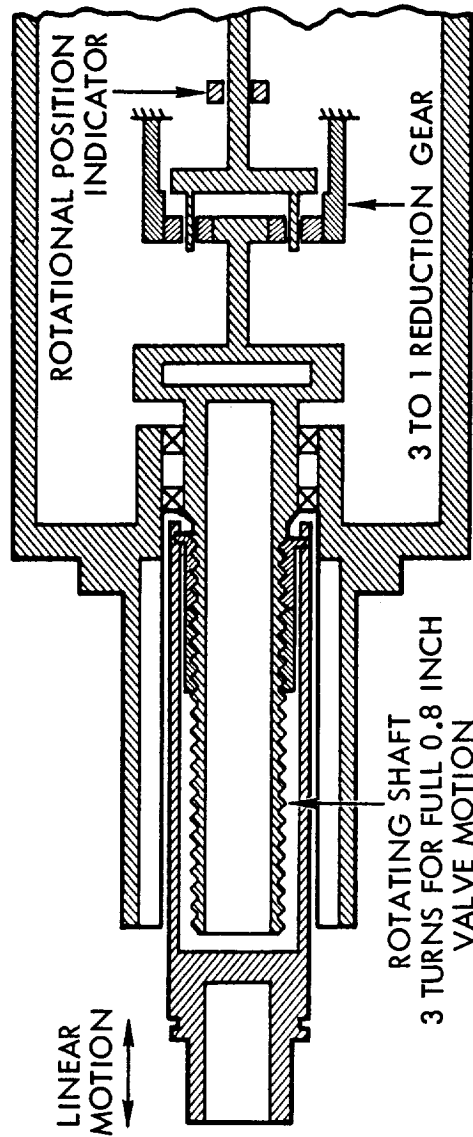
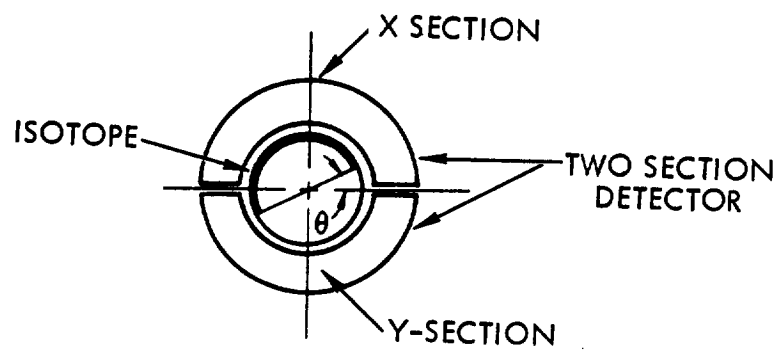Figure 4-4. Rotational Positioning Device

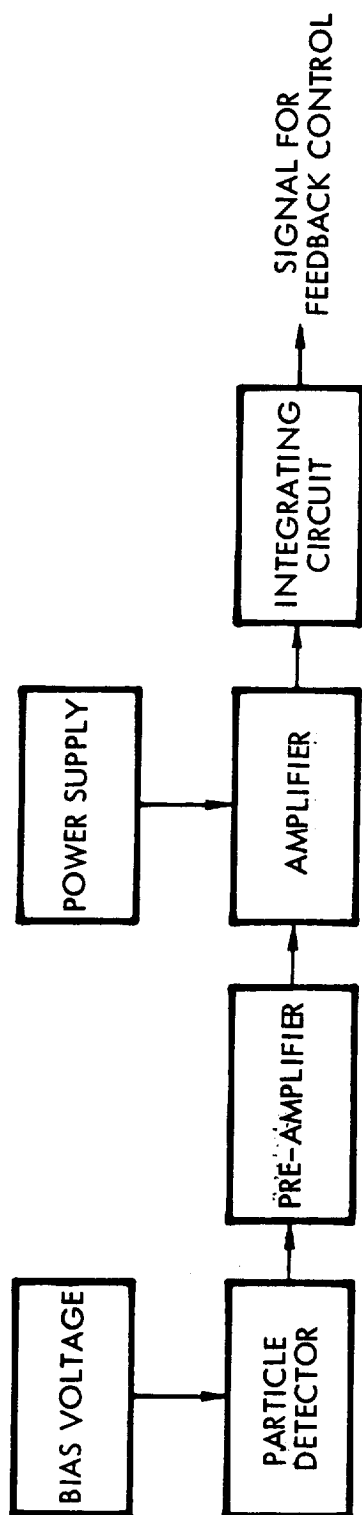Figure 4-5. Linear Output Rotational Positioning Device

Figure 4-6. Radioisotope Positioner Electronic Components

APPENDIX A

## Solid Angle Position Indicator

The relationships between the various parameters of interest for the
solid angle positioning device are derived in Reference 1 and will
not be discussed here. Curves, of interest from a valve position
measurement standpoint, are presented in Figures A-1 through A-5.

Figure A-1 shows the solid angle subtended by a point source on a
detector as a function of the ratio of source-to-detector distance
to the detector radius, $d/r$. Since the count rate from the detector
is directly proportional to the solid angle subtended by the source,
Figure A-1 shows the detector output as a function of source to
detector distance. As may be observed, the output is nonlinear. It
should be further noted, with respect to Figure A-1, that a signifi-
cant decrease in source size may be obtained by shifting the $d/r$
ratio limits to the left, i.e., by moving the source as close to the
beryllium target as possible and having as large a target radius
as practical. For example, Figure A-1 shows that a change in the
$d/r$ ratio of from 5.0 to 1.0 decreases the required source size for
comparable output by a factor of about 10. Assuming the same target
radius and minimum $d/r$ value, valves with short strokes will require
even smaller sources.

Figures A-2 and A-3 show the alpha source sizes required to produce
various total resolution percentages for the alpha source/beryllium
target approach. Curves are presented for two values of $d/r$ and
for three different counting times. Counting time was determined
by dividing the resolution interval into either 1, 5, or 10 counting
times as given by equation A-1:

$$t = \frac{(\triangle L)_r \; L_{tot}}{n \; v \; (100)} \tag{A-1}$$

where t   =   counting time, seconds

$\triangle L_r$    =   percentage total resolution, per cent

$L_{tot}$    =   total linear valve stroke, inches (taken as 0.8 inch)

n   =   the number of counting times per resolution interval (1, 5, or 10)

v   =   maximum valve velocity, in/sec (taken as 1 in/sec)

Figure A-2 is based upon a d/r ratio of 5.0 which corresponds to the LEM valve at 100 per cent stroke. Figure A-3 is based upon a d/r ratio of 1.0 and corresponds to the LEM valve at zero per cent stroke. The resolution for the LEM valve actuator is given as ± 0.3 per cent of full stroke in the LEM valve actuator specifications.

Figures A-4 and A-5 are similar to Figures A-2 and A-3 except for the fact that Figures A-4 and A-5 are for a system in which the source particles are detected directly, i.e., no beryllium target is used.

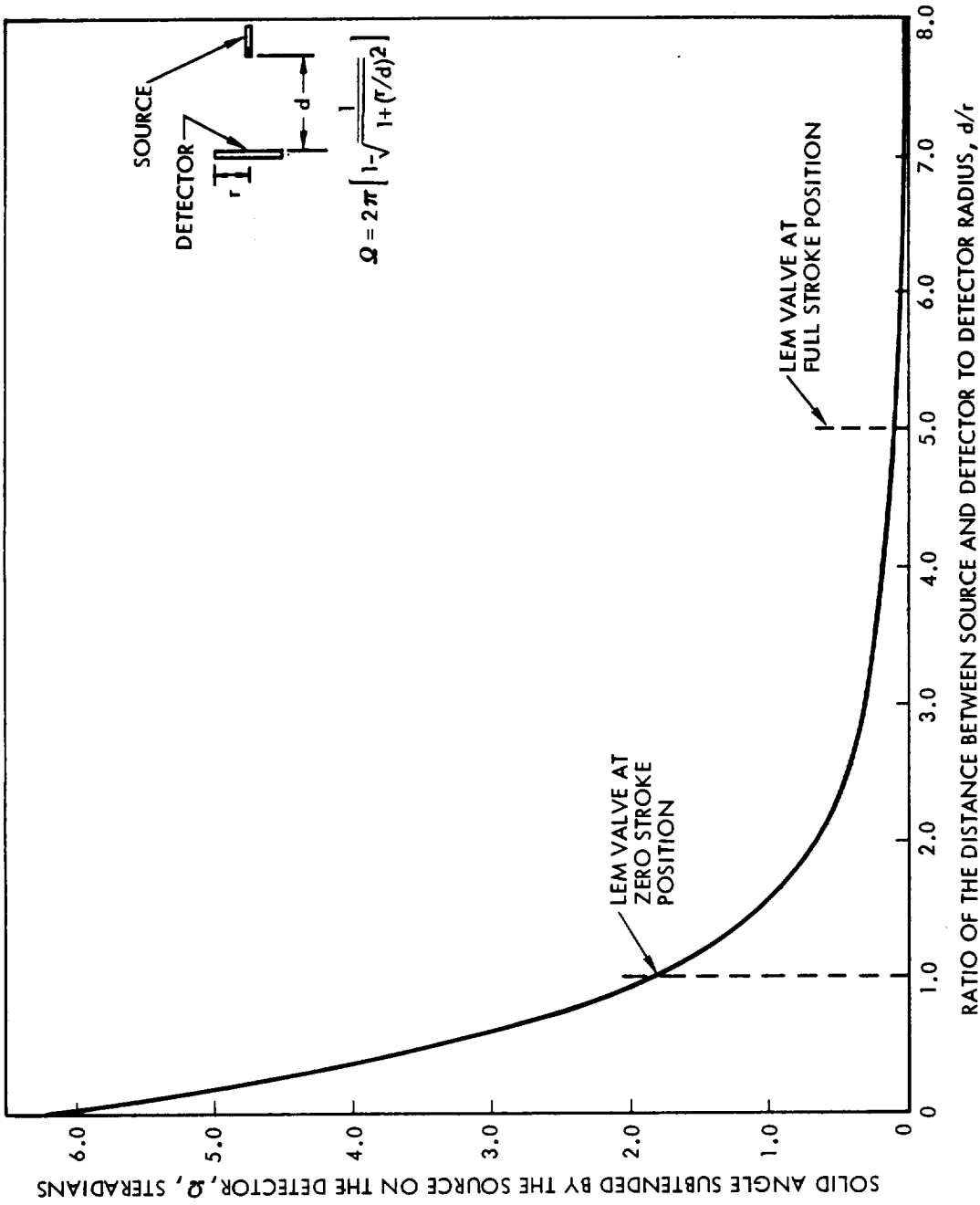$$\Omega = 2\pi \left[ 1 - \sqrt{\frac{1}{1+(r/d)^2}} \right]$$

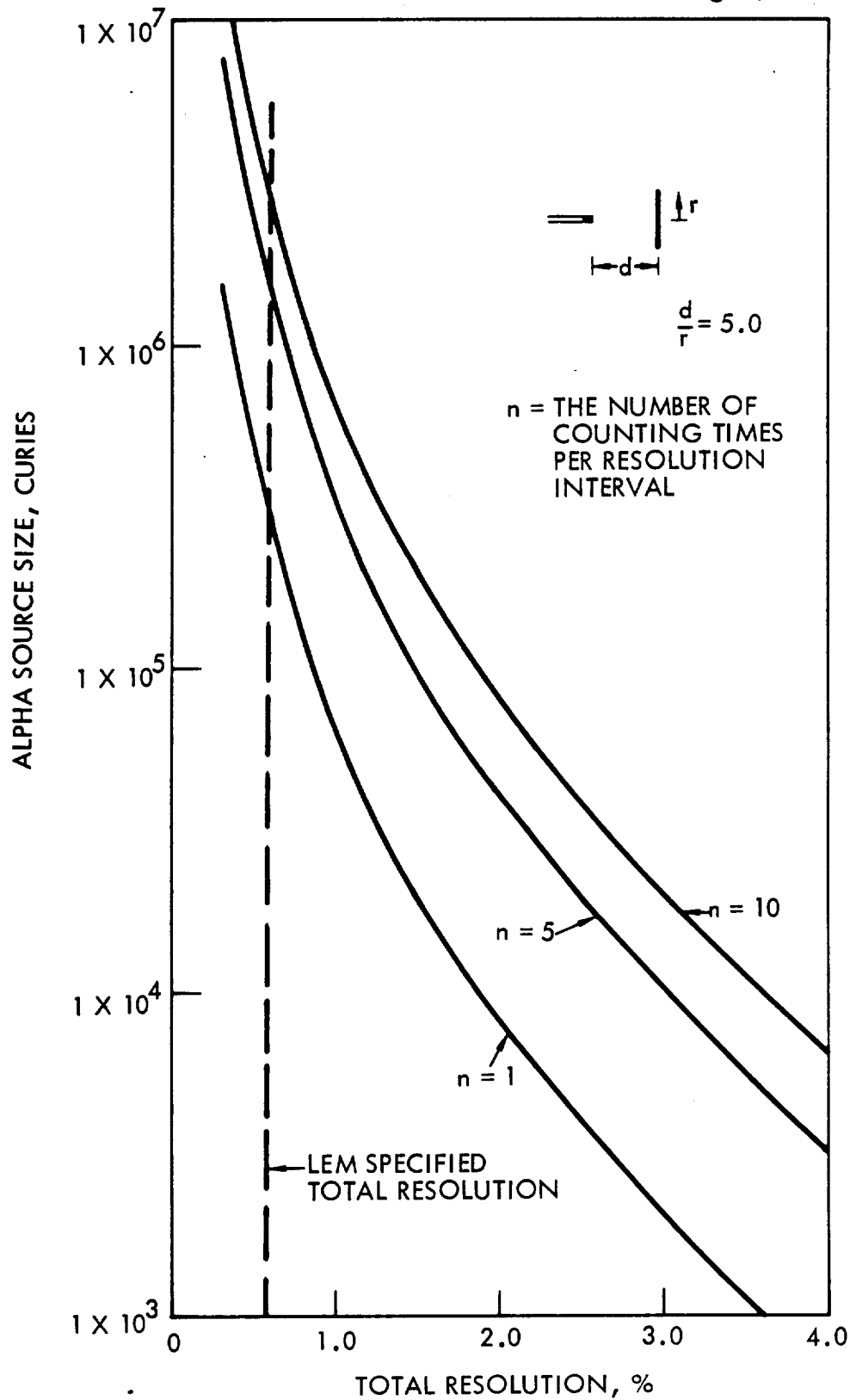Figure A-1.   Output From the Solid Angle Position Indicator

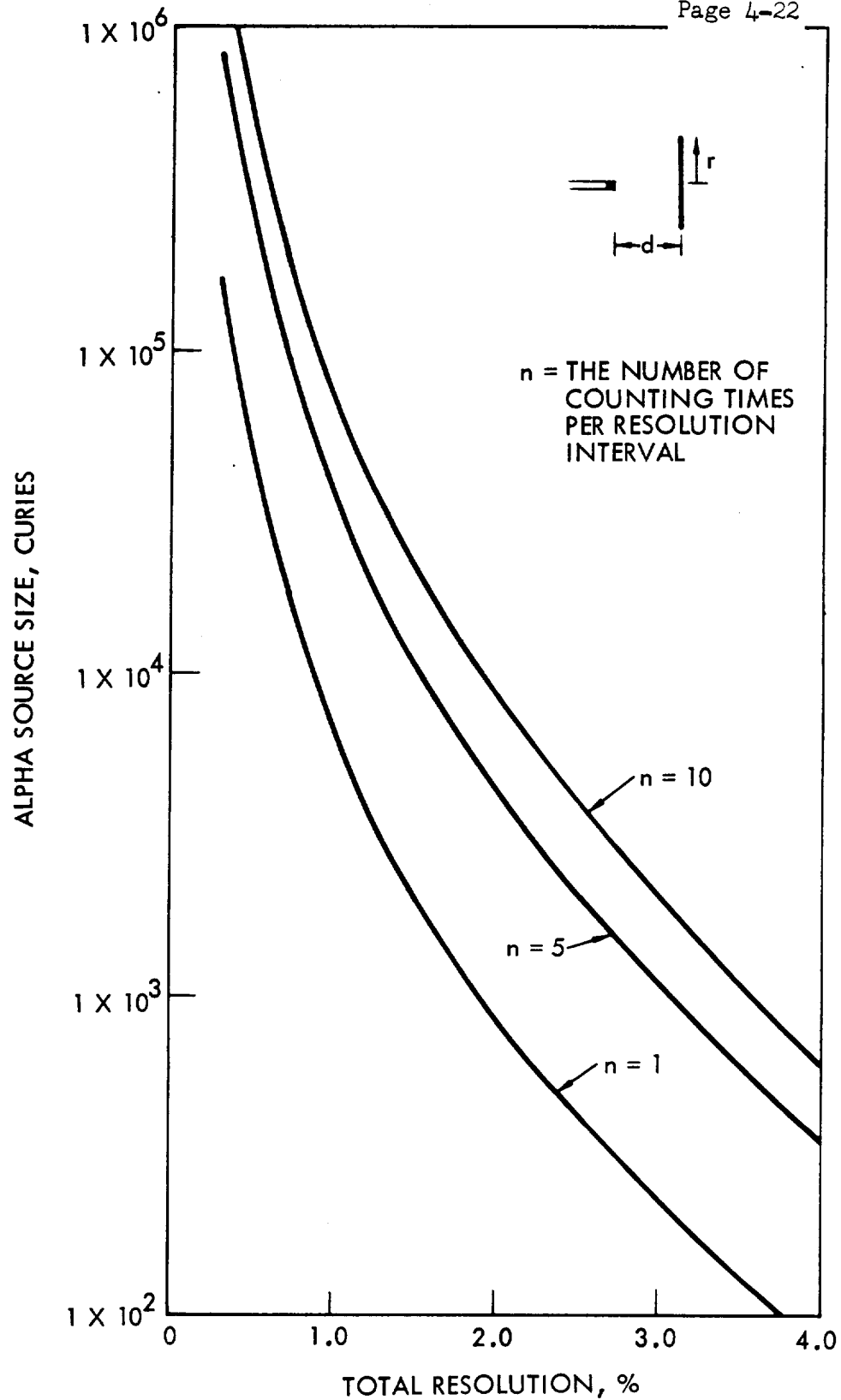Figure A-2. Source Size for the Alpha Source/Beryllium Target Solid-Angle Position Indicator for d/r = 5.0

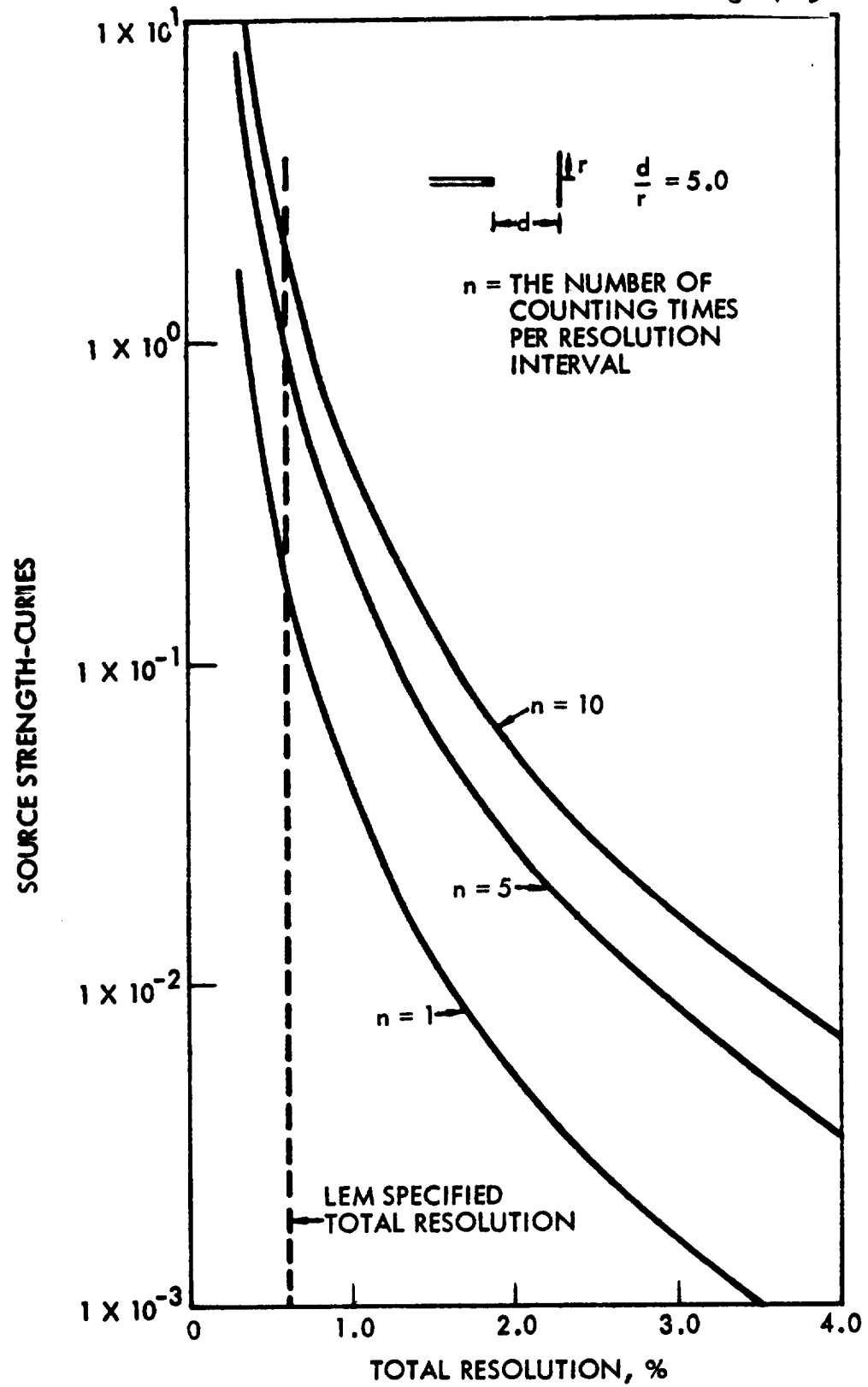Figure A-3. Source Size for the Alpha Source/Beryllium Target Solid Angle Position Indicator for d/r = 1.0

Figure A-4. Source Size for the Solid Angle Position Indicator
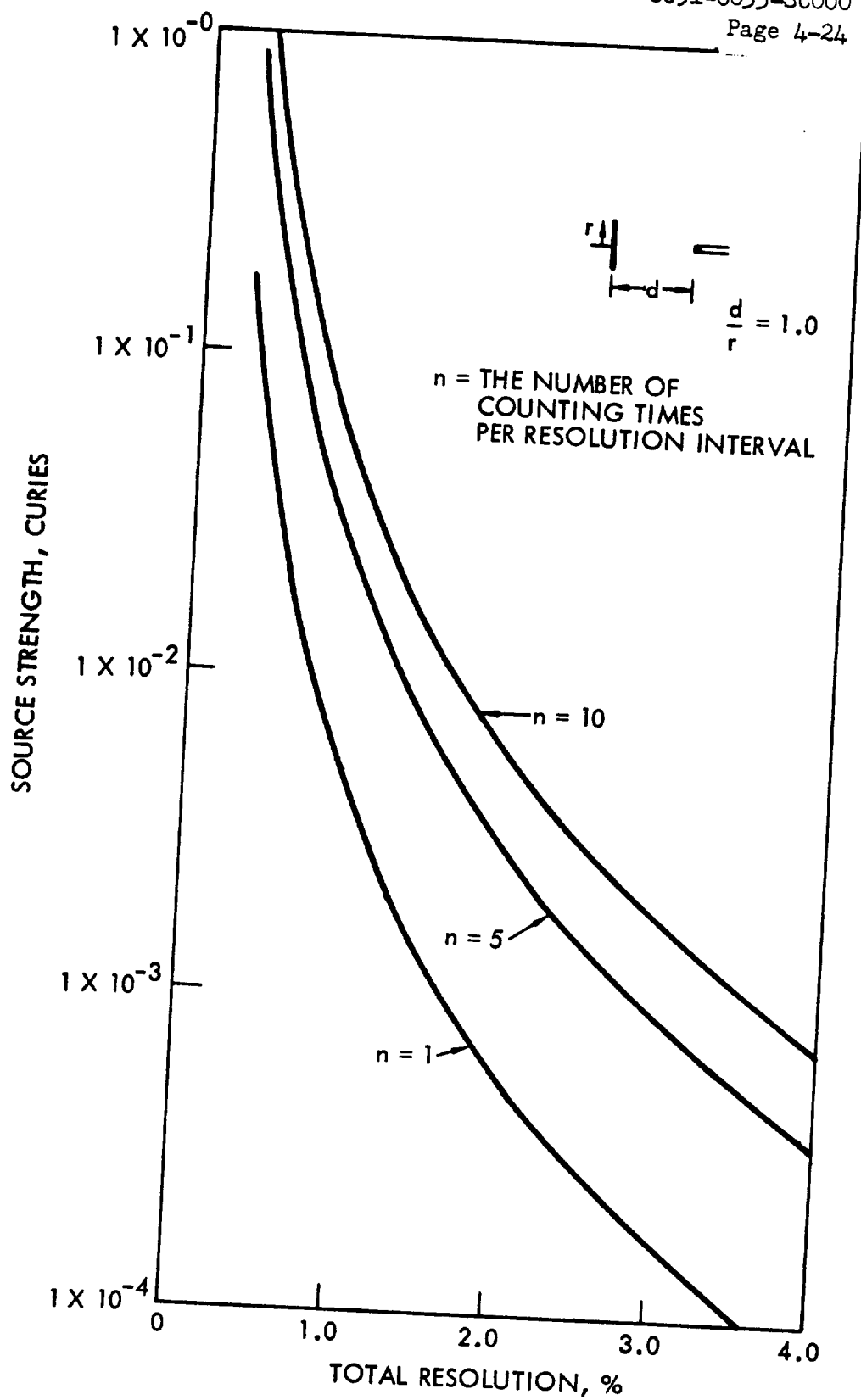Which Detects Source Particles (d/r = 5.0)

Figure A-5. Source Size for the Solid Angle Position Indicator Which Detects Source Particles (d/r = 1.0)

APPENDIX B

The Four-Quadrant Rotational Position Indicator

Figure 4-3 shows a sketch of the four quadrant rotational positioner. The count rates from the x- and y-quadrants of the detector for the position shown in Fig. 4-3 are given by equations B-1 and B-2.

$$R_x = \frac{2SKG}{\pi} \left(\frac{\pi}{2} - \Theta\right) \qquad (B-1)$$

$$R_y = \frac{2SKG}{\pi} (\Theta) \qquad (B-2)$$

where:   $R_x$   = count rate from the x-quadrant, cps

$S$    = radioisotope source strength, cps
(1 curie = $3.7 \times 10^{10}$ cps)

$K$    = detector efficiency (taken as 1.0 for a solid state detector)

$G$    = source-to-detector geometry factor (taken as 0.5)

$\Theta$    = angle through which the shaft has rotated from the zero position, radians

$R_y$    = count rate from the y-quadrant, cps

The sum of the count rates is a constant, assuming that detector efficiencies and geometry factors for the two quadrants are equal. An x-y plot of the theoretical output from the detector is shown in Figure B-1.

The angle $\Theta$, through which the shaft rotates is directly proportional to the linear motion of the LEM valve, and is related to the angle, $\propto$, shown in Figure B-1 by equation (B-3). The count rate ratio defines

$$\propto = \arctan \frac{R_y}{R_x} = \arctan \frac{\Theta}{\frac{\pi}{2} - \Theta} \qquad (B-3)$$

the angle, $\alpha$ , and thus defines the angle, $\theta$, and the valve position. The tolerable error in $\theta$ is then directly reflected in a tolerable error in $\alpha$ and, in turn, a tolerable error in the count rate ratio. From statistics:

$$\sigma_\alpha = \left[ \left( \frac{\partial \alpha}{\partial R_x} \right)^2 \sigma_{R_x}^2 + \frac{\partial \alpha}{\partial R_y}^2 \sigma_{R_y}^2 \right]^{1/2} \quad (B-4)$$

where: $\sigma$ = the standard deviation in the quantity of interest

$$\sigma_{R_x} = \sqrt{\frac{R_x}{t}}$$

$$\sigma_{R_y} = \sqrt{\frac{R_y}{t}}$$

Taking the partial derivatives indicated in equation B-4, utilizing equation B-3 and substituting back into B-4:

$$\sigma_\alpha = \frac{1}{R_x^2 + R_y^2} \left\{ \frac{R_y^2 R_x}{t} + \frac{R_x^2 R_y}{t} \right\}^{1/2} \quad (B-5)$$

and,

$$\sigma_\alpha = \frac{d\alpha}{d\theta} \sigma_\theta$$

Taking the derivative and substituting:

$$\sigma_\alpha = \frac{2\pi}{\pi^2 - 4\pi\theta + 8\theta^2} \sigma_\theta \quad (B-6)$$

Measuring differences in $\alpha$ :

$$\sigma_\alpha = \left( \sigma_{\alpha_1}^2 + \sigma_{\alpha_2}^2 \right)^{1/2}$$

For measuring small differences, $\alpha_1$, is equivalent to $\alpha_2$ and:

$$\sigma_{\Delta\alpha} = \sqrt{2}\ \sigma_\alpha \tag{B-7}$$

The relationship given by B-6 holds for difference measurements as well as for direct measurements. Substituting equations B-1, B-2, B-6, and B-7 into equation B-5:

$$\sigma_{\Delta\theta} = \frac{\left[\theta\ (\pi-2\theta)\right]^{1/2}}{\sqrt{SGKt}} \tag{B-8}$$

For the differential measurement, $\Delta\theta$, to have a 95.4 per cent probability of falling within $\Delta\theta \pm 2\sigma_{\Delta\theta}$, the resolution in a $\Delta\theta$ measurement, $\Delta\theta_r$, is given by:

$$\Delta\theta_r = 4\sigma_{\Delta\theta} \tag{B-9}$$

Substituting B-9 into B-8:

$$\Delta\theta_r\sqrt{SKGt} = 4\left[\theta\ (\pi-2\theta)\right]^{1/2} \tag{B-10}$$

Figure B-2 is a plot of equation B-10 and shows the theoretical resolution obtainable in a shaft position measurement for a constant source strength as a function of shaft position. Although the plot pertains only to a single quadrant, similar plots may be obtained for each of the four quadrants.

Figure B-3 shows the source strength required as a function of total resolution for the four quadrant device.
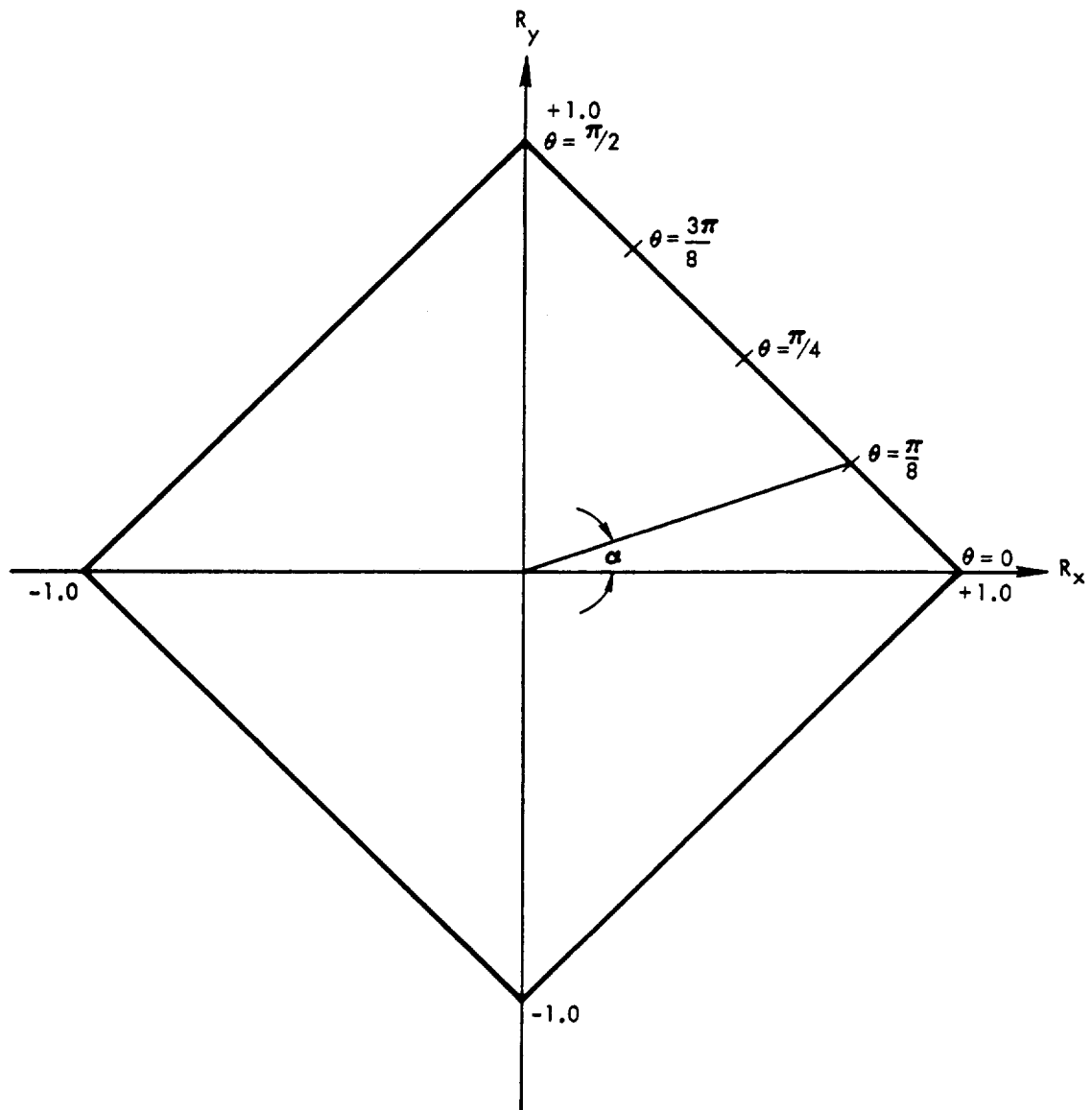
Four-Quadrant Detector Output

FIGURE B-1
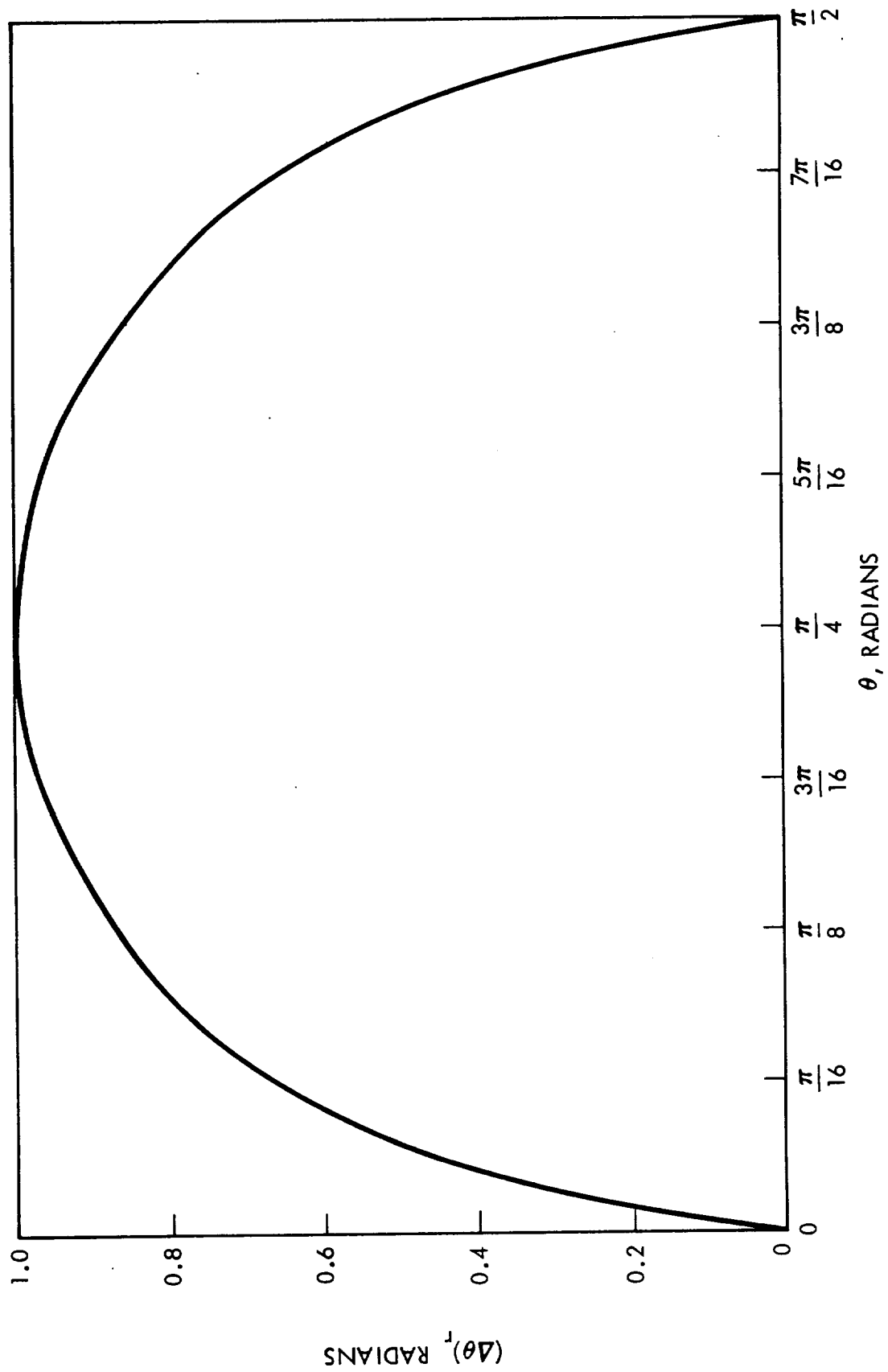
Error in Shaft Position Measurement As a Function of Shaft Position
For Constant Source Strength

FIGURE B-2

n = THE NUMBER OF
COUNTING TIMES
PER RESOLUTION
INTERVAL
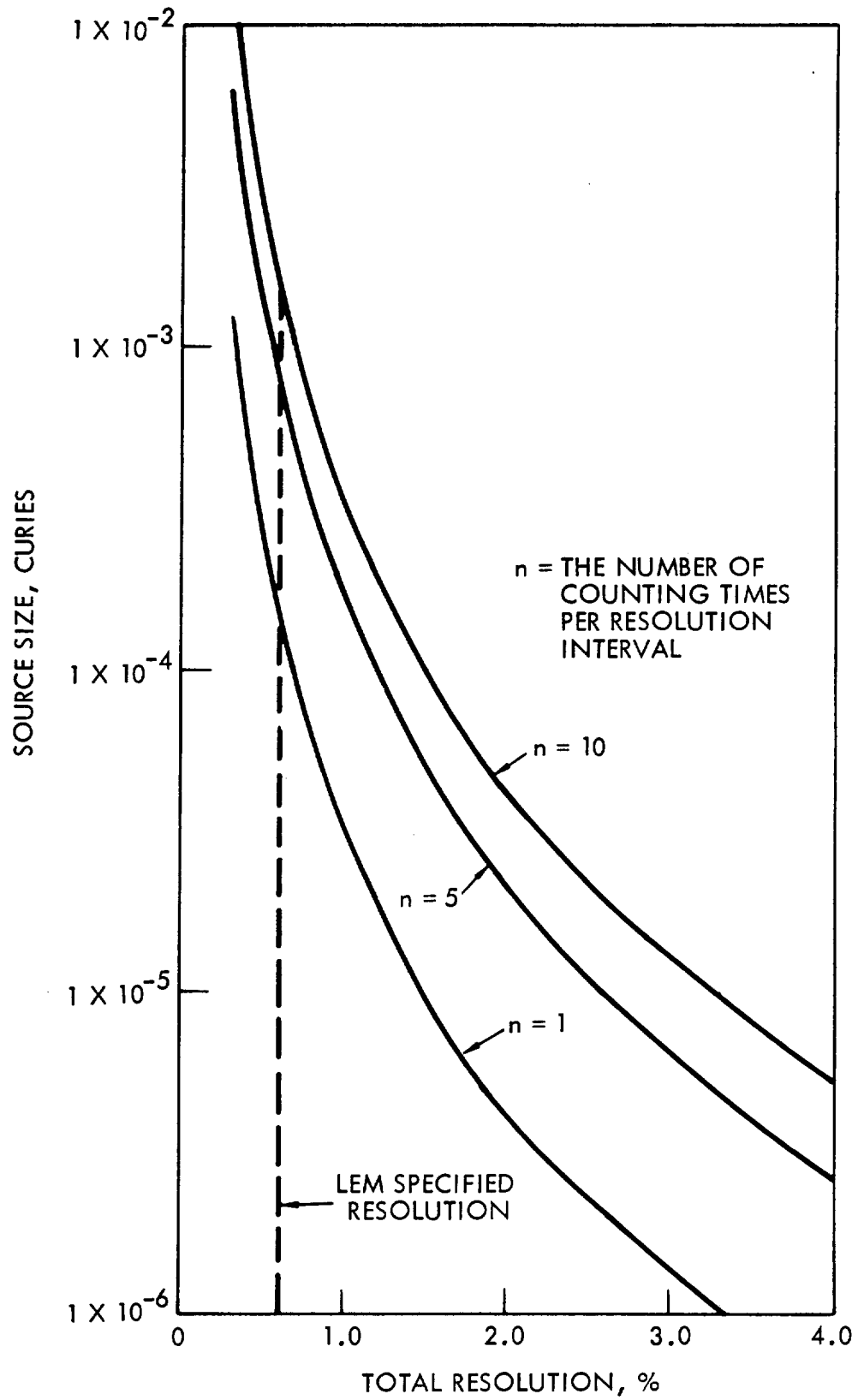
n = 10

n = 5

n = 1

LEM SPECIFIED
RESOLUTION

Figure B-3. Source Size Required for the Four Quadrant
Rotational Positioner

APPENDIX C

Divided Detector Position Indicator

Figure 4-5 shows a sketch of the divided detector. The count rates from the x and y detectors are given by:

$$R_x = \frac{SGK}{\pi}(\pi-\theta) \qquad 0 \le \theta < \pi$$
$$\text{and } R_x = \frac{SGK}{\pi}(\theta-\pi) \qquad \pi \le \theta \le 2\pi \qquad \text{(C-1)}$$

$$R_y = \frac{SGK}{\pi}\theta \qquad 0 \le \theta \le \pi$$
$$\text{and } R_y = \frac{SGK}{\pi}(2\pi-\theta) \qquad \pi < \theta \le 2\pi \qquad \text{(C-2)}$$

where:   $R_x$ = count rate from x detector, cps

   $R_y$ = count rate from y detector, cps

   S = source strength, cps

   G = the geometry factor, (taken as 0.5)

   K = the detector efficiency, (taken as
       1 for a solid state detector)

   $\theta$ = shaft displacement angle, radians

Taking the difference between count rates, we have:

$$R = R_y - R_x = \frac{SGK}{\pi}(2\theta - \pi) + I_o \qquad 0 < \theta \le \pi$$
$$\text{and } R = R_y - R_x = \frac{SGK}{\pi}(3\pi - 2\theta) + I_o \qquad \pi < \theta \le 2\pi \qquad \text{(C-3)}$$

The detector output is superimposed upon some constant signal, $I_o$, to obtain an output signal which is always positive. By substituting $\theta = 0$ into equations C-3, we obtain $I_o$ = SGK, and equations C-3 become:

$$R = \frac{SGK}{\pi}(2\theta - \pi) + SGK \qquad 0 \le \theta - \pi$$

$$\text{and } R = \frac{SGK}{\pi}(3\pi - 2\theta) + SGK \qquad \pi \le \theta \le 2\pi$$

$$\left. \right\} \quad (C-4)$$

Figure C-1 shows the detector output as a function of $\theta$.

Using methods similar to those applied in Appendix B, the following expression was developed for the relationship between tolerable error in shaft position measurement, source size and counting time:
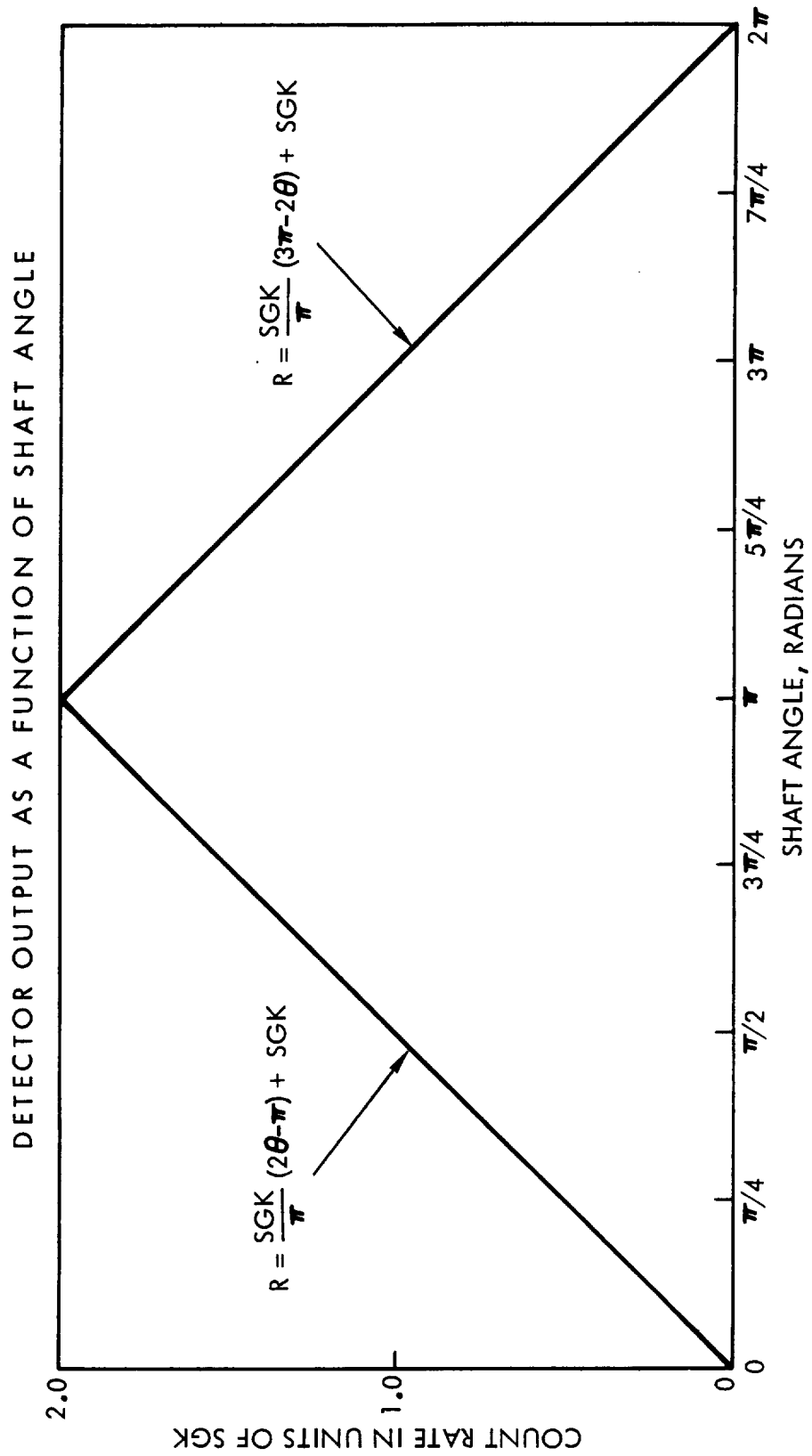
$$S = \frac{16\pi\theta}{KGt(\Delta\theta_r)^2} \qquad (C-5)$$

where: S, K, G, $\theta$ and t are as defined previously and

$\Delta\theta_r$ = the tolerable error in shaft angular position measurement, radians

Figure C-2 is a plot of equation C-5 for constant source strength.

Figure C-3 shows the radioisotope source size as a function of total tolerable resolution.

DETECTOR OUTPUT AS A FUNCTION OF SHAFT ANGLE

$$R = \frac{SGK}{\pi}(2\theta - \pi) + SGK$$

$$R = \frac{SGK}{\pi}(3\pi - 2\theta) + SGK$$

SHAFT ANGLE, RADIANS

COUNT RATE IN UNITS OF SGK

Detector Output As a Function of Shaft Angle

Figure C-1

RESOLUTION AS A FUNCTION OF SHAFT POSITION

RESOLUTION, $\Delta\theta_r$, RADIANS

SHAFT POSITION, $\theta$, RADIANS
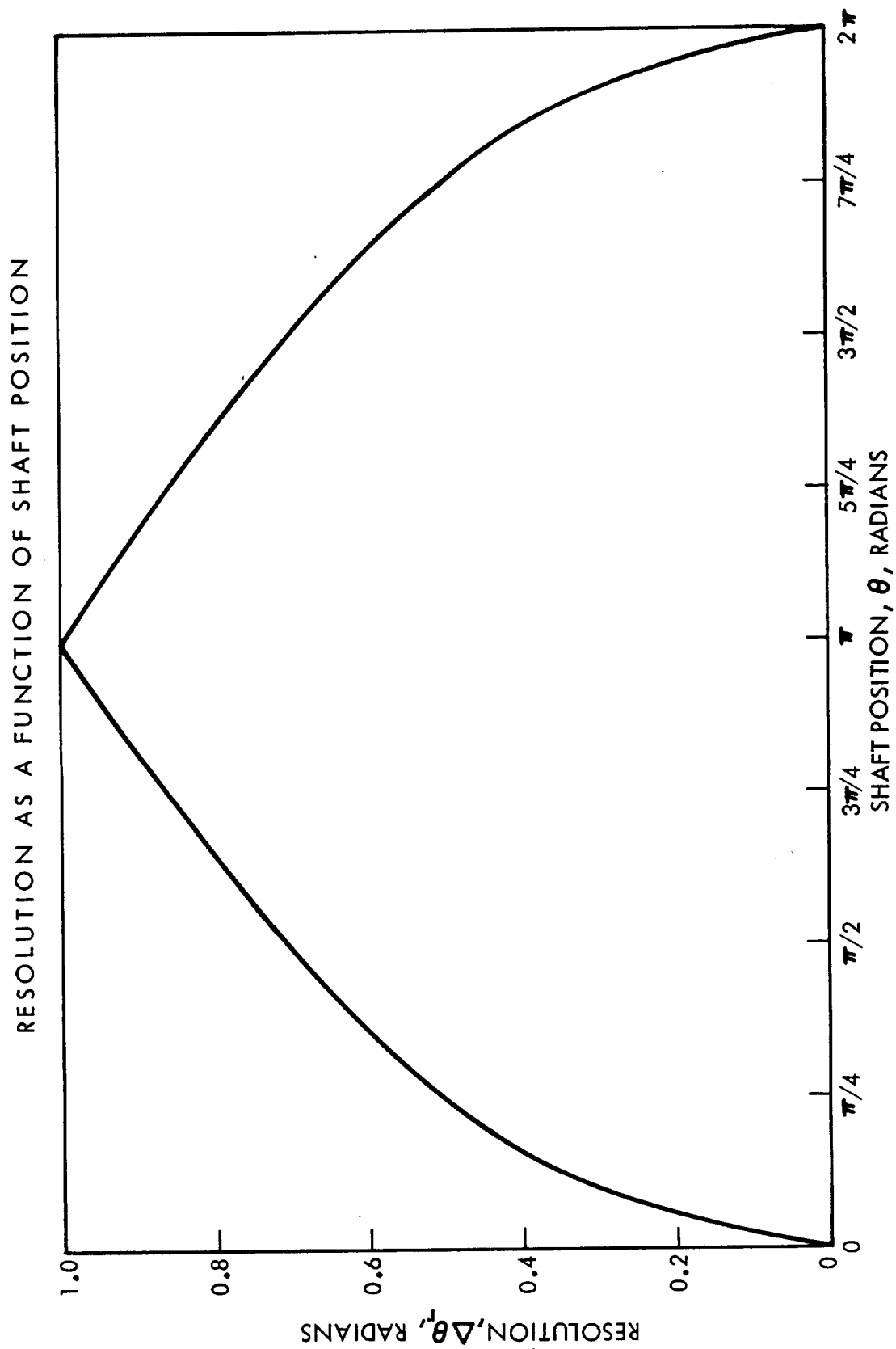
FIGURE C-2

SOURCE SIZE FOR A TOTAL
ROTATION OF $2\pi$ RADIANS

n = THE NUMBER OF
COUNTING TIMES
PER RESOLUTION
INTERVAL

n = 10

n = 5

n = 1

LEM SPECIFIED
RESOLUTION
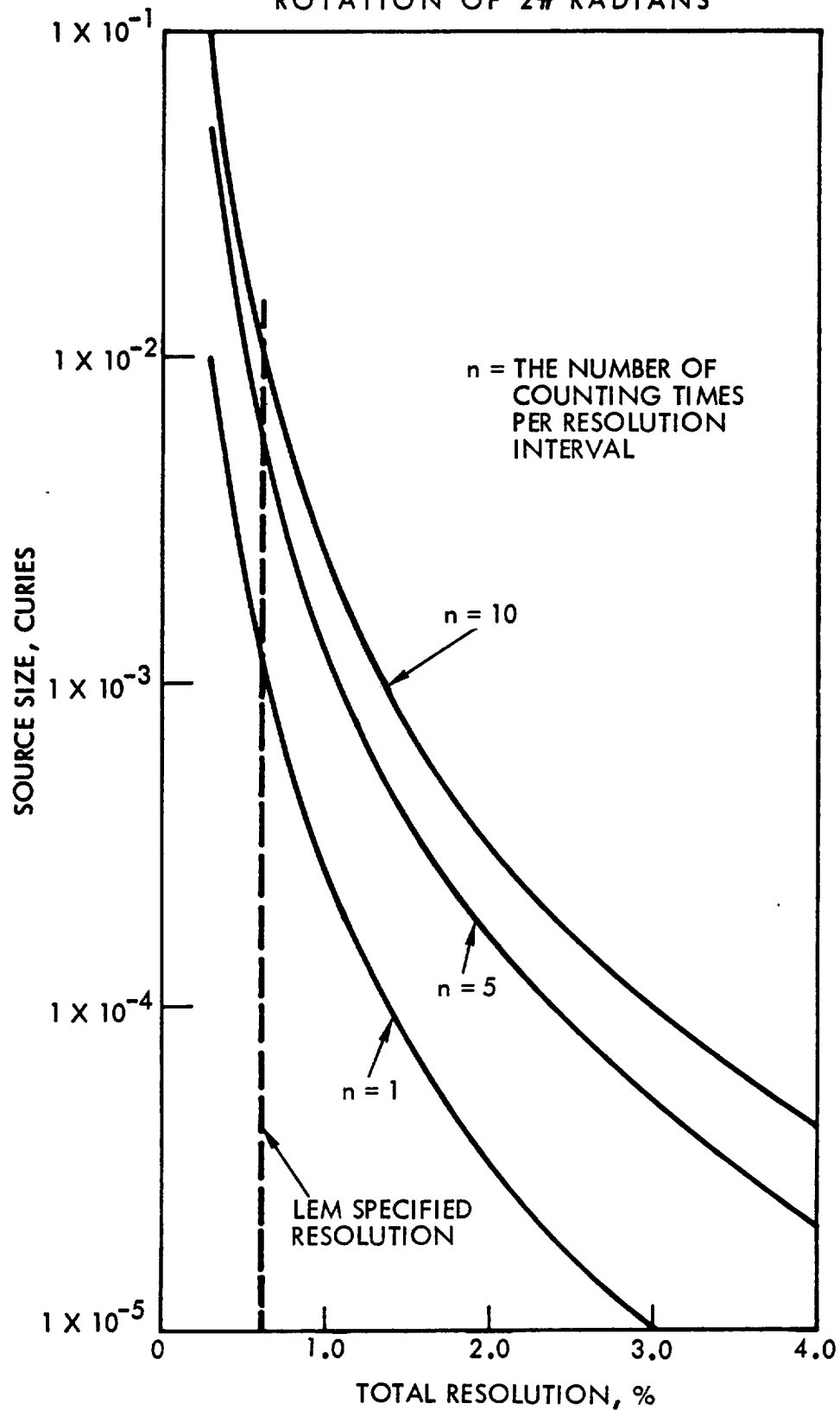
SOURCE SIZE, CURIES

TOTAL RESOLUTION, %

Figure C-3.   Source Size Required for the Divided Detector
Rotational Positioner

RADIOACTIVE PROXIMETER

REFERENCE LITERATURE AND BIBLIOGRAPHY

1.  I. E. Lamb, et al.  "Radioactive, Independent Transducer-Receiver System,"  Report Number AGN 3027-15,
    Contract Number AT(04-3)-251, P.A.3, November 1960,
    Aerojet-General Corporation.

2.  L. Dumont.  "Specification, Actuator, Throttle,
    Electromechanical,"  Specification Number EQ2-12B,
    7 January 1964, TRW Space Technology Laboratories

3.  "Preliminary Design Report, L.E.M. Throttle Actuator for
    Space Technology Laboratories,"  Eclipse-Pioneer Division,
    Bendix Corporation, 4 November 1963.

4.  H. E. Ethington.  Nuclear Engineering Handbook,
    McGraw Hill, 1958.

5.  Mosteller, et al.  Probability with Statistical Application,
    McGraw Hill, 1958.

FINAL REPORT DISTRIBUTION LIST

CONTRACT NAS7-107

NASA HEADQUARTERS
Washington, D.C.  20546

Mr. Henry Burlage, Jr.
Chief, Liquid Propulsion Technology, RPL

Scientific and Technical Information Facility
NASA Representative, CRT
P. O. Box 5700
Bethseda, Maryland  20014

NASA Western Operations Office
150 Pico Boulevard
Santa Monica, California  90405

    Office of Technical Information
    Contracting Officer
    Patent Office

TECHNICAL MANAGER

Mr. Louis Toth
Jet Propulsion Laboratory
California Institute of Technology
4800 Oak Grove Drive
Pasadena, California  91103

## NASA FIELD CENTERS

Ames Research Center
Moffett Field, California  94035

Goddard Space Flight Center
Greenbelt, Maryland  20771

Jet Propulsion Laboratory
California Institute of Technology
4800 Oak Grove Drive
Pasadena, California  91103

Langley Research Center
Langley Field, Virginia    23365

Lewis Research Center
21000 Brookpark Road
Cleveland, Ohio  44135

Marshall Space Flight Center
Huntsville, Alabama  35812

Manned Spacecraft Center
Houston, Texas  77001

# GOVERNMENT INSTALLATIONS

Advanced Research Projects Agency
Pentagon, Room 3D154
Washington 25, D. C.

Aeronautical Systems Division
Air Force Systems Command
Wright-Patterson Air Force Base, Ohio

Air Force Missile Development Center
Holloman Air Force Base, New Mexico

Air Force Missile Test Center
Patrick Air Force Base, Florida

Air Force Office of Aerospace Research
Temporary Building D
Washington 25, D. C.

Air Force Systems Command, Dyna-Soar
Air Force Unit Post Office
Los Angeles 45, California

Army Ordnance Missile Command
Redstone Arsenal, Alabama

A S T I A
Arlington Hall Station
Arlington 12, Virginia

Arnold Engineering Development Center
A. E. O. R.
Tullahoma, Tennessee

Bureau of Naval Weapons
Department of the Navy
Washington 25, D. C.

Headquarters, United States Air Force
Washington 25, D. C.

Office of Naval Research
Washington 25, D. C.

Picatinny Arsenal
Dover,
New Jersey

Rocket Research Laboratories
Edwards Air Force Base, California

U. S. Naval Ordnance Test Station
China Lake,
California

U. S. Atomic Energy Commission
Technical Information Services
P. O. Box P
Oak Ridge, Tennessee

U. S. Atomic Energy Commission
Chief, Analysis and Applications
Germantown, Maryland
(Mailing Address:
 Washington, D.C.  20546)

C P I A

Chemical Propellant Information Agency
Johns Hopkins University
Applied Physics Laboratory
8621 Georgia Avenue
Silver Spring, Maryland

# C O M M E R C I A L   C O N T R A C T O R S

Aerojet-General Corporation
P. O. Box 296
Azusa, California

Aerojet-General Corporation
P. O. Box 1947
Sacramento 9, California

Aeronutronic
A Division of Ford Motor Company
Ford Road
Newport Beach, California

Aerospace Corporation
2400 East El Segundo Boulevard
El Segundo, California

Arthur D. Little, Inc.
Acorn Park
Cambridge 40, Massachusetts

Astropower, Inc., Subsidiary of
Douglas Aircraft Company, Inc.
2968 Randolph Avenue
Costa Mesa, California

Astrosystems, Inc.
82 Naylon Avenue
Livingston, New Jersey

Atlantic Research Corporation
Edsall Road and Shirley Highway
Alexandria, Virginia

Beech Aircraft Corporation
Boulder Facility
Box 631
Boulder, Colorado

Bell Aerosystems Company
P. O. Box 1
Buffalo 5, New York

Bendix Systems Division
Bendix Corporation
Ann Arbor, Michigan

Boeing Company
P. O. Box 3707
Seattle 24, Washington

Convair (Astronautics)
Division of General Dynamics Corp.
P. O. Box 2672
San Diego 12, California

Curtiss-Wright Corporation
Wright Aeronautical Division
Wood-ridge, New Jersey

Douglas Aircraft Company, Inc.
Missile and Space Systems Division
3000 Ocean Park Boulevard
Santa Monica, California

Fairchild Stratos Corporation
Aircraft Missiles Division
Hagerstown, Maryland

General Electric Company
Re-entry Systems Department
Box 8555
Philadelphia, Pennsylvania 19101

General Electric Company
Rocket Propulsion Units
Building 300
Cincinnati 15, Ohio

Grumman Aircraft Engineering Corp
Bethpage, Long Island, New York

Kidde Aero-Space Division
Walter Kidde and Company, Inc.
675 Main Street
Belleville 9, New Jersey

Lockheed Aircraft Corporation
Missile and Space Division
Sunnyvale, California

Lockheed Propulsion Company
P. O. Box 111
Redlands, California

# COMMERCIAL CONTRACTORS

Marquardt Corporation
16555 Saticoy Street
Box 2013 - South Annex
Van Nuys, California

Martin Division
Martin Marietta Corporation
Baltimore 3, Maryland

Martin Denver Division
Martin Marietta Corporation
P. O. Box 179, Denver, Colorado

McDonnell Aircraft Corporation
P. O. Box 6101
Lambert Field, Missouri

North American Aviation, Inc.
Space & Information Systems Div.
Downey, California

Northrop Space Laboratories Corp.
1001 East Broadway
Hawthorne, California

Pratt & Whitney Aircraft Corp.
Florida Res. & Dev. Center
West Palm Beach, Florida

Radio Corporation of America
Astro-Electronics Division
Defense Electronic Products
Princeton, New Jersey

Reaction Motors Division
Thiokol Chemical Corporation
Denville, New Jersey

Republic Aviation Corporation
Farmingdale
Long Island, New York

Rocketdyne (Library Dept. 586-306)
Division of North American Aviation, I₁
6633 Canoga Avenue
Canoga Park, California

Space General Corporation
9200 Flair Avenue
El Monte, California

Space Technology Laboratories
P. O. Box 95001
Airport Station
Los Angeles 45, California

Stanford Research Institute
333 Ravenswood Avenue
Menlo Park, California

TAPCO Division
Thompson-Ramo-Wooldridge, Inc.
23555 Euclid Avenue
Cleveland 17, Ohio

Thiokol Chemical Corporation
Redstone Division
Huntsville, Alabama

United Aircraft Corporation
East Hartford Plant
400 Main Street
Hartford, Connecticut

United Technology Corporation
587 Methilda Avenue
Sunnyvale, California

Vought Astronautics
Box 5907
Dallas 22, Texas

B. H. Hadley, Inc.
P. O. Box 31
1427 South Garey Avenue
Pomona, California